NASA CR-72596

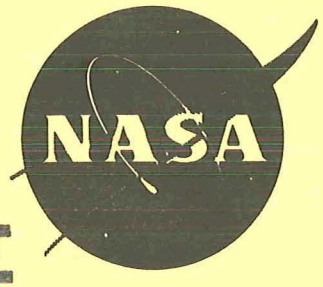

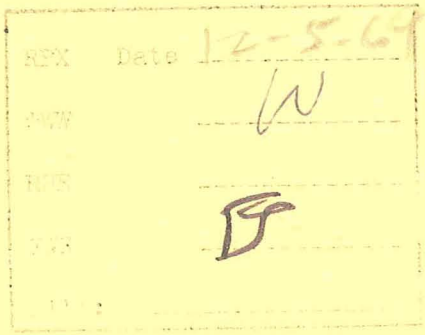

DEVELOPMENT OF A PROTECTIVE COATING SYSTEM FOR REGENERATIVELY COOLED THRUST CHAMBERS

by

C. G. Ruderer,
R. L. Heestand, and D. E. Kizer

prepared for

NATIONAL AERONAUTICS AND SPACE ADMINISTRATION

NASA Lewis Research Center
CONTRACT NAS 3-11186

BATTELLE MEMORIAL INSTITUTE
COLUMBUS LABORATORIES

Requests for copies of this report should be referred to

National Aeronautics and Space Administration
Scientific and Technical Information Facility
P.O. Box 33
College Park, Md. 20740

NASA CR-72596

FINAL TECHNICAL REPORT

DEVELOPMENT OF A PROTECTIVE COATING SYSTEM FOR REGENERATIVELY COOLED THRUST CHAMBERS

by

C. G. Ruderer,
R. L. Heestand, and D. E. Kizer

BATTELLE MEMORIAL INSTITUTE
Columbus Laboratories
505 King Avenue
Columbus, Ohio 43201

prepared for

NATIONAL AERONAUTICS AND SPACE ADMINISTRATION

May 31, 1969

CONTRACT NAS 3-11186

NASA Lewis Research Center
Cleveland, Ohio

Charles Zalabak, Project Manager
Chemical and Nuclear Rocket Division

DISTRIBUTION LIST

	Copies
National Aeronautics and Space Administration Lewis Research Center 21000 Brookpark Road Cleveland, Ohio 44135	
Attention: Contracting Officer Chemical Rocket Procurement Section Mail Stop 500-210	13
National Aeronautics and Space Administration Washington, D. C. 20546	
Attention: Code RPL	2
Code RPX	1
Code RRM	1
Scientific and Technical Information Facility NASA Representative, Code CRT P. O. Box 33 College Park, Maryland 20740	6
National Aeronautics and Space Administration Langley Research Center Langley Station Hampton, Virginia 23365	
Attention: Robert R. Howell Mail Stop 208	1
Librarian	1
National Aeronautics and Space Administration Goddard Space Flight Center Greenbelt, Maryland 20771	
Attention: Librarian	1
National Aeronautics and Space Administration Marshall Space Flight Center Huntsville, Alabama 35812	
Attention: K. Chandler, R-P&VE-PA	1
Librarian	1
V. F. Seitzinger, R-P&V-MNC	1
National Aeronautics and Space Administration Ames Research Center Moffett Field, California 94035	
Attention: Librarian	1
National Aeronautics and Space Administration Manned Spacecraft Center Houston, Texas 77085	
Attention: J. G. Thibodaux	1
Librarian	1
Jet Propulsion Laboratory 4800 Oak Grove Drive Pasadena, California 91103	
Attention: Librarian	1
National Bureau of Standards U. S. Department of Commerce Washington, D. C. 20546	1
Department of the Air Force Air Force Materials Laboratory (AFSC) Wright Patterson Air Force Base, Ohio 45433	
Attention: MAMC (J. J. Krochmal)	1
Department of the Air Force Air Force Rocket Propulsion Laboratory Edwards Air Force Base, California 93523	
Attention: RPM	1
Department of the Army Picatinny Arsenal Scientific & Technical Information Branch Dover, New Jersey 07601	
Attention: SMUPA-VAG, Librarian	1
U. S. Army Materials Research Agency Watertown, Massachusetts	1
Department of the Navy Naval Research Laboratory Washington, D. C. 20390	
Attention: Code 2027	1
Department of the Navy Naval Air Systems Command Washington, D. C. 20360	
Attention: AIR-330	1
DMIC Battelle Memorial Institute Columbus Laboratories 505 King Avenue Columbus, Ohio 43201	
Attention: Information Specialist	1
Defense Ceramic Information Center Battelle Memorial Institute Columbus Laboratories 505 King Avenue Columbus, Ohio 43201	
Attention: Manager of Technical Information	1

DISTRIBUTION LIST
(Continued)

	Copies
Chemical Propulsion Information Agency Applied Physics Laboratory - JHW 8621 Georgia Avenue Silver Spring, Maryland 20910	2
Battelle Memorial Institute Columbus Laboratories 505 King Avenue Columbus, Ohio 43201	20
Aerojet-General Corporation P. O. Box 15847 Sacramento, California 95813 Attention: W. J. Lewis, Dept. 0726	1
Aerojet-General Corporation P. O. Box 15847 Sacramento, California 95813 Attention: Technical Library - 2432-2015A	1
Rocketdyne Division North American Rockwell Corporation 6633 Canoga Avenue Canoga Park, California 91304 Attention: Dr. R. P. Frohmberg	1
Rocketdyne Division North American Rockwell Corporation 6633 Canoga Avenue Canoga Park, California 91304 Attention: Library, Dept. 086-306	1
Aerospace Corporation P. O. Box 95085 Los Angeles, California 90045 Attention: Technical Information Center - Document Group	1
Bell Aerosystems Company P. O. Box 1 Buffalo, New York 14240 Attention: Technical Library	1
Bell Telephone Laboratories Mountain Avenue Murray Hill, New Jersey 07974	1
Boeing Company P. O. Box 3999 Seattle, Washington 98124 Attention: Aerospace Library 8k-38	1
DuPont Company Eastern Division Gibbstown, New Jersey 08027 Attention: Report Clerk, A. R. Steward	1
General Dynamics Corporation P. O. Box 12009 San Diego, California 92112 Attention: Library & Information Services	1
General Electric Company Building 700, Mail Zone N-32 Cincinnati, Ohio 45215 Attention: FPD Technical Information Center	1
General Motors Technical Center 12 Mile and Mound Road Warren, Michigan Attention: Dr. Richard Murie, Dept. 55	1
General Telephone & Electronics Laboratory, Inc. Bayside, New York	1
IIT Research Institute 10 West 35th Street Chicago, Illinois 60616 Attention: Document Library	1
International Harvester Company Solar Division San Diego, California 92112	1
Itek Corporation Vidya Division 1450 Page Hill Road Palo Alto, California 94304 Attention: Librarian	1
LTV Aerospace Corporation LTV Vought Aeronautics Division P. O. Box 5907 Dallas, Texas 75222 Attention: Librarian	1
The Marquardt Corporation P. O. Box 2013 South Annex Van Nuys, California 91409 Attention: Librarian	1
Central Research Laboratory Allied Chemical Corporation P. O. Box 309 Morristown, New Jersey 07960 Attention: E. R. Degginger	1

DISTRIBUTION LIST
(Continued)

	Copies
McDonnell-Douglas Corporation P. O. Box 516 St. Louis, Missouri 63166 Attention: Librarian	1
McDonnell-Douglas Corporation Douglas Missile and Space Systems Division 3000 Ocean Park Blvd. Santa Monica, California 90406 Attention: Librarian A2-260	1
Monsanto Research Corporation 1515 Nicholas Road Dayton, Ohio 45407 Attention: Security Office	1
Norton Research Corporation 70 Memorial Drive Cambridge, Massachusetts 02142 Attention: Technical Information Center	1
Philco Ford Corporation Aeronutronic Division Ford Road Newport Beach, California 92663 Attention: Technical Information Service Acquisitions	1
Southern Research Institute Menlo Park, California	1
Stanford Research Institute Document Center for Propulsion Sciences 333 Ravenswood Avenue Menlo Park, California 94025	1
Sylvania Electric Products, Incorporated Silcor Divison Hicksville, New York	1
Teleflex, Incorporated Sermetal Division P. O. Box 187 125 South Main Street North Wales, Pennsylvania 19454	1
TRW Systems, Incorporated One Space Park Redondo Beach, California 90278 Attention: Technical Information Center	1
Union Carbide Corporation P. O. Box 324 Tuxedo, New York 10987 Attention: Technical Librarian	1
United Aircraft Corporation 400 Main Street East Hartford, Connecticut 06108 Attention: Acquisitions Librarian	1
United Technology Center P. O. Box 358 Sunnyvale, California 94088 Attention: Technical Library	1
University of California Lawrence Radiation Laboratory P. O. Box 808 Livermore, California 94550 Attention: Technical Information Division	1
University of Dayton Dayton, Ohio	1
University of Denver Denver Research Institute P. O. Box 10127 Denver, Colorado 80210 Attention: Security Officer	1
University of Utah Salt Lake City, Utah 84112 Attention: Dr. S. D. Brown	1
Vitro Laboratories West Orange, New Jersey	1

FOREWORD

This report summarizes the efforts performed by Battelle-Columbus under NASA Contract NAS 3-11186 from July 1, 1967, through March 31, 1969. The technical manager was Mr. Charles Zalabak, Chemical and Nuclear Rocket Division, National Aeronuatics and Space Administration, Lewis Research Center, Cleveland, Ohio 44135.

The authors wish to acknowledge the contributions of several individuals to the work described in the report. Dr. J. R. Thompson conducted the materials survey and initial selection of coating systems with the assistance of Dr. C. A. Alexander. Mr. G. R. Whitacre performed the necessary heat-transfer analysis, and Dr. J. C. Gerdeen performed the thermal-stress analysis. Dr. T. R. Wright advised on procedures and techniques for plasma spraying. Rocket testing was conducted by Mr. J. L. Harp and Mr. R. E. Robinson with Dr. E. W. Ungar acting in a consulting capacity.

ABSTRACT

The results of a study on coatings to reduce the effective heat flux in regeneratively cooled nozzles is reported. Task I involved the selection of materials for graded plasma-sprayed coatings, including metals, ceramics, and cermets and combinations of these applied as graded coatings. Consideration was given to compatibility of the materials with each other and the rocket environment, thermal conductivity of the coating system, and resistance to spalling as a result of thermal or mechanical shock. Sixteen potential systems were formulated, and on the basis of thermal and stress analyses four systems were selected for fabrication and testing.

Task II involved fabrication of the four candidate systems and testing in a hydrogen-oxygen rocket motor. On the basis of short-duration rocket tests with no cooling of the specimen, one coating system was selected for tests of longer duration employing water cooling. These tests revealed that the coating system (consisting of stainless steel BeO mixtures with an outer layer of thoria) finally selected has the capability of withstanding restarts of the rocket motor but that additional process development is required to obtain optimum deposits by plasma spraying.

TABLE OF CONTENTS

DEVELOPMENT OF A PROTECTIVE COATING SYSTEM FOR REGENERATIVELY COOLED THRUST CHAMBERS

C. G. Ruderer,
R. L. Heestand, and D. E. Kizer

SUMMARY

The goal of this program was to provide coating systems capable of reducing the potential heat flux in a regenerative hydrogen-cooled rocket motor from 50 to 60 Btu/(sec)(in.^{2}) to approximately 20 Btu/(sec)(in.^{2}). Plasma-arc spraying was selected as a method to apply the coatings since a wide variety of materials could be deposited in thin layers and the technique was readily applicable to coating existing motors. Although all materials having melting points on the order of 4000 F were considered, chemical compatibility requirements dictated that only oxides would withstand the environmental conditions.

Thermal- and mechanical-property data were used to conduct thermal-stress analyses and design ten systems having the compositional gradients required to give good mechanical compatibility with the substrate. Four of these coating systems were selected on the basis of minimum thermal-gradient-induced stresses for short-time rocket tests. Oxygen-hydrogen rocket tests were conducted at short times on several uncooled specimens of each of the four types for the first step in evaluation. Coatings which spalled in these tests were those which also had low adherence strength as determined by room-temperature tests. At this point, one system showed potential for success. The system was thoria over beryllia graded with stainless steel to a stainless steel substrate.

In water-cooled rocket tests on this system, the thoria layer successfully withstood the test conditions for time periods up to 5 sec. The coating would also withstand consecutive 1-sec firings of the motor, but failure occurred in the BeO on runs of longer duration. Further development of the spraying process for BeO or a modification eliminating BeO is indicated. A coating system which would withstand the required environment and service conditions was not found. However, a method for the formulation and selection of coating systems is presented, and recommendations are made in the report for the further development of coating systems based on the results of the program.

INTRODUCTION

This report describes work done on a research and development program conducted to extend the capabilities of regeneratively cooled rocket engines by applying a thermal/oxidation protective coating to the interior walls of the thrust chambers. The purpose of such an approach is to reduce the temperature of the metallic chamber wall and to lower the heat flux to the coolant to a level that permits effective heat dissipation. Specifically, the coating developed was intended for potential service in the throat region of an advanced hydrogen-oxygen, regeneratively cooled rocket engine operating at an exposed

surface temperature of approximately 4000 F. Desired characteristics of the coating were ability to maintain a coating/wall interface temperature of 1600 F or less and to reduce heat flux from approximately 60 Btu/(sec)(in.^{2}) to approximately 20 Btu/(sec)(in.^{2}).

The general program approach was to define the material characteristics required, select suitable materials on the basis of literature data and computer analyses, devise, analyze, and select potential coating systems incorporating these materials, and fabricate, test, and evaluate the candidate coating systems selected. State-of-the-art plasma-arc powder spraying was used to apply several multilayer, graded-composition coatings to uncooled substrates. Coated specimens were subjected to short-term service as nozzle inserts in a stationary laboratory rocket engine. On the basis of these tests, the final coating system was selected, applied to cooled substrates, and exposed to similar rocket firings of extended duration.

SELECTION OF MATERIALS

Material Requirements

The first requirement of the program was the selection of materials or materials systems for service as thermally and chemically protective plasma-sprayed coatings in the thrust chamber of a regeneratively cooled hydrogen-oxygen rocket engine. Target capabilities for the coating included an ability to reduce the heat flux from 60 Btu/(sec)(in.^{2}) to approximately 20 Btu/(sec)(in.^{2}) and to maintain a substrate temperature not exceeding 1600 F.

In qualitative terms, the ideal coating system would:

(1) Withstand the operating temperature of the thrust chamber

(2) Be chemically stable in the thrust-chamber environment

(3) Have a low overall thermal conductivity at the temperature encountered

(4) Resist erosion

(5) Resist thermal and mechanical shock

(6) Be impervious to the combustion gases at the temperatures encountered

(7) Be chemically and structurally compatible with the substrate at operating temperature

(8) Form a bond with the substrate sufficiently strong to prevent coating loss during operation

(9) Have a low density

(10) Consist of materials which are readily available, easily fabricated, low in cost, and require no special handling or precautions during fabrication or in service.

In order to establish a more quantitative basis for materials selection, the conditions present in the operating thrust chamber were defined and analyzed (Table 1). Calculations indicated that the exposed surface of the coating must withstand a high-pressure, high-velocity oxidizing/reducing atmosphere at a temperature of about 3920 F.

Initial Materials Selection

First consideration was given to the material which would be directly exposed to the thrust-chamber environment. Because a minimum requirement for the exposed material was that it be able to withstand thrust-chamber operating temperatures, only materials able to accommodate 4000 F temperatures without melting, decomposing, subliming, or undergoing disruptive phase transformations were considered for use in the exposed coating layer.

A review of available data [1-27] revealed approximately 130 materials having the required temperature capability; these materials are listed in Table 2. Little or no data were available for many of the materials listed, and these were deleted from further consideration. Also deleted were those materials which form liquid protective surface layers at temperature. Such materials were not considered suitable because the high-velocity chamber gases would tend to mechanically remove the liquid layer, and the composition, thickness, properties, and behavior of the coating system would be different for each restart of the rocket engine. Other materials were rejected on the basis of available data indicating excessive reactivity at the temperature and/or in the atmosphere of the thrust chamber.

A computer code was used to compare the stabilities of the various classes of materials fulfilling the minimum temperature requirement. The compounds HfB_2, ZrC, and TaN were selected for detailed study because their free energies of formation indicated them to be among the most stable compounds of their respective material classifications. Oxides were excluded because of their known stability. Calculations were based on a closed system containing 1 mole of the compound and 1 mole of the thrust-chamber gases at a temperature of 2500 K (4000 F) and a pressure of 77.62 atm. Initial concentrations were assumed for all possible chemical species present, using 1×10^{-10} mole as the minimum concentration permitted in the computer code. A typical analysis, that for ZrC, is given in Table 3. It is evident from Table 3 that the conditions of thrust-chamber operation favor the oxidation of ZrC to ZrO_2. Similarly, analyses showed that HfB_2 and TaN would be oxidized to HfO_2 and molten Ta_2O_5, respectively. In each case, oxidation would proceed until no initial compound remained. While data regarding reaction rates and kinetics were not available for these materials at the temperature of interest, the rates may be expected to be rapid. The thrust-chamber operating conditions also favor oxidation of the other nonoxide materials (elements, silicides, intermetallics, and sulfides) listed in Table 2. The above analyses demonstrated the inadequacy of most material types, but showed that oxides were the most stable materials under the conditions of thrust-chamber operation. Therefore, only the 30 single and mixed oxides listed in Table 2 remained as potential exposed-surface materials.

The candidate oxide materials were next compared and evaluated on the basis of the thermal impedance they could provide. An exposed-surface temperature of 3920 F (4380 R) was assumed, and the equation given below was used to calculate the minimum

TABLE 1. NOZZLE THROAT THERMODYNAMIC AND TRANSPORT PROPERTIES

Gas-Stream Flow Conditions	
Total Pressure (P_o)	136 atm
Static Pressure (P_s)	77.62 atm
Total Temperature (T_o)	3591 K
Static Temperature (T_s)	3117 K
Average Velocity (V)	4940 ft/sec
Thermodynamic Properties	
Enthalpy (H), cal/g	-662.2
Entropy (S), cal/(g)(K)	4.2197
Molecular Weight (M)	13.236
$\frac{\partial \ln M}{\partial \ln P}_T$	0.00802
$\frac{\partial \ln M}{\partial \ln T}_P$	-0.1587
Specific Heat Ratio (γ)	1.1602
Gas-Composition Mole Fractions	
H_1, g	0.01499
H_2, g	0.28234
H_2O, g	0.68814
O_1, g	0.00047
O_2, g	0.00046
O_1H_1, g	0.01353
Transport Properties	
Viscosity (μ), poises	880
Conductivity (k), cal/(cm)(sec)(K)	2444[a]
Specific Heat at Constant Pressure, (C_p), cal/(g)(K)	1.3873
Prundtl Number (Pr)	0.5085
Lewis Number (Le)	1.5525

(a) Includes reaction (diffusion and recombination) effects.

TABLE 2. POTENTIAL COATING MATERIALS FOR SERVICE AT 4000 F

Elements

Graphite	Niobium	Ruthenium
Iridium	Osmium	Tantalum
Molybdenum	Rhenium	Tungsten

Borides

AlB_{10}	Mo_2B	NdB_6	Ta_3B_4	UB_4	β-WB
BaB_6	β-MoB	ScB_2	TaB_2	VB	W_2B_5
CaB_6	MoB_2	SmB_6	ThB_4	V_3B_4	YB_6
HfB	NbB	SrB_6	TiB_2	VB_2	ZrB_2
HfB_2	NbB_2	TaB	UB_2	W_2B	ZrB_{12}

Carbides and Mixed Carbides

Al_4C_3	LaC_2	PrC_2	ThC_2	W_2C	$ZrC \cdot 8TaC$
B_4C	Mo_2C	SiC	TiC	WC	
CeC_2	MoC	Ta_2C	UC	YC_2	
HfC	Nb_2C	TaC	UC_2	ZrC	
$HfC \cdot 4TaC$	NbC	ThC	VC	$ZrC \cdot 4TaC$	

Nitrides

BN	Nb_2N	ScN	ThN	YN
Be_3N_2	NbN	Ta_2N	TiN	ZrN
HfN	PuN	TaN	UN	

Oxides and Mixed Oxides

$BaO \cdot ThO_2$	$CaO \cdot ZrO_2$	HfO_2	Pu_2O_3	ThO_2
$BaO \cdot ZrO_2$	$CeO \cdot Cr_2O_3$	La_2O_3	PuO_2	$ThO_2 \cdot ZrO_2$
BeO	CeO_2	$La_2O_3 \cdot 2HfO_2$	Sm_2O_3	UO_2
$3BeO \cdot 2ZrO_2$	Cr_2O_3	MgO	SrO	Y_2O_3
CaO	Dy_2O_3	Nb_2O_3	$SrO \cdot ZrO_2$	Yb_2O_3
$CaO \cdot HfO_2$	Gd_2O_3	$Nd_2O_3 \cdot 2HfO_2$	Tb_2O_3	ZrO_2

Silicides

Hf_5Si_3	Ta_2Si	W_3Si_2	Zr_4Si_3
Nb_5Si3	Ta_5Si_3	Zr_5Si_3	Zr_6Si_5
Ta_5Si	$TaSi_2$	Zr_3Si_2	Zr_6Si_5

Intermetallics, Sulfides, and Composites[a]

$HfMo_2$	PrS	Boride Z
$HfRe_2$	ThS	Borolite-101
Mo_2Re_3	US	
PtRe		
Re_3W_2		

(a) Melting point data are not available for many other developmental composite materials.

TABLE 3. BEHAVIOR OF ZrC IN THRUST-CHAMBER ENVIRONMENT[a]

Material[b]	Calculated Composition, mole	
	Initial	Final
ZrC(s)	1.0	0.76462
C(s)	1×10^{-6}	5.5622×10^{-7}
H(g)	0.01499	0.00309
H_2(g)	0.28234	0.97611
H_2O	0.68814	0.00125
O(g)	0.00047	1.7279×10^{-9}
O_2(g)	0.00046	9.2278×10^{-13}
OH(g)	0.01353	8.2601×10^{-7}
ZrO_2(g)	1×10^{-10}	5.0717×10^{-9}
ZrO_2(s)	1×10^{-6}	0.23538
CH(g)	1×10^{-10}	7.7088×10^{-9}
CHO(g)	1×10^{-10}	8.6483×10^{-5}
CH_2(g)	1×10^{-10}	1.2072×10^{-7}
CH_2O(g)	1×10^{-10}	8.5091×10^{-6}
CH_3(g)	1×10^{-10}	2.6456×10^{-4}
CH_4(g)	1×10^{-10}	0.00218
CO(g)	1×10^{-10}	0.23084
CO_2(g)	1×10^{-10}	4.8757×10^{-5}
C_2H_2(g)	1×10^{-10}	9.3408×10^{-4}
C_2H_4(g)	1×10^{-10}	3.8938×10^{-5}
C_2H_4O(g)	1×10^{-10}	3.2285×10^{-12}
C_3O_2(g)	1×10^{-10}	2.3394×10^{-9}
HO_2(g)	1×10^{-10}	7.6629×10^{-15}
HZr(g)	1×10^{-10}	2.0531×10^{-10}

(a) Closed system containing 1 mole of ZrC and 1 mole of gas at a temperature of 2500 K and a pressure of 77.62 atm. Minimum allowable concentration = 1×10^{-10} mole.

(b) Major constituents of final composition are underlined.

thermal impedence required for a 0.005-in.-thick* oxide coating to reduce the temperature to 2000 F (2460 R). It was assumed that intermediate coating layers necessary to match thermal expansion of the oxide to that of the substrate would provide the additional thermal impedance required to insure a maximum substrate temperature of 1600 F.

$$k_c = \frac{t_c}{T_w - T_{n+1}} \left[\frac{c\,(6380 - T_w)}{\left(\frac{T_w}{1000} + 6.03 \right)^{0.68}} \right] ,$$

where

k_c = thermal conductivity of the coating

t_c = coating thickness

T_w = temperature of exposed surface (4380 R)

T_{n+1} = temperature of coating/substrate interface (2460 R)

c = a constant = 0.0497.

The maximum permissible thermal conductivity was calculated to be 2.273 Btu/(ft)(hr)(R).

On the basis of available thermal-conductivity data for dense material and considering that the coating material would have a lower density[3, 6, 7], only ZrO_2, HfO_2**, UO_2, ThO_2, CeO_2, and, perhaps, Y_2O_3 were considered acceptable exposed-surface materials. After considering a number of factors, including availability, completeness of characterization, and ease of handling, the choice was limited to ZrO_2, HfO_2, and ThO_2. Because such a limited number of oxides had potential as the exposed-surface coating material, HfO_2 and ThO_2 were retained as candidate materials in spite of their high cost and the radioactivity of ThO_2. It should be emphasized that ZrO_2 and HfO_2 must be stabilized to the cubic phase by addition of CaO or Y_2O_3 to prevent the disruptive phase transformations which occur in the unstabilized materials. Future references to ZrO_2 and HfO_2 should be taken to mean the Y_2O_3-stabilized materials.

Although ZrO_2, HfO_2, and ThO_2 have adequate thermal impedance to achieve the required temperature and heat-flux gradients, none of these materials can be used alone as the total coating system because of:

(1) Large thermal-expansion mismatch with candidate substrate materials (Hastelloy X and Type 347 stainless steel)

(2) Poor resistance to oxygen diffusion

(3) Poor thermal-shock resistance

(4) Inability to form a strong bond directly with the substrate materials when deposited by plasma spraying.

*Calculations indicated that excessive thermal stresses would be developed in oxide coatings thicker than about 0.005 in.

**Thermal conductivity of HfO_2 was assumed to be the same as that of ZrO_2, although no data were found.

To overcome these difficulties, it was necessary to develop multilayer coating systems which would permit stepwise and comparatively gradual transition of property values from those of the substrate to those of the exposed oxide coating, provide a more effective barrier against oxygen diffusion to the substrate, and increase the thermal-shock resistance of the total coating system. In essence, the multilayer coatings would consist of a thin plasma-sprayed layer of the substrate material (or a material with chemical and expansion characteristics compatible with those of the substrate) to provide optimum substrate adhesion, several layers containing successively greater ceramic-metal ratios, and, finally, the exposed oxide layer. Such an approach helped resolve the oxide-substrate mismatch, permitted the outer oxide layer to be thinner (and, hence, more thermal-shock resistant), provided a degree of reinforcement for the shock-sensitive materials, resulted in smaller temperature gradients across individual layers, and permitted introduction of "special purpose" layers, such as those to impede oxygen diffusion or to replenish any spalled areas of surface oxide. Consideration was also given to incorporating small amounts of refractory-metal reinforcement in oxide layers to improve thermal-shock resistance; in these cases, niobium was selected on the basis of its high strength, ductility, and insensitivity to embrittlement by oxygen. Consideration of the above factors led to development of the generalized candidate coating systems shown in Table 4. The advantages, limitations, and compatibilities of the materials listed were assessed by qualitative or semiquantitative evaluations.

TABLE 4. POTENTIAL MATERIALS FOR USE IN INTERMEDIATE LAYERS OF PROTECTIVE COATING SYSTEMS

Surface Coating Materials	ThO_2	Y_2O_3-Stabilized ZrO_2	Y_2O_3-Stabilized HfO_2
Intermediate Layer 1	BeO ThO_2-ZrO_2 Reinforced Al_2O_3 Reinforced ThO_2	BeO Borolite-101 SrO-ZrO_2 Hypereutectic ZrC Metal-rich ZrB_2 Boride Z	BeO HfB_2 + 10 v/o $MoSi_2$ Hypereutectic HfC Metal-rich HfB_2 HfB_2 + SiC
Intermediate Layer 2	Graded layers between materials of Intermediate Layer 1 and (1) Hastelloy C or Hastelloy X (2) Type 304 or Type 347 stainless steel (3) Me_xBe_{12}		
Substrate	Hastelloy X or Type 347 stainless steel		

Of the candidate materials for the first layer(s), it was concluded that the Hastelloys and stainless steels would provide maximum compatibility with substrates of the corresponding materials. Of the dodecaberyllides, $TiBe_{12}$ has been found to be highly oxidation resistant. It is suitable for plasma spraying, adheres well to metal substrates, and has a thermal expansion compatible with that of Hastelloy X. Thermodynamic calculations suggest that $TiBe_{12}$ and the residual carbon in Hastelloy X may react to form titanium carbide, although reaction rates are expected to be slow at the moderate temperatures encountered by the lower coating layers.

More severe difficulties were foreseen for some of the materials initially considered for use in the intermediate layer(s). The zirconates were deleted because the available data were insufficient to permit realistic evaluation of their compatibilities with other materials of interest. Likewise, the HfB_2/SiC composite was omitted because it was thought that this material could not be successfully plasma sprayed without an extensive development program. More detailed thermodynamic considerations indicated the use of hypereutectic carbides to be inadvisable because of the possible reduction of the outermost oxide layer by the carbide or free carbon. Of greater consequence, if the carbides were heated sufficiently they could carburize adjacent metal constituents and be oxidized to form large quantities of CO. The gas generated could expand and build up sufficient pressure behind the impervious outer coating layers to spall off some or all of the outer layers. Similarly, composites containing $MoSi_2$ such as Boride Z and $HfB_2/MoSi_2$ would endanger the coating by potential generation of volatile molybdenum oxide. In addition, the silicide could react with adjacent metals to form low-melting eutectics. The borides including the Borolite-101 composite could also oxidize with the generation of gases, but were not thought to pose as serious a problem.

Inclusion of a BeO layer seemed desirable as a barrier to oxygen diffusion, but this oxide reacts in the presence of water vapor and becomes volatile at high temperatures. Although water vapor is a major constituent of the thrust-chamber gas (Table 1), the BeO should not attain the critical reaction temperature, which is generally reported as 3000 F. In addition, the relatively impervious oxidation-resistant outer layer should help prevent water-vapor contact with the BeO underlayer. In any event, BeO was considered only for intermediate layers because of the health hazard resulting from volatilization of BeO from an exposed-surface layer.

Refractory-metal reinforcement was considered for strengthening intermediate layers of ThO_2 or Al_2O_3. Although all metals considered may be oxidized, it was expected that the outer coating layers would somewhat protect the metal from oxidizing atmosphere. Niobium was selected as the reinforcing metal on the basis of its ductility and insensitivity to embrittlement by oxygen.

Preliminary Coating Systems

After consideration of the material possibilities indicated in Table 4 and the limitations of these materials as discussed above, 15 preliminary coating systems were devised. In all cases, the thickness of individual coating layers was 0.002 in. or greater, but did not exceed 0.005 in. These values represent the minimum practical thickness for reliable plasma-spray deposition and the maximum thickness not resulting in excessively high thermal stresses, respectively. Five of the initial systems were not considered further because of the presence of hypereutectic carbides or $MoSi_2$ or because they were very similar to other systems. Table 5 lists the composition, thickness, and calculated interface temperature for each layer of the ten multilayer coating systems still under consideration at this point. Preliminary thermal calculations indicated that all coating systems would maintain the coating-substrate interface at a temperature well below the 1600 F maximum permissible temperature.

More accurate thermal analyses were made for each of the above coating systems using the TWODHT computer program applicable to time-dependent heat conduction in two dimensions. A subroutine within the program adjusts the values of

TABLE 5. PRELIMINARY COATING SYSTEMS

System	Layer	Layer Composition[a], v/o	Layer Thickness, in.	Calculated Interface Temperature, F
				3920
A	5	ThO_2	0.0035	1740
	4	BeO	0.002	1600
	3	50 BeO-50 $TiBe_{12}$	0.002	1495
	2	20 BeO-80 $TiBe_{12}$	0.002	1390
	1	$TiBe_{12}$	0.002	1290
	Substrate	Hastelloy X	0.010	
				3920
B	5	ThO_2	0.0035	1740
	4	BeO	0.002	1600
	3	50 BeO-50 Type 304 stainless	0.002	1502
	2	25 BeO-75 Type 304 stainless	0.002	1400
	1	Type 304 stainless	0.002	1270
	Substrate	Type 347 stainless	0.010	
				3920
C	5	ZrO_2	0.0035	1916
	4	BeO	0.003	1732
	3	50 BeO-50 $TiBe_{12}$	0.003	1606
	2	20 BeO-80 $TiBe_{12}$	0.002	1519
	1	$TiBe_{12}$	0.002	1429
	Substrate	Hastelloy X	0.010	
				3920
D	5	HfO_2	0.0035	1850
	4	BeO	0.003	1715
	3	50 BeO-50 $TiBe_{12}$	0.003	1587
	2	20 BeO-80 $TiBe_{12}$	0.002	1500
	1	$TiBe_{12}$	0.002	1403
	Substrate	Hastelloy X	0.010	
				3920
E	4	ZrO_2	0.0035	1916
	3	ZrB_2	0.003	1714
	2	50 ZrB_2-50 Hastelloy X	0.003	1527
	1	20 ZrB_2-80 Hastelloy X	0.003	1345
	Substrate	Hastelloy X	0.010	
				3920
F	4	HfO_2	0.0035	1850
	3	50 HfO_2-50 Type 304 stainless	0.003	1532
	2	20 HfO_2-80 Type 304 stainless	0.003	1295
	1	Type 304 stainless	0.002	1158
	Substrate	Type 347 stainless	0.010	

temperature-dependent properties to those appropriate to instantaneous thermal conditions. A second subroutine accounts for the geometry of the simulated specimen, which in this case was a cylindrical substrate-coating shell with azimuthal symmetry. Several preliminary computer runs established that there was no significant variation of heat transfer from point to point in the axial direction. Accordingly, the problem was treated as a one-dimensional heat-transfer analysis. Polar coordinates were retained in the simplified analysis, and the area increase corresponding to increasing radius (decreasing depth below coating surface) was taken into account.

The steady-state heat flux and substrate-coating interface temperature were used as criteria for assessing how well the computer program simulated the actual operating conditions expected. In every case, the heat flux was very nearly the desired 20 Btu/(sec)(in.^{2}). The calculated substrate surface temperature exceeded the desired 1600 F in some instances, but in no case attained a value as high as 1800 F. It was believed that all computer calculations approximated the expected operating conditions well enough to be considered valid analyses. As expected, all calculations showed that the outermost coating layer would encounter the most severe temperature gradient; considering all coating systems, the temperature difference across the outermost layer averaged 2011 F, while that across all other layers taken together averaged 716 F.

Selection of Candidate Coating Systems

Thermal stresses in the above coating systems were evaluated by a one-dimensional elastic analysis of the cylindrical thin-shell model considered in the thermal analyses. The analysis assumed axial symmetry and plane strain and, hence, considered only changes in temperature and stress in the radial direction (i.e., across the thickness of the coated substrate). The constancy of temperature along the cylinder length indicated by the thermal calculations permitted end effects to be neglected, and neglecting end effects was equivalent to specifying that the cylinder was unrestrained. For unrestrained cylinders, stresses in the central portions are greater than those near the ends. The analysis therefore was thought to provide a good estimate of the maximum stress present in the coating system.

Stress analyses were made with the aid of the AXISOL computer program. AXISOL is the Battelle-Columbus version of the "Wilson" finite-element program[27] for stress analysis of general bodies of revolution in which the body is considered to be a series of ring elements with rectangular cross sections. This program is particularly useful for analysis of multilayer thin-shelled structures because it permits arbitrary variations of composition and temperature across the thickness of the shell. To obtain stresses in the central portion of the cylindrical shell (i.e., the maximum stress in the coating system) it was necessary to consider only a thin slice perpendicular to the symmetry axis which corresponded to a single row of ring elements. By imposing the conditions that axial strain remained constant within the slice and that no net axial load was transmitted through the slice, it was assured that the stresses calculated corresponded to the maximum stress levels present in the coating under the geometrical and thermal conditions imposed.

It was assumed that all materials behaved elastically, and room-temperature values of elastic constants were used when elevated-temperature data were not available. However, calculated stress values exceeded the substrate yield strength, indicating that

the substrate would deform, particularly at elevated temperatures. The 1 to 2 percent deformation expected would reduce the level of stress present in the coating. Although the calculations therefore gave stresses larger than those anticipated in actual service, they were thought to be adequate for computing relative stress levels among the various coating systems.

Stresses under conditions of thermal shock (sudden initial heating on startup) were found to be not significantly greater than those under steady-state conditions. Most stress occurred in the outermost heated layer during initial transient heating, but all layers were highly stressed at steady state. Accordingly, steady-state stresses were judged to be the most critical and were emphasized in interpretation of the analyses. As desired, hotter surfaces were in compression and cooler surfaces were in tension at all times and under all conditions. Of greater significance, the analyses showed that subsurface tensile stresses would be developed within all the coating systems considered except two. Because all coating systems met the thermal requirements of the application and because of the brittle nature of many of the coating constituents, subsurface tensile stress was taken as the major criterion for evaluation and selection of coating systems. Table 6 ranks the coating systems in order of increasing subsurface tensile stress and tabulates corresponding stresses (Z) at the outer surface of the coating and the inner surface of the metal tube.

TABLE 6. RANKING OF COATING SYSTEMS BY MAXIMUM TENSILE STRESSES IN THE COATINGS

Ranking	Coating	Z-Stress on Hot Surface, 10^5 psi	Z-Stress on Cold Surface, 10^5 psi	Maximum Subsurface Tensile Stress, 10^5 psi
1	M	-2.24	2.34	0.0
2	G	-1.86	2.63	0.0
3	N	-2.60	2.90	0.18
4	D	-1.86	2.32	0.32
5	B	-2.32	2.25	0.83
(a)	Rocketdyne	-4.2	2.22	1.16
6	H	-1.22	2.11	1.89
7	A	-1.26	3.83	1.97
8	F	-6.52	2.68	2.11
9	K	-3.82	2.68	2.35
10	C	-5.19	4.84	3.32

(a) The Rocketdyne coating, included here for purpose of comparison, was a plasma-sprayed graded Inconel/zirconia system. This coating had a thermal resistance of 200 in^2./(sec)(F)(Btu), and was able to reduce the surface temperature of a nickel cooling ring from 2600 F to 1500 F. Effective heat flux to the substrate was reduced from 50 to 25 Btu/($in.^2$)(sec) with the coating. The coating system withstood 100 thermal shocks from 4000 F to 65 F surface temperature.
Reference: H. W. Carpenter, "Heat Barrier Coatings for Rocket Engines", Summary of the Thirteenth Meeting of the Refractory Composites Working Group, DMIC Memorandum 227, pp 16-17, September 1, 1967.

Coating systems selected for further investigation, fabrication, and testing were those having the lowest calculated values of subsurface tensile stress. Although Coating System G did not develop a subsurface tensile stress, it was not selected as a candidate system because thermal analysis indicated that the metallic component of the outermost intermediate layer would be subjected to excessive temperatures. Coating Systems M, N, D, and B were selected for further study, and were redesignated Coating Systems 1, 2, 3, and 4, respectively. Tables 7 through 10 summarize the calculated temperatures and thermal stresses expected to be present during steady-state operation of the rocket engine at layer interfaces of the four candidate coating systems selected. Since property data was not available in some instances at the required temperatures, recalculation of systems should be conducted as data becomes available to obtain a more accurate state of stress.

PREPARATION OF SPECIMENS AND COATINGS TESTS

Plasma-Spraying Equipment, Materials, and Techniques

All plasma spraying was done in the stainless steel spray chamber shown in Figure 1. Prior to spraying, the chamber was evacuated to at least 10^{-4} torr and backfilled with 99.998 percent pure argon passed through a bed of activated alumina. A modified Plasmadyne Model SG-1B hand-held plasma-arc powder spray gun was used in all cases; standard gun electrodes were used for spraying most of the coatings applied in the early stages of the program. Arc and powder carrier gases were argon of the same grade and dryness used to backfill the spray chamber. Arc power was supplied by a rectifier having an open-circuit output voltage of 80 v and capable of continuous operation at 40 kw. Powder material was injected into the powder carrier-gas stream by means of a Plasmadyne Rotofeed 1000 powder hopper.

Since state-of-the-art plasma spraying was to be utilized in preparing the coatings and it was not intended to optimize all the materials required for testing program, parameters for plasma spraying which had been determined previously were utilized in the program. However, some development was required since many of the materials had not been sprayed as thin coatings onto thin substrates as consecutive layers.

Initial experiments were conducted to determine spraying parameters for the various materials on the thin substrates required in the program. Coatings were applied to small 0.020- or 0.040-in.-thick coupons of Type 347 stainless steel or Hastelloy X clamped to a water-cooled copper chill plate. Later experiments, including fabrication of specimens for bond- and tensile-strength specimens, involved coating 2 by 4-in. areas of the 3 by 5 by 0.010-in. sheet and required the fabrication of the special cooling jig depicted in Figure 2. This jig provided effective cooling by a thin curtain of rapidly flowing water at 60 psig in direct contact with the substrate and prevented melting or severe warping of thin substrates during plasma spraying. Increasing substrate temperature usually enhances adhesion; however, in this case, because of the thin substrates, this variable could not be utilized.

TABLE 7. CALCULATED TEMPERATURES AND THERMAL STRESSES AT INTERFACES IN COATING SYSTEM 1

	Layer Composition, v/o	Thickness, mils	Interface Temperature, F	Coefficient of Thermal Expansion, 10^{-6}/F	Elastic Modulus, 10^6 psi	Poissons Ratio, ν	Z-Stress, 10^5 psi
			4040				
				7.0	12.8	0.275	-2.24
Hot Surface	ThO_2	3.0					
			2360	5.4	12.8	0.275	-2.90
Interface 1				5.4	12.8	0.280	-0.64
	ThO_2 + 10 v/o Nb Reinforcement	2.0					
			1870	5.2	12.8	0.280	-0.29
Interface 2				6.95	20.6	0.290	-1.16
	50 ThO_2/Nb 50 Hastelloy C	2.0					
			1610	6.8	20.6	0.290	-0.77
Interface 3				7.64	26.4	0.296	-1.23
	80 Hastelloy C 20 ThO_2/Nb	2.0					
			1390	7.5	26.4	0.296	-0.77
Interface 4				7.9	30.0	0.300	-0.83
	Hastelloy C	2.0					
			1200	7.7	30.0	0.300	-0.36
Interface 5				8.6	28.6	0.320	-0.21
	Hastelloy X	10.0					
Cold Surface			370	7.7	28.6	0.320	2.34

TABLE 8. CALCULATED TEMPERATURE AND THERMAL STRESSES AT INTERFACES IN COATING SYSTEM 2

	Layer Composition, v/o	Thickness, mils	Interface Temperature, F	Coefficient of Thermal Expansion, 10^{-6}/F	Elastic Modulus, 10^6 psi	Poissons Ratio, ν	Z-Stress, 10^5 psi
			4010	7.0	16.4	0.306	-2.60
Hot Surface	50 ThO_2 50 Stabilized ZrO_2	3.0					
			2210	5.4	16.4	0.306	-0.69
Interface 1				5.7	48.0	0.300	-1.86
	BeO	3.0					
			1920	5.7	50.0	0.300	-0.88
Interface 2				7.3	40.0	0.300	-2.02
	50 BeO 50 Hastelloy C	3.0					
			1670	7.1	40.0	0.300	-1.17
Interface 3				7.6	34.0	0.300	-1.15
	80 Hastelloy C 20 BeO	3.0					
			1420	7.5	34.0	0.300	-0.39
Interface 4				7.9	30.0	0.300	-0.32
	Hastelloy C	2.0					
			1220	7.7	30.0	0.300	0.18
Interface 5				8.6	28.6	0.320	0.32
	Hastelloy X	10.0					
Cold Surface			380	7.7	28.6	0.320	2.90

TABLE 9. CALCULATED TEMPERATURE AND THERMAL STRESSES AT INTERFACES IN COATING SYSTEM 3

	Layer Composition, v/o	Thickness, mils	Interface Temperature, F	Coefficient of Thermal Expansion, 10^{-6}/F	Elastic Modulus, 10^6 psi	Poissons Ratio, ν	Z-Stress, 10^5 psi
			3970	6.60	8.0	0.300	-1.86
Hot Surface	Stabilized HfO_2	3.5					
			1840	6.60	8.0	0.300	-0.48
Interface 1				5.71	50.0	0.300	-1.04
	BeO	3.0					
			1620	5.71	50.0	0.300	-0.34
Interface 2				6.55	49.0	0.300	-1.12
	50 BeO 50 $TiBe_{12}$	3.0					
			1470	6.55	49.0	0.300	-0.55
Interface 3				6.10	49.5	0.300	0.04
	80 $TiBe_{12}$ 20 BeO	2.0					
			1370	6.10	49.5	0.300	0.32
Interface 4				8.53	50.0	0.300	-1.77
	$TiBe_{12}$	2.0					
			1250	8.53	50.0	0.300	-1.22
Interface 5				8.60	28.6	0.320	-0.24
	Hastelloy X	10.0					
Cold Surface			400	7.80	28.6	0.320	2.32

TABLE 10. CALCULATED TEMPERATURES AND THERMAL STRESSES AT INTERFACES IN COATING SYSTEM 4

	Layer Composition, v/o	Thickness, mils	Interface Temperature, F	Coefficient of Thermal Expansion, 10^{-6}/F	Elastic Modulus, 10^6 psi	Poissons Ratio, ν	Z-Stress, 10^5 psi
			3870	7.15	12.8	0.275	-2.32
Hot Surface	ThO_2	3.5					
			1720	5.4	17.1	0.275	0.03
Interface 1				5.71	48.0	0.300	0.38
	BeO	2.0					
			1570	5.71	49.0	0.300	0.83
Interface 2				7.86	38.5	0.290	-0.98
	50 BeO 50 Type 304 stainless	2.0					
			1460	7.86	38.5	0.290	-0.63
Interface 3				8.93	33.0	0.285	-1.16
	75 Type 304 stainless 25 BeO	2.0					
			1440	8.93	33.0	0.285	-1.10
Interface 4				10.0	28.0	0.280	-1.25
	Type 304 stainless	2.0					
			1210	10.0	28.0	0.280	-0.66
Interface 5				10.6	28.0	0.280	-0.76
	Type 347 stainless	10.0					
Cold Surface			440	9.5	28.0	0.280	2.25

34296

FIGURE 1. TURBULENT FLOW D-C ARC PLASMA SPRAYING TORCH AND SPRAY CHAMBER

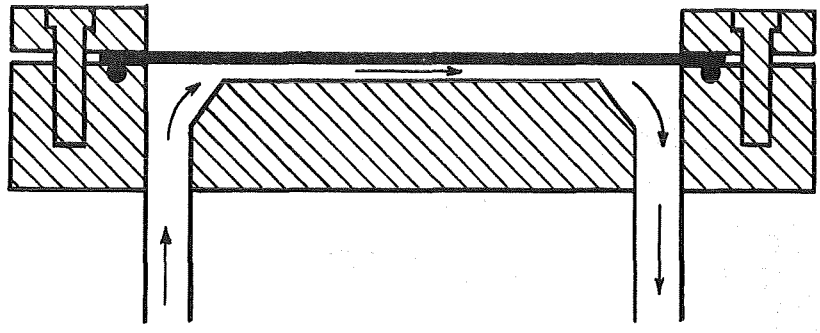

FIGURE 2. WATER-COOLED FIXTURE FOR PLASMA SPRAYING FLAT SPECIMENS

All substrates were prepared for coating by vapor blasting to obtain a roughened surface and were rinsed in water and ultrasonically cleaned in both trichlorethylene and ethyl alcohol. Surface roughnesses, in microinches rms, were measured with a Model BL110 Brush Surfindicator. Details of surface preparation are given in following sections. In all cases, coating thicknesses were determined by micrometer measurements taken at several locations both before and after coating deposition. Samples were examined metallographically for density and coating adhesion.

Spray powders used in this program were:

(1) Molybdenum: Plasmalloy 111-M, minus 200 plus 325 mesh

(2) Niobium: Atlantic Equipment Engineers, plasma-spray grade

(3) Type 304 stainless steel: Plasmalloy 213-M, minus 200 plus 325 mesh

(4) Hastelloy C: Plasmalloy 211-M, minus 200 plus 325 mesh

(5) Nichrome: Plasmalloy 207-M, nickel-20 w/o chromium, minus 200 plus 325 mesh

(6) Al_2O_3: Plasmalloy 331-M, minus 200 plus 325 mesh

(7) ZrO_2: Atlantic Equipment Engineers, fused, stabilized, plasma-spray grade

(8) HfO_2: Atlantic Equipment Engineers, fused, reactor plasma-spray grade, 99.9 percent, minus 150 plus 325 mesh

(9) ThO_2: Atlantic Equipment Engineers, high-density, fused, plasma-spray grade, TH-265

(10) BeO: Brush Beryllium Company, CGHF grade, minus 20 mesh (hot pressed and crushed before use – see below)

(11) NiAl: Atlantic Equipment Engineers, prealloyed, plasma-spray grade

(12) $TiBe_{12}$: synthesized at Battelle-Columbus.

With the exception of BeO, all materials were used in the as-received condition. Material blends were prepared by weighing appropriate amounts of the constituents into a polyethylene jar and mixing by rolling on ball-mill rolls.

From previous work it was known that the low density and extremely fine particle size of BeO made this material extremely difficult to plasma spray. Therefore, the coarsest grade of BeO commercially available (20 mesh) was ordered with the intention of crushing it to an appropriate size, such as minus 100 plus 200 mesh. However, the received material was found to consist of agglomerates of extremely fine particles, so no advantage was obtained with this material. Various attempts to plasma spray the as-received material met with little success. In one attempt an ultrahigh-velocity electrode insert was employed. While the insert did not solve the problems of plasma spraying of BeO, it was found to be helpful in spraying the highly refractory ThO_2, HfO_2, and ZrO_2. Accordingly, the ultrahigh-velocity insert was used throughout the remainder of the program for these materials; minor modification of spraying parameters permitted use of this insert to deposit the less-refractory metals and alloys as well.

The difficulties with BeO were resolved by in-house processing of the as-received material. Billets approximately 2 in. in diameter by 3 in. were hot pressed from the as-received material at 3000 F and 1000 psi. The hot-pressed billets were hand crushed and screened to minus 100 plus 200- and minus 200 plus 325-mesh size ranges. Both size ranges were found to be acceptable for plasma spraying, and hot-pressed, crushed, and sized BeO was used throughout the remainder of the program.

The final parameters for applying plasma-sprayed coatings to the specimens are listed in Table 11. These values are not to be considered as optimum since the development of optimized coating techniques in respect to density, adhesion, or efficiency for all the materials studied was not within the scope of the program. Table 12 lists the composition and thickness of the layers for the four types of specimens selected for rocket testing.

Substrate Tensile Strength

The dependence of substrate tensile strength on surface roughness and on heating occurring during application of plasma-sprayed coatings was investigated by two series of measurements. In the first series, the tensile strengths of uncoated substrates roughened to various degrees by vapor blasting and by dry grit blasting were determined. The second series involved specimens all roughened to the same degree, but coated with various plasma-sprayed materials and material systems. For both series of measurements, 3 by 5 by 0.010-in. coupons of annealed Type 347 stainless steel or Hastelloy X were machined to form three specimens from each coupon. Final specimen dimensions were 5 by 0.75 by 0.010 in., with a 2.5-in.-long central section reduced to a 0.50-in. width.

For the first series of tests, substrates were roughened to nominal roughnesses of 5, 25, 30, and 50 μ in. rms by vapor blasting with silica grit at 0, 20, 50, and 95 psig, respectively. A few additional substrates were roughened to 150 μ in. rms by dry grit blasting at 30 psig, but were deformed appreciably. Effects of distortion on tensile strips as a result of roughening are shown in Figure 3. Attainment of greater surface roughness was impractical with a fine-particle-size blasting media because the thin substrates were severely deformed at high blasting pressures. In addition, defects caused by roughening above 50 μ in. rms would reduce the strength of the substrate. For example, surface roughness above 60 μ in. rms requires minus 120-mesh grit, which contains particles having sizes up to 0.0049 in. At blasting pressures of 50 psi these particles would introduce defects up to 0.003 in. deep in the 0.010-in. material.

TABLE 11. PLASMA-SPRAYING PARAMETERS[a] FOR COATING SYSTEMS SELECTED FOR ROCKET TESTS

	Coating System 1					Coating System 2				
	Layer 1	Layer 2	Layer 3	Layer 4	Layer 5	Layer 1	Layer 2	Layer 3	Layer 4	Layer 5
Current, amps	300	400	500	600	700	300	500	550	600	700
Arc-Gas Pressure, psig	100	100	100	100	100	100	100	100	100	100
Arc-Gas Flow, cfm	0.92	0.65	0.65	0.65	0.65	0.92	0.65	0.65	0.65	0.65
Powder-Gas Pressure, psig	50	50	50	50	50	50	50	50	50	50
Powder-Gas Flow, cfm	0.19	0.14	0.10	0.09	0.08	0.17	0.12	0.11	0.14	0.16
Powder Feeder Setting	20	20	20	20	20	20	20	20	20	20
Spraying Distance, in.	3	3	3	2	2	3	3	3	1	3
Nominal Layer Thickness, in.	0.002	0.002	0.002	0.002	0.003	0.002	0.003	0.003	0.003	0.003
	Coating System 3					Coating System 4				
	Layer 1	Layer 2	Layer 3	Layer 4	Layer 5	Layer 1	Layer 2	Layer 3	Layer 4	Layer 5
Current, amps	650	650	650	650	700	400	450	500	650	700
Arc-Gas Pressure, psig	100	100	100	100	100	100	100	100	100	100
Arc-Gas Flow, cfm	0.65	0.65	0.65	0.65	0.65	1.00	0.92	0.65	0.65	0.65
Powder-Gas Pressure, psig	50	50	50	50	50	50	50	50	50	50
Powder-Gas Flow, cfm	0.16	0.19	0.19	0.13	0.10	0.20	0.16	0.16	0.14	0.16
Powder Feeder Setting	20	20	20	20	20	10	10	10	20	20
Spraying Distance, in.	3	3	2	1	3-4	4-5	3-4	1	1	3
Nominal Layer Thickness, in.	0.002	0.002	0.003	0.003	0.0035	0.002	0.002	0.002	0.002	0.0035

(a) All coatings were plasma sprayed in dry argon using an ultrahigh-velocity spray gun. Substrates were cooled by direct contact with flowing water at 60 psig on the back of the substrate. Commercial plasma-spray-grade materials were used except for BeO, which was hot pressed and crushed to minus 100 plus 200 mesh.

TABLE 12. COMPOSITION OF COATING SYSTEMS SELECTED FOR ROCKET TESTING

Coating System	Layer		Nominal Composition, v/o	Actual Composition of Blend, w/o[a]	Nominal Thickness, mils
1	5	ThO_2	100	100	3.0
	4	ThO_2/Nb	90/10	90/10	2.0
	3	ThO_2/Nb/Hastelloy C	45/5/50	48/4.5/47.5	2.0
	2	ThO_2/Nb/Hastelloy C	18/2/80	20/1/79	2.0
	1	Hastelloy C	100	100	2.0
	Substrate	Hastelloy X	--	--	10.0
2	5	ZrO_2/ThO_2	50/50	35/65	3.0
	4	BeO	100	100	3.0
	3	BeO/Hastelloy C	50/50	35/65	3.0
	2	BeO/Hastelloy C	20/80	15/85	3.0
	1	Hastelloy C	100	100	2.0
	Substrate	Hastelloy X	--	--	10.0
3	5	HfO_2	100	100	3.5
	4	BeO	100	100	3.0
	3	BeO/$TiBe_{12}$	50/50	65/35	3.0
	2	BeO/$TiBe_{12}$	20/80	50/50	2.0
	1	$TiBe_{12}$	100	100	2.0
	Substrate	Hastelloy X	--	--	10.0
4	5	ThO_2	100	100	3.5
	4	BeO	100	100	2.0
	3	BeO/Type 304 stainless	50/50	40/60	2.0
	2	BeO/Type 304 stainless	25/75	20/80	2.0
	1	Type 304 stainless	100	100	2.0
	Substrate	Type 347 stainless	--	--	10.0

(a) As formulated; as-deposited compositions were not determined.

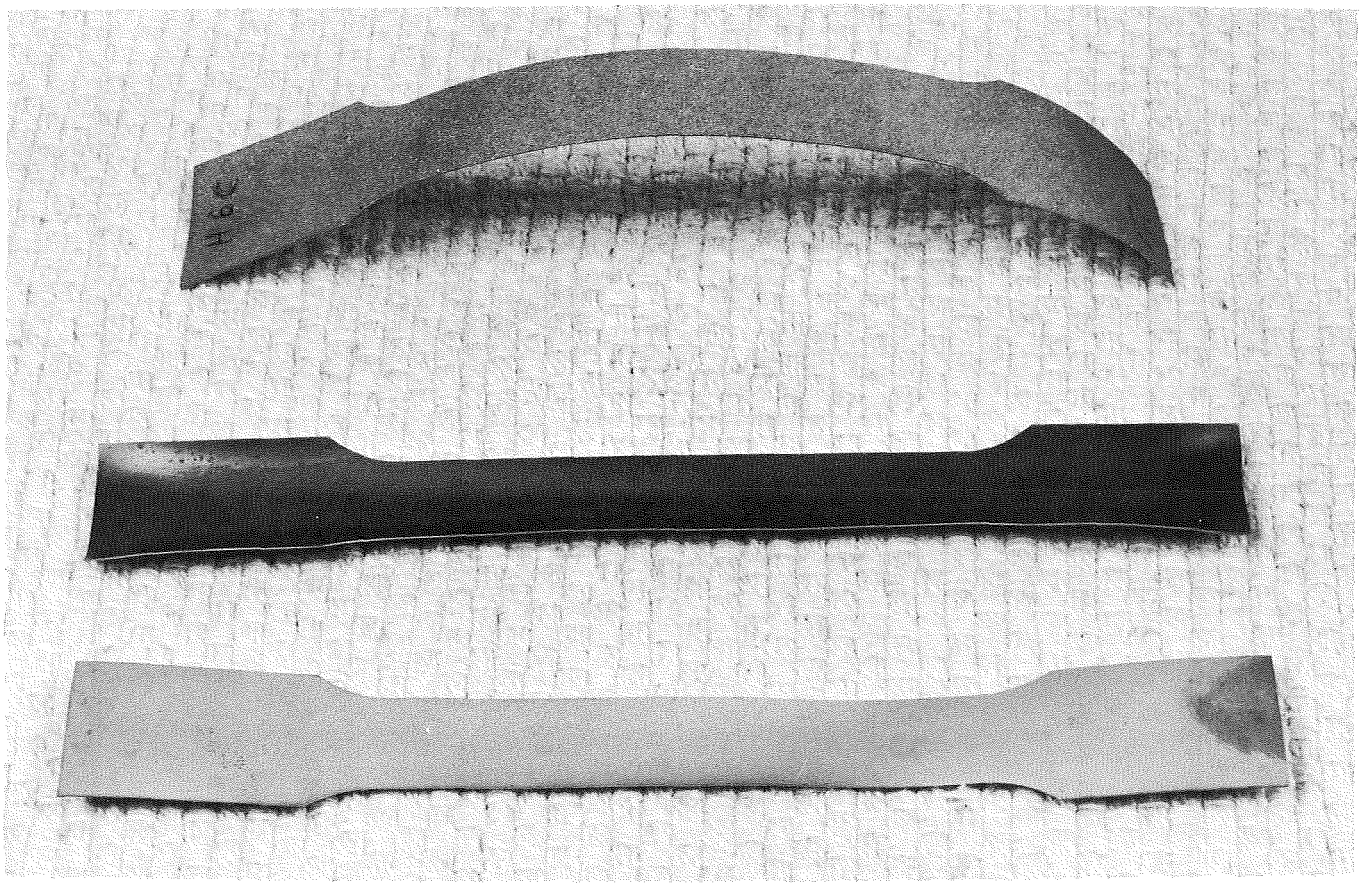

FIGURE 3. DEFORMATION OF SUBSTRATES AS A RESULT OF ROUGHENING

Top: Dry-grit blasted on both sides at 12-inch distance, 30-psi pressure. Surface roughness of 150 μin. rms.

Middle: Vapor blasted on one side at 4-inch distance, 95-psi pressure. Surface roughness of 55 μin. rms.

Bottom: Vapor blasted on both sides at 4-inch distance, 95-psi pressure. Surface roughness of 55 μin. rms.

Although it could not be eliminated, distortion was reduced somewhat by roughening both sides of the substrates.

Tensile tests were conducted at a loading rate (crosshead speed) of 0.2 in. per min using a 1-in. extensometer. The high rate was used to minimize testing time and costs, and did not impair reproducibility of measured values. Ultimate strength was calculated by dividing load at fracture by the initial cross-sectional area. Yield stress and elastic modulus were determined from the recorded stress/strain curve. Elongation was estimated from the initial and final specimen lengths. Since the gripped ends were not deformed during testing but were included in length measurements, reported elongation values are somewhat low, although they are adequate for purposes of comparison. Results of tensile strength measurements are given in Tables 13 and 14.

Vapor blasting at pressures of 50 psig or less had little effect on ultimate strength, yield strength, or ductility, but decreased elastic modulus by up to about 20 percent. Vapor blasting at higher pressures and dry-grit blasting at even low pressures severely deformed the substrates, introduced defects, resulted in work hardening, and caused appreciable reduction in ductility. On the basis of these measurements, all substrates subsequently prepared during the course of this program were roughened by vapor blasting at a pressure not more than 50 psig.

Each 3 by 5 by 0.010-in. substrate coupon for the second series of tests was roughened to approximately 30 μ in. rms by vapor blasting at 50 psi and was ultrasonically cleaned in both trichlorethylene and absolute ethyl alcohol. The uncoated substrate thickness was measured and the coupon was plasma sprayed in the water-cooled jig shown in Figure 2 using the spraying parameters listed in Table 11. Three tensile specimens of the size and configuration described above were machined from each coupon. Before tensile testing, some specimens were used for coating bond-strength measurements (as described in the next section). The absence of coating in localized areas was thought to have no detectable effect on the values relative to those of the substrate, and all coating material flaked off the substrate during tensile testing.

Specimens were sealed in plastic bags to prevent release of BeO and ThO_2 dust to the open air. Because this precaution prevented use of an extensometer to measure strain, yield strength and elastic-modulus data were not obtained. As before, a strain rate (crosshead speed) of 0.20 in. per min was used. Ultimate strength was calculated by dividing load at fracture by the initial cross-sectional area of the uncoated substrate, and the percent elongation was estimated from the change in overall specimen length.

Results of this series of measurements, listed in Table 15 showed that the thermal environment imposed during deposition of plasma-sprayed coatings had the general effect of decreasing the tensile strength and ductility of the substrate material by a relatively small amount. While in no case did the substrate strength loss exceed 15 percent, substrate strength losses for Systems 2, 3, and 4 were five to six times that for the System 1 substrate. This result implied that the System 1 coating resulted in a lower substrate temperature and, hence less decrease in substrate strength.

TABLE 13 TENSILE PROPERTIES OF ANNEALED AND VAPOR-BLASTED HASTELLOY X UNCOATED SUBSTRATES

Specimen	Vapor-Blast Pressure, psig	Roughness, microinches	Area, 10^{-5} in.^{2}	Ultimate Strength, 10^3 psi	0.2 Percent Offset Yield Strength, 10^3 psi	Elastic Modulus, 10^6 psi	Estimated Elongation, percent	Averages (Same Units)	
H1A	0	5-6	525	108.19	--	--	16.2	U. S.	110.25
B	0	7	530	110.00	48.9	24.6	17.4	Y. S.	48.8
C	0	5-6	519	110.79	49.6	24.6	17.8	E. M.	25.5
								E.	17.6
H2A	0	5-6	524	110.69	48.2	25.8	18.4		
B	0	5-6	524	111.07	49.1	24.6	16.8		
C	0	5-6	520	110.77	48.1	27.9	17.8		
H3A	50	25	535	107.48	48.6	20.5	17.6	U. S.	110.23
B	50	25	530	108.87	47.8	19.8	18.6	Y. S.	49.2
C	50	25	524	90.08	47.4	20.3	8.6	E. M.	19.6
								E.	18.3
H4B	50	25	510	113.14	52.4	18.6	18.4		
C	50	25	525	111.43	51.0	18.6	18.4		
H5A	95	50	525	96.19	59.0	17.6	12.2	U. S.	97.17
B	95	55	530	93.02	54.4	15.1	13.0	Y. S.	56.7
C	95	55	519	102.31	--	--	17.6	E. M.	16.4
								E.	14.3
H6A	30[a]	150	515	118.00	89.4	26.6	9.4	U. S.	122.27
B	30[a]	150	514	127.43	97.5	24.2	8.4	Y. S.	93.5
C	30[a]	150	519	121.39	--	--	10.6	E. M.	25.4
								E.	9.5
H9A	20	30	516	113.37	49.4	21.4	17.0	U. S.	111.15
B	20	30	530	112.83	49.1	21.0	17.6	Y. S.	48.5
C	20	25-30	520	111.54	--	--	16.2	E. M.	21.4
								E.	17.8
H10A	20	25-30	520	108.08	47.5	19.9	20.4		
B	20	25	511	109.98	--	--	17.0		
C	20	25	500	111.07	47.8	23.4	18.4		

(a) Dry-grit blasted at 30 psig.

TABLE 14. TENSILE PROPERTIES OF ANNEALED AND VAPOR-BLASTED TYPE 347 STAINLESS STEEL UNCOATED SUBSTRATES

Specimen	Vapor-Blast Pressure, psig	Roughness, microinches	Area, 10^{-5} in.^{2}	Ultimate Strength, 10^3 psi	0.2 Percent Offset Yield Strength, 10^3 psi	Elastic Modulus, 10^6 psi	Estimated Elongation, percent	Averages (Same Units)	
S1A	0	5-6	530	96.60	40.5	22.0	28.6	U. S.	98.42
B	0	5-6	519	98.26	40.5	21.9	28.0	Y. S.	41.3
C	0	5-6	520	97.50	40.8	25.4	28.0	E. M.	24.1
								E.	26.2
S2A	0	6-7	545	99.08	41.6	22.5	24.4		
B	0	6	530	99.06	42.5	23.6	24.4		
C	0	5-6	525	100.00	42.0	29.6	24.4		
S3A	50	30-35	515	100.97	45.6	15.8	22.6	U. S.	100.49
B	50	30-35	540	99.07	42.0	19.5	26.4	Y. S.	43.1
C	50	35	515	100.97	44.1	19.4	22.6	E. M.	18.7
								E.	24.9
S4A	50	25	520	100.97	41.4	18.0	26.0		
B	50	25	519	101.16	43.5	19.8	25.6		
C	50	25	535	99.81	42.1	19.7	26.0		
S5A	95	50	516	99.47	54.8	18.4	14.0	U. S.	97.08
B	95	50	505	99.01	53.3	21.2	17.8	Y. S.	53.7
C	95	30	525	100.76	43.0	20.2	22.4	E. M.	19.9
								E.	18.1
S6A	30[a]	150	535	107.48	42.0	9.5	13.2	U. S.	111.66
B	30[a]	150	524	115.84	--	7.5	8.2	Y. S.	42.0
								E. M.	8.5
								E.	10.7
S9A	20	40	547	96.53	44.8	13.7	22.0	U. S.	98.22
B	20	35-40	542	98.15	44.4	17.8	22.8	Y. S.	43.7
C	20	35-40	547	96.34	46.3	11.9	23.4	E. M.	15.8
								E.	23.6
S10A	20	30-35	521	98.08	43.2	19.3	24.0		
B	20	40	516	98.84	44.5	13.5	25.0		
C	20	35	511	101.37	38.8	18.5	24.2		

(a) Dry-grit blasted at 30 psig.

TABLE 15. TENSILE STRENGTH AND ELONGATION OF PLASMA-SPRAYED SUBSTRATES

Coating[a]	Number of Specimens	Average Tensile Strength, psi	Average Strength Loss, percent	Average Estimated Elongation, percent
		Hastelloy X Substrates		
(Reference)	4	110,230	0	18.3
System 1	4	108,280	1.8	16.5
System 2	4	100,460	8.9	17.6
System 3	4	96,470	12.5	16.2
		Type 347 Stainless Steel Substrates		
(Reference)	4	100,490	0	24.9
Type 304 stainless	4	94,150	6.3	23.2
System 4	4	84,050	14.1	24.1

(a) Reference specimens were uncoated substrates previously measured (Tables 13 and 14). The geometry, size, annealing procedure, vapor-blasting pressure, and testing strain rate were identical for coated specimens and corresponding reference specimens.

It may be noted (Table 12) that BeO and BeO blends constituted over half the total coating thickness for all coating systems except System 1, which contained no BeO. Since the room-temperature thermal conductivity of BeO is roughly 10 times that of $TiBe_{12}$ and 20 times that of ThO_2*, the overall thermal conductivity of System 1 may be expected to be lower than that for any other system under consideration. However, calculations made in connection with coating system selection indicated substrate interface temperatures of 1200 to 1250 F and temperature gradients across the entire coating of 2660 to 2840 F for all coating systems. The calculated differences among the various systems seem insufficient to account for the differences in substrate strength loss. The validity of these and other calculations is open to question, however, on the basis that, while accurate data are available on the properties of conventionally prepared materials, little is known of the effect of plasma spraying on material properties or of the actual property values for plasma-sprayed deposits. The discrepancy between calculated and actual property values of plasma-sprayed materials was clearly demonstrated by a 20-fold difference between calculated and measured values of thermal diffusivity for Coating System 4. (These measurements will be discussed below.)

An alternate explanation for the high strength of substrate coated with System 1 is that, while the thermal conductivity of the coating itself was not grossly different from that of other systems, the effective coating/substrate interface conductivity was lower than for the other coating systems. The very low bond strength found for System 1, as discussed in the next section, seems to support this explanation in that a low conductivity would result from a poor bond.

In consideration of the above discussion and on the basis of available information, it may be stated with confidence only that application of the particular coating systems deposited under the conditions employed in this program resulted in substrate strength losses on the order of 10 percent, except for Coating System 1, for which the substrate strength loss was very minor. Further study to arrive at a complete and satisfactory explanation for the low strength loss of System 1 substrates was beyond the scope of this program.

*Based on values for dense polycrystalline materials: J. F. Lynch, C. G. Ruderer, W. H. Duckworth, "Engineering Properties of Ceramics", AFML-TR-66-52 (June, 1966).

Coating Bond Strength

The purpose of this work was threefold: (1) to estimate the general level of coating-substrate bond strength of plasma-sprayed coating, (2) to establish the general degree of dependence of coating bond strength on substrate surface roughness, and (3) to determine the approximate bond strength of candidate coating materials.

Experiments to achieve the first two of the above objectives were conducted concurrently with materials selection efforts, and, therefore, employed coating materials of the general types expected to be selected for the candidate coating systems. Materials used in this first series of measurements of coating bond strength were ZrO_2, Al_2O_3, 75 v/o NiAl-25 v/o ZrO_2, and ZrO_2 applied over underlayers of various metals or NiAl. Bond strengths of candidate coating systems were measured later in a second series of tests conducted after these systems had been selected. Substrate preparation, plasma spraying, and bond-strength testing procedures were substantially as described below in all cases; modifications in the procedures will be noted where appropriate in later discussions.

In all cases, 3 by 5 by 0.010-in. Hastelloy-X or Type 347 stainless steel substrates were roughened by vapor blasting and ultrasonically cleaned in both trichlorethylene and absolute ethyl alcohol. After measurement of thickness and surface roughness, substrates were clamped in the direct-contact water-cooled fixture shown in Figure 2 and plasma-spray coated using the spraying parameters established for each material. Coated substrates were cut and/or machined to desired dimensions, abraded on the uncoated side, and washed with acetone. A stainless steel tensile rod, 5/16 in. in diameter by ~2 in. long was cemented to the coating, and a second identical rod was cemented to the uncoated side of the substrate directly opposite and in alignment with the first. Cementing was accomplished by placing a small coupon of FM-1000 film adhesive between the surface to be joined, holding the assembly together under a light clamping pressure, and curing the adhesive for 1 hr at 300 to 350 F. This adhesive was selected for high strength and lack of penetration into the coating. Figure 4 shows a specimen assembly in place in the testing machine. The upper tensile rod was held in the stationary chuck of a universal testing machine and the lower rod was connected to the movable crosshead by a wire-mesh strap looped over a tool-steel pin inserted through the tensile rod. This arrangement minimized shear stresses by permitting the specimen to align itself in the testing machine. All specimens were tested to fracture at a crosshead speed of 0.010 in./min; this rapid testing rate was considered adequate for obtaining comparative values of coating bond strength. Blank tests indicated a tensile strength of 3000 to 4000 psi for the adhesive under the conditions used for application and testing.

Specimens failed by the fracture modes depicted in Figure 5 or by combinations of these. The exact location of fractures could not be accurately determined for specimens of the multilayer candidate coating systems; fractures are reported as occurring within the coating (Type 6 fracture) or at the substrate (Type 5 fracture). Many fracture surfaces were curved (Types 3, 4, and 6) or extended slightly beyond the edges of the tensile rods, but the approximate data desired did not justify efforts to measure the exact fracture area. Accordingly, fracture strengths were calculated by dividing the tensile load at fracture by the cross-sectional area of the tensile rod. This approximation, together with the variety of fracture modes and the small number of specimens, resulted in scattered and somewhat inconclusive data, particularly for the first series of specimens.

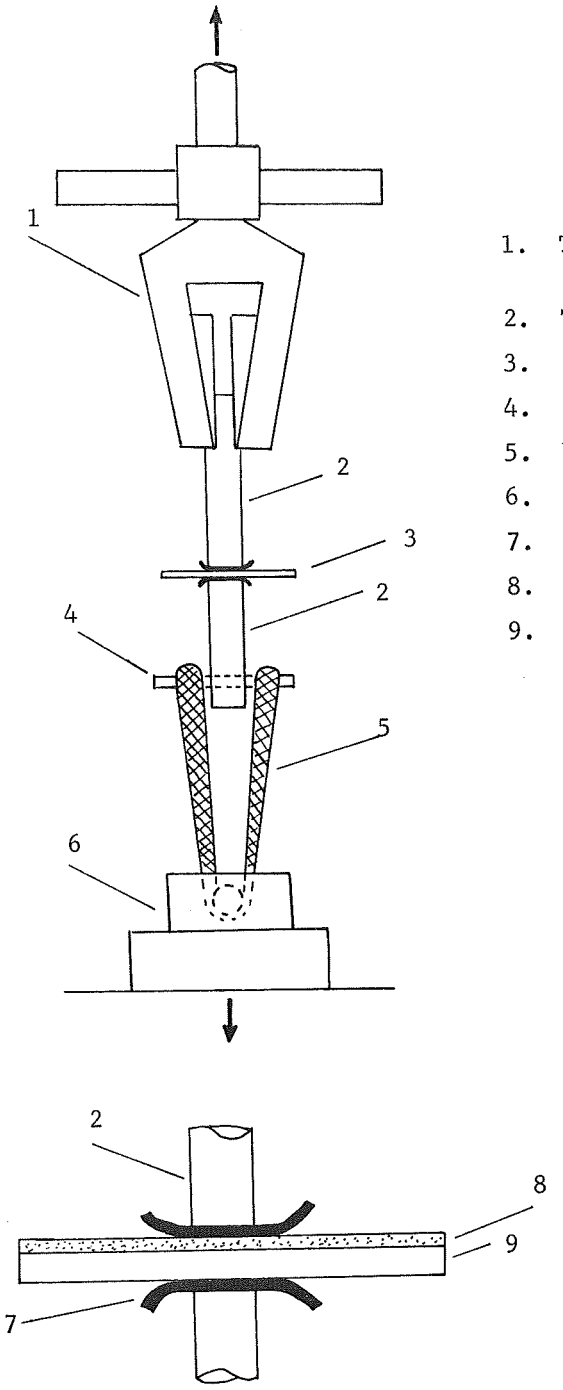

1. Testing Machine Stationary Chuck
2. Tensile Rod
3. Specimen
4. Pin
5. Wire Mesh Strap
6. Testing Machine Crosshead
7. Film Adhesive
8. Plasma-Sprayed Coating
9. Substrate

Detail of Specimen

FIGURE 4. TESTING ARRANGEMENT FOR BOND STRENGTH MEASUREMENTS

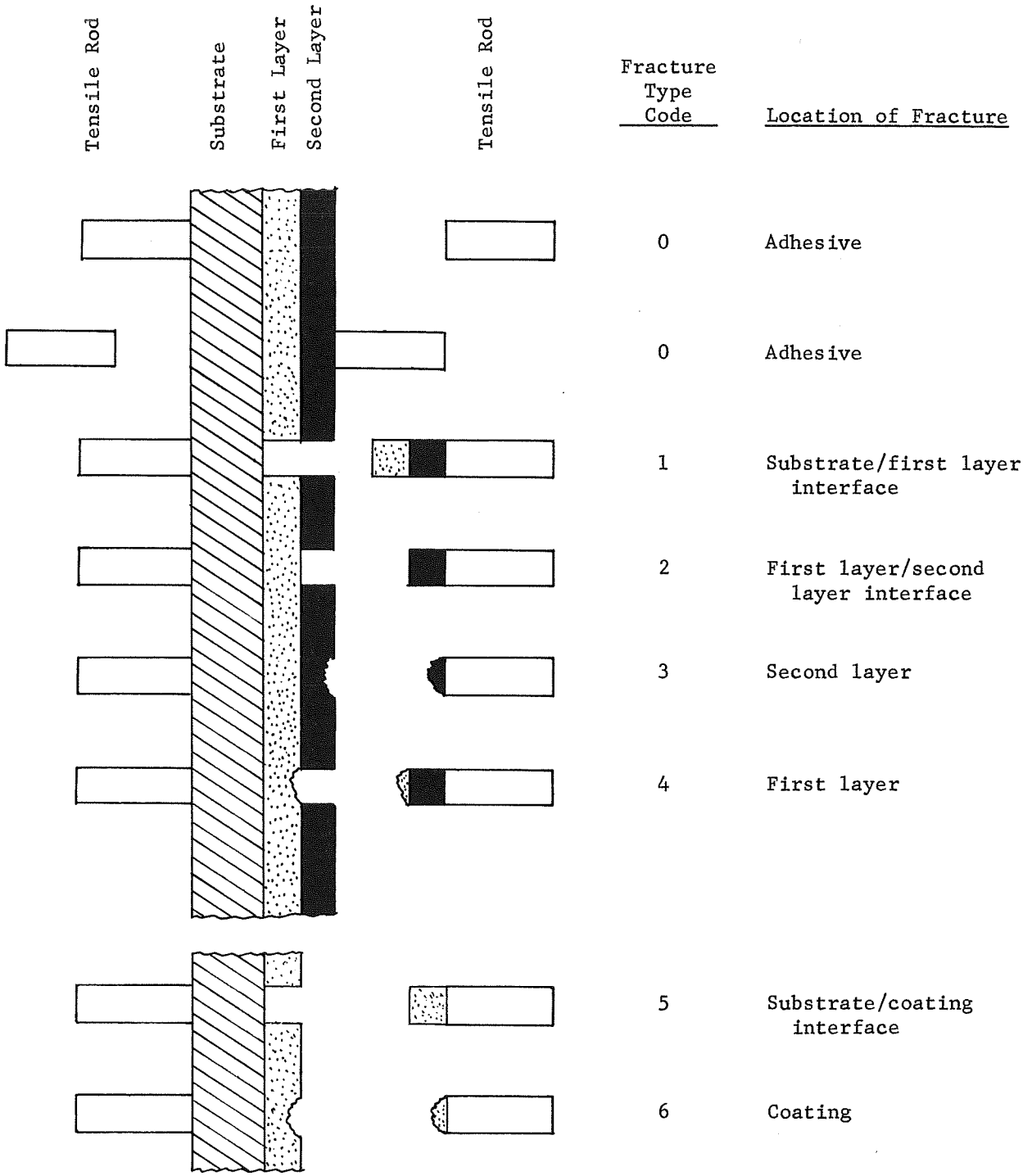

FIGURE 5. TYPES OF COATING FRACTURE

TABLE 16. CHARACTERIZATION AND COATING BOND STRENGTH OF HASTELLOY-X SPECIMENS

Specimen	Surface Roughness, microinches (rms)	Coating-1 Thickness, mils	Coating-2 Thickness, mils	Strength, psi	Type Fracture
H-1A	18	ZrO_2 (5.1)	--	665	4
H-1B	45	ZrO_2 (5.1)	--	795	4
H-2A	28	ZrO_2 (4.9)	--	1030	4
H-2B	50	ZrO_2 (4.9)	--	1300	4
H-3A	20	NiAl (2.7)	ZrO_2 (2.8)	1260/1680	2,3/1,3
H-3B	45	NiAl (2.7)	ZrO_2 (2.8)	1650	2,3
H-4A	28	NiAl (2.7)	ZrO_2 (3.5)	2735	1,2
H-4B	53	NiAl (2.7)	ZrO_2 (3.5)	815	2
H-5A	20	Hastelloy C (3.4)	ZrO_2 (2.8)	1190	1
H-5B	42	Hastelloy C (3.4)	ZrO_2 (2.8)	975	2,3
H-6A	25	Hastelloy C (3.2)	ZrO_2 (3.3)	780	2
H-6B	50	Hastelloy C (3.2)	ZrO_2 (3.3)	885/1590	3/2
H-7A	20	75 v/o NiAl, 25 v/o ZrO_2 (5.6)	--	2510	4
H-7B	42	75 v/o NiAl, 25 v/o ZrO_2 (5.6)	--	2290	4,5
H-8A	28	75 v/o NiAl, 25 v/o ZrO_2 (5.6)	--	1600	4
H-8B	52	75 v/o NiAl, 25 v/o ZrO_2 (5.6)	--	2940	4
H-9A	20	Mo (2.1)	ZrO_2 (3.2)	585	2,3
H-9B	45	Mo (2.1)	ZrO_2 (3.2)	770	2
H-10A	25	Mo (2.8)	ZrO_2 (2.9)	665	2
H-10B	55	Mo (2.8)	ZrO_2 (2.9)	890	2
H-11A	17	Nichrome (2.8)	ZrO_2 (3.6)	850	3
H-11B	45	Nichrome (2.8)	ZrO_2 (3.6)	1550	1,3
H-12A	28	Nichrome (2.2)	ZrO_2 (3.8)	1485	3
H-12B	55	Nichrome (2.2)	ZrO_2 (3.8)	815/1210	2,3/2,3

TABLE 17. CHARACTERIZATION AND COATING BOND STRENGTH OF TYPE 347 STAINLESS STEEL SPECIMENS

Specimen	Surface Roughness, microinches (rms)	Coating 1 Thickness, mils	Coating-2 Thickness, mils	Strength, psi	Type Fracture
S-1A	20	ZrO_2 (4.7)	--	515	4
S-1B	45	ZrO_2 (4.7)	--	430	4
S-2A	30	ZrO_2 (3.9)	--	525	4
S-2B	53	ZrO_2 (3.9)	--	870	4
S-3A	17	NiAl (2.2)	ZrO_2 (2.9)	895	2
S-3B	45	NiAl (2.2)	ZrO_2 (2.9)	2470	1,2
S-4A	32	NiAl (2.0)	ZrO_2 (3.3)	1390	3
S-4B	52	NiAl (2.0)	ZrO_2 (3.3)	1195	3
S-5A	20	304 stainless steel (2.2)	ZrO_2 (3.4)	870	2,3
S-5B	45	304 stainless steel (2.2)	ZrO_2 (3.4)	350	3
S-6A	30	304 stainless steel (2.8)	ZrO_2 (3.8)	655	2,3
S-6B	52	304 stainless steel (2.8)	ZrO_2 (3.8)	1260	2
S-7A	18	75 v/o NiAl, 25 v/o ZrO_2 (7.7)	--	310	4
S-7B	45	75 v/o NiAl, 25 v/o ZrO_2 (7.7)	--	1430	4
S-8A	30	75 v/o NiAl, 25 v/o ZrO_2 (4.4)	--	1270	4
S-8B	55	75 v/o NiAl, 25 v/o ZrO_2 (4.4)	--	>2560	4
S-9A	18	Mo (2.1)	ZrO_2 (3.5)	640	2
S-9B	45	Mo (2.1)	ZrO_2 (3.5)	1050	2
S-10A	32	Mo (1.9)	ZrO_2 (3.6)	1235	2
S-10B	50	Mo (1.9)	ZrO_2 (3.6)	940	2
S-11A	18	Nichrome (2.8)	ZrO_2 (3.5)	570	2,3
S-11B	45	Nichrome (2.8)	ZrO_2 (3.5)	730	2,3
S-12A	32	Nichrome (2.8)	ZrO_2 (3.5)	645	2
S-12B	50	Nichrome (2.8)	ZrO_2 (3.5)	675	2,3

The initial series of bond-strength measurements employed coatings applied to substrates roughened to nominal values of 20, 27, 45, and 55 μ in. rms by vapor blasting at pressures of approximately 20, 30, 70, and 95 psig, respectively. A few substrates were roughened to values as high as 130 μ in. rms by dry grit blasting at 30 psig. Results of this series of bond-strength measurements are given in Tables 16, 17, and 18 and Figures 6 and 7. Although data were scattered, a general trend toward increasing bond strength with increasing surface roughness was discernible. That this tendency persisted even in two-layer coatings which fractured at locations other than the coating-substrate interface suggested that the effect of substrate surface roughness may be carried through to the second coating layer.

TABLE 18. CHARACTERIZATION AND FRACTURE STRENGTH OF PLASMA-SPRAYED ALUMINUM OXIDE COATINGS

Specimen	Surface Roughness, microinches	Applied Force, lb	Strength, psi	Type Fracture
		Hastelloy-X Substrates		
H-3A-A[a]	10	3.7	~2.8[c]	4
H-3B-A[b]	10	0.9	~0.6[d]	4
H-1B-A	30	52.5	680	5
H-2B-A	125	63.5	825	4
		Type 347 Stainless Steel Substrates		
S-1B-A	20	43	560	4,5
S-1A-A	30	42	545	4,5
S-2A-A	80	32	415	4
S-4B-A	110	32	415	5
S-4A-A	130	32	415	5

(a) Washed in alcohol before coating.
(b) Ultrasonically cleaned in trichlorethylene before coating.
(c) Coating stripped off in large sheet. Area of coating removed ~1.3 square inches.
(d) Coating stripped off in large sheet. Area of coating removed ~1.6 square inches.

On the basis of six fractures occurring wholly within a ZrO_2 layer, the cohesive strength of plasma-sprayed ZrO_2 was estimated to be 1030 psi. Average values of 940 and 950 psi were obtained for the 13 fractures at ZrO_2-underlayer interfaces and for the 30 fractures partially in the ZrO_2 layer and partially at ZrO_2-underlayer interfaces, respectively. The similarity of these values to each other and to the indicated cohesive strength of ZrO_2 suggested that fractures at ZrO_2-underlayer interfaces may have resulted from ZrO_2 failure at or very near the interface.

The fracture strength of ZrO_2 deposited over metallic undercoatings was not closely dependent on the type of undercoating, and strengths of these double-layer coatings were not consistently or markedly different from that of ZrO_2 applied directly to a substrate. However, both single- and double-layer coatings incorporating NiAl with ZrO_2 had significantly greater strengths, as high as 3000 psi. The self-bonding nature of NiAl was thought to give it high cohesive strength and to help bond ZrO_2 grains to each other. The improved bond to the substrate may have been due to the as-sprayed properties of the NiAl being intermediate between those of the substrate and those of the ZrO_2.

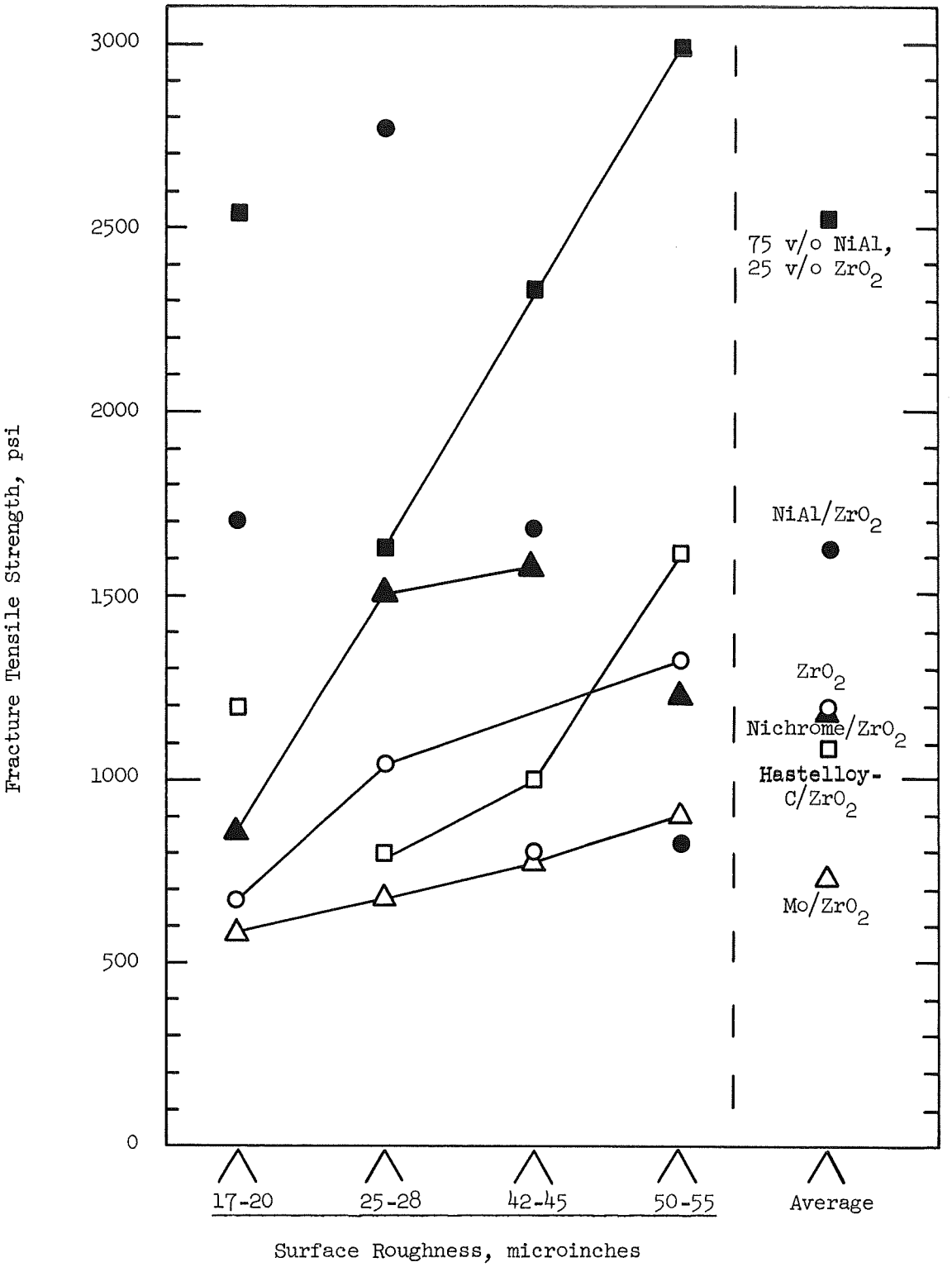

FIGURE 6. EFFECT OF ROUGHNESS AND COATING SYSTEM ON STRENGTH OF SPECIMENS WITH HASTELLOY-X SUBSTRATES

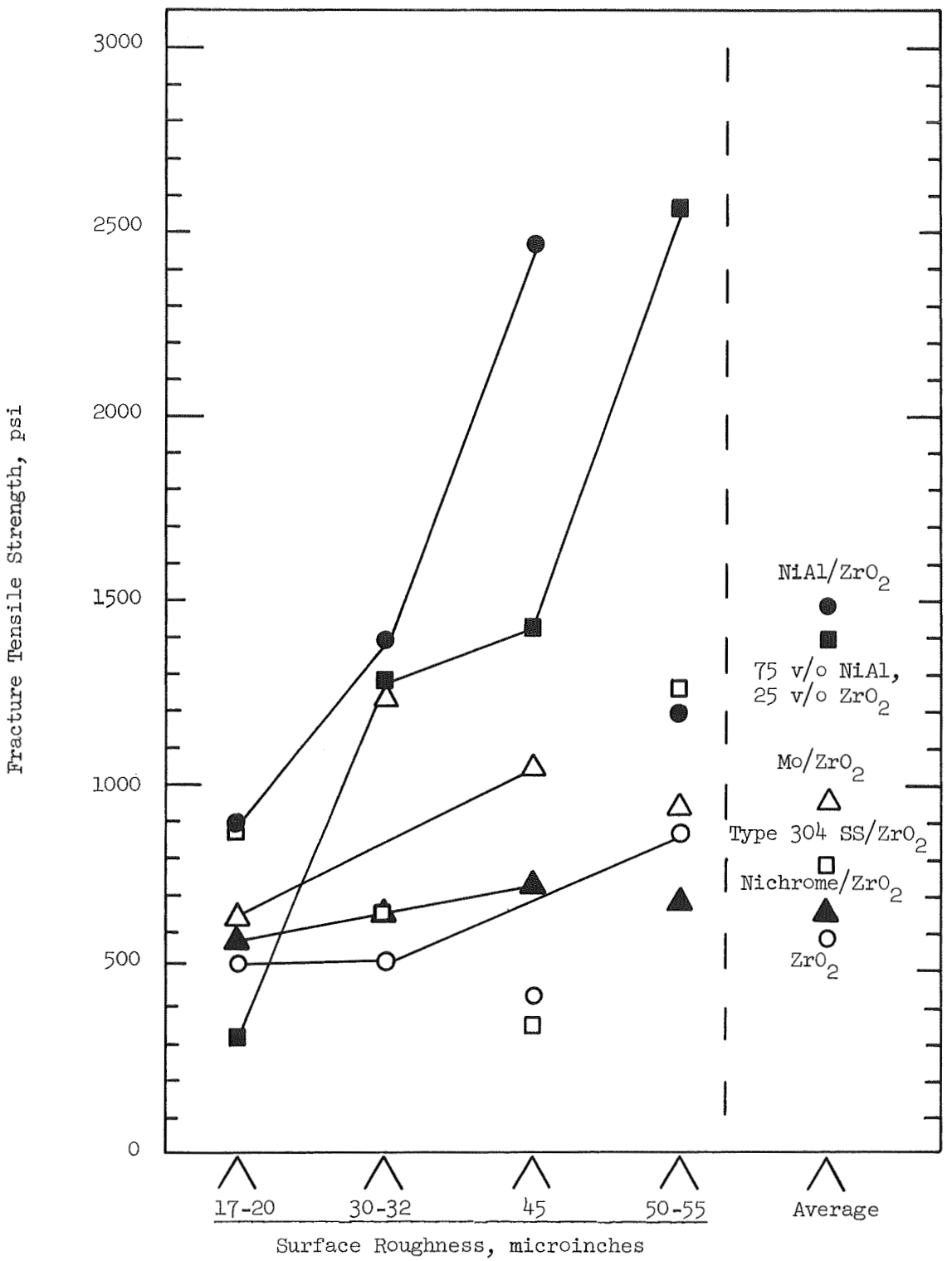

FIGURE 7. EFFECT OF ROUGHNESS AND COATING SYSTEM ON STRENGTH OF SPECIMENS WITH TYPE 347 STAINLESS STEEL SUBSTRATES

Specimens for the second series of bond-strength measurements were prepared and tested according to the procedures discussed above, except that all substrates were vapor blasted at 50 psig. This blasting pressure was selected as the highest practical value which did not cause appreciable substrate deformation; surface roughnesses of approximately 30 μ in. rms were obtained. Substrates were cleaned and coated as already discussed. Coated substrates were machined into tensile specimens so that coating bond strength and tensile strength of coated substrates could be determined on the specimens. After coating bond strengths were measured, substrates were pulled to failure, as discussed above.

Results of bond-strength measurements for the four candidate coating systems and for single layers of plasma-sprayed Hastelloy X and Type 304 stainless steel are summarized in Table 19; average values of bond strengths determined in the first series of measurements are included for comparison.

TABLE 19. BOND STRENGTHS OF PLASMA-SPRAYED COATINGS

Coating	Quantity Tested	Quantity in Average[a]	Average Coating Bond Strength, psi	Location of Fracture[b]
		Second Series of Measurements[c]		
Type 304 stainless[d]	8	4	4130	Substrate
Hastelloy C	4	2	3870	Substrate
System 1	4	4	760	Substrate
System 2	4	4	1330	Coating
System 3	4	4	1385	Coating
System 4[d]	6	2	3985	Coating
		First Series of Measurements[e]		
ZrO_2 over molybdenum	4	4	730	Coating
ZrO_2	4	4	950	Substrate
ZrO_2 over Hastelloy C	5	5	1085	Coating
ZrO_2 over Nichrome	5	5	1180	Coating
ZrO_2 over NiAl	5	5	1630	Coating
75 v/o NiAl-25 v/o ZrO_2	4	4	2335	Substrate
Al_2O_3	5	5	470	Coating/substrate

(a) Specimens tested but not included in average are those for which failure occurred in the adhesive without fracture of the coating.

(b) "Substrate" denotes failure at the coating-substrate interface which exposed a bare substrate. "Coating" fractures are those which occurred elsewhere in the coating system.

(c) Hastelloy X substrates roughened to ~30 μin. rms by vapor blasting at 50 psig.

(d) Type 347 stainless steel substrates roughened to ~30 μin. rms by vapor blasting at 50 psig.

(e) Hastelloy X substrates roughened to 17 to 55 μin. rms (cf. Table 16).

(f) Type 347 stainless steel vapor blasted or dry grit blasted to roughnesses of 20 to 130 μin. rms (cf. Table 18).

Single layers of Hastelloy C and Type 347 stainless steel formed bonds of approximately 4000 psi with the substrate materials. In all cases, complete coating systems fractured at lower stress levels and in most cases failure appeared to occur within a

single layer rather than at layer interfaces. These observations indicated that the cohesive strength for at least one of the four outermost layers of the coating system was appreciably less than the strength of the first layer-substrate bond. System 1 was an exception in that all fractures occurred at the first layer-substrate interface. This result was inconsistent because the bond strength of the first layer alone was five times that of the first layer when it was incorporated into the complete five-layer coating system. Moreover, even though the first layer, the plasma-spraying parameters for the first layer, the substrate, and the substrate preparation were identical for Systems 1 and 2, System 2 fractures occurred within the coating and at stress levels nearly twice those sufficient to cause fracture at the first layer-substrate interface of System 1. Comparison of coating system compositions (Table 12) and plasma-spraying parameters (Table 11) indicates that, even though the compositions of Systems 1 and 2 were somewhat different, the parameters used for plasma spraying corresponding layers of the two systems were nearly identical.

It is apparent that the bond at the first layer-substrate interface of System 1 was somehow degraded during deposition of subsequent layers, and that the conditions or mechanisms causing this degradation were not present or were not as significant for the first layer-substrate interface of System 2. Sufficient information concerning the nature and properties of plasma-sprayed deposits and the effects of plasma spraying additional layers over preexisting coatings was not available at this time to permit a satisfactory explanation for the poor bonding of System 1 and the excellent bonding of System 4, and studies to acquire the information required were beyond the scope of this portion of the program.

While it could not easily be definitely established, most in-coating fractures appeared to occur in the BeO layer, which may be expected to be more weak and brittle than any other layer.* However, Coating System 4 exhibited very high fracture strengths even though it contained a BeO layer. Four System 4 specimens tested but not included in the average in Table 19 failed in the adhesive. Two of these failures occurred at very low stress levels as a result of improper bonding of the tensile rod to the substrate, but the other two failed in the adhesive at stresses in excess of 3500 psi.

In summary, the bond and cohesive strengths of System 4 were excellent, the bond strength of System 1 was poor and less than the cohesive strength, and the cohesive strengths of Systems 2 and 3 were moderate and less than the coating bond strength.

Thermal Diffusivity

At the request of the project monitor, a task was added to the program to determine the thermal diffusivity of one specimen of a complete plasma-sprayed coating system. Coating System 4 was selected for study because literature data were available for the properties of all the component materials.

The selected plasma-spraying parameters were used to deposit Coating System 4 on a 1/8-in.-thick copper plate clamped to a water-cooled copper chill plate. The thickness of each coating layer was increased to approximately 0.005 in. in order to obtain

*Based on published data for dense polycrystalline materials prepared by conventional techniques.

the total thickness of about 0.030 in. required for the measurement, and an extra layer of Type 304 stainless steel was applied over the ThO_2 outer layer to eliminate optical transparency encountered with thoria at elevated temperatures. Six 1/2-in.-diameter disks were cut and ground from the coated substrate, and the coatings were removed by etching away the copper substrate in nitric acid. Etched specimens were thoroughly cleaned in water to remove residual acid and ultrasonically cleaned in trichlorethylene and absolute ethyl alcohol. One specimen was selected for measurement and a second was sectioned and polished to provide a pre-test reference microstructure (Figure 8).

Thermal diffusivity was measured by a "flash laser" technique in which the specimen is brought to thermal equilibrium in a vacuum furnace and heated by a brief laser pulse directed at one face of the disk specimen. The time-temperature history of the opposite face as the heat pulse propagates through the specimen is directly related to the thermal diffusivity of the specimen. Specimen-surface temperature was monitored for approximately 1 hr after a laser pulse at each of four furnace temperatures between 300 and 1040 C; measured values of thermal diffusivity as a function of temperature are shown in Figure 9. No time dependence of thermal diffusivity was detected at temperatures less than 1000 C.

Using published property values for each material comprising the coating system, a computer analysis of transient thermal response predicted an overall thermal diffusivity of 0.005 cm^2/sec at 500 C. The value measured at this temperature, 0.0024 cm^2/sec, was roughly 20 times lower than the predicted result, a discrepancy much too large to be accounted for by the estimated ±15 percent experimental error, inaccuracy of layer thickness measurement, or the effects of porosity and oriented structure in plasma-sprayed materials. Thermal diffusivity (D) is related to thermal conductivity (k), density (ρ), and specific heat (C_p) by the expression: $D = k/\rho C_p$. The density of plasma-sprayed materials is generally in excess of 80 percent theoretical, and may be measured and taken into account in diffusivity predictions. Appreciable changes in specific heat can occur only by gross changes in chemical composition or by crystallographic modification. Even extreme changes in density and specific heat would account for only about 1/50 to 1/30 of the difference between predicted and measured diffusivity values. Thus, it was concluded that the discrepancy in values was primarily due to a gross reduction of thermal conductivity resulting from the plasma-spraying process. Boganov, et al.[28], also found thermal conductivities of flame-sprayed materials to be much lower than those of the same materials prepared by conventional sintering; they reported conductivities of six flame-sprayed oxides to be 1/5 to 1/10 the values predicted.

The following explanation appears to account satisfactorily for the low thermal-conductivity of coatings deposited by plasma or flame spraying. During coating application, molten particles are flattened and rapidly quenched onto the substrate to form a lamellar coating. Interparticle and particle-substrate bonding is of a predominantly or exclusively mechanical nature as a result of the rapid quenching of particles as they are deposited and the relatively low levels of heat they encounter during subsequent deposition of additional material. The low cohesive and bond strength of plasma-sprayed oxide coatings was confirmed by measurements reported in the preceding section. The thermal resistance at particle boundaries arising from poor interparticle bonding leads to a drastic reduction in overall heat conduction through the coating even though the thermal conductivity of individual particles is equivalent to that of dense, well-sintered material. Particularly severe reduction of overall thermal conductivity may be expected for plasma-sprayed coatings of oxides and other materials susceptible to fracture by thermal shock. Particle cracking and fracture of such materials introduces additional discontinuities which further impede thermal transfer. The above explanation is consistent

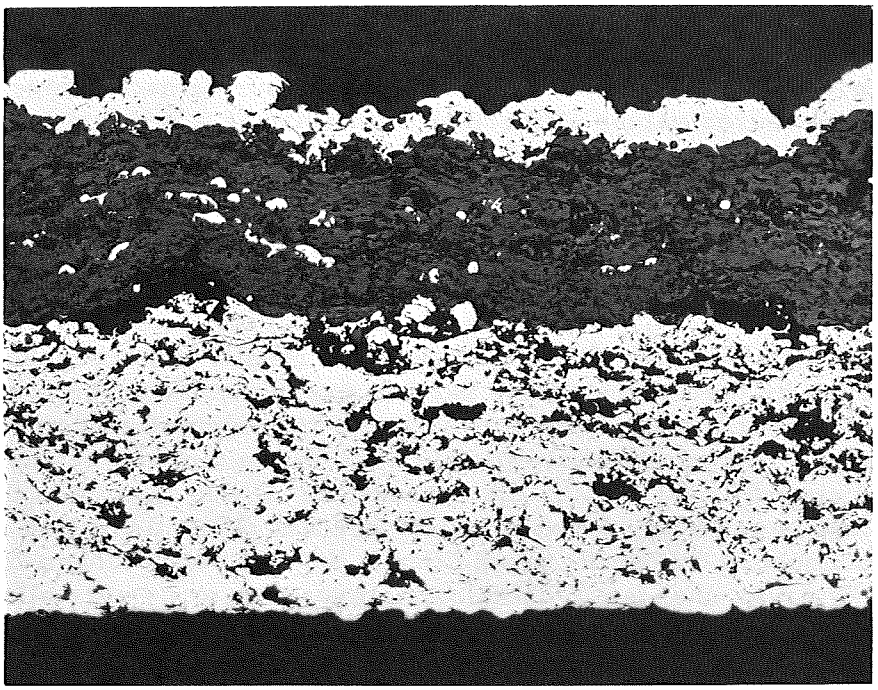

100X 5D446

FIGURE 8. COATING-SYSTEM-4 SAMPLE PREPARED FOR DIFFUSIVITY TEST

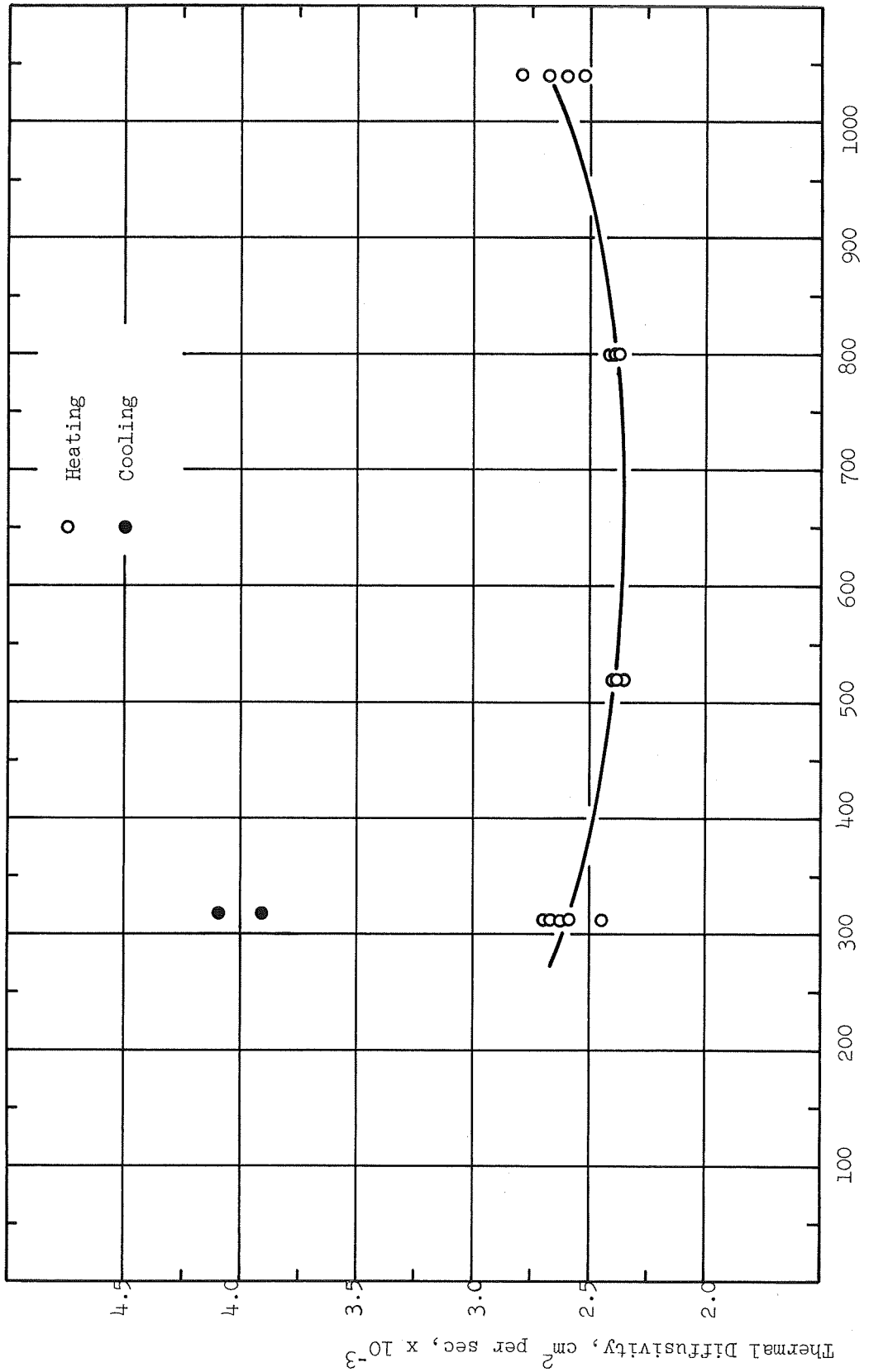

FIGURE 9. THERMAL DIFFUSIVITY OF SYSTEM 4, SPECIMEN 6 COMPOSITE MATERIAL

with experimental observations and implies that some reduction in overall thermal conductivity is an unavoidable consequence of plasma spraying, particularly for materials which are sensitive to thermal shock.

It has been demonstrated that the thermal conductivity of plasma-sprayed materials may be increased by sintering or hot isostatic compaction after spraying. The latter process may be expected to promote coating-substrate bonding and to effect densification of the coating in addition to enhancing interparticle bonding. Such post-spraying operations were not feasible for the coatings of this program in that the temperatures required to sinter the oxide layers are in excess of the melting points of the metallic underlayers.

Preparation of Uncooled Specimens for Rocket Testing

The final specimen configuration for uncooled rocket firings evolved from the series of designs depicted in Figure 10. In all cases, overall specimen dimensions were 1 by 1 by 1-1/4 in. to conform to the dimensions of the existing rocket facility.

The initial design (Figure 10a) proposed for use as a rocket-test specimen was a U-shaped 0.010-in.-thick substrate clamped to a water-cooled copper block during coating deposition. The 0.010-in. thickness was selected because this was the substrate thickness intended for use in the final full-scale rocket engine. The upper surface of the specimen substrate was to be plasma sprayed with a candidate coating system while on the cooling block, after which a thermocouple was to be welded to the uncoated backside of the substrate and the instrumented specimen mounted in place in the rocket nozzle by imbedding all but the coated surface in plaster. While substrates of this design had been previously plasma sprayed with apparent success for rocket tests using thicker substrates, the thin substrates buckled when removed from the cooling block as a result of distortion due to thermal stresses set up on the plasma-sprayed surface of the substrate.

A second, similar, approach was tried in which a block of plaster was cast into the interior of the U-shaped substrate prior to plasma spraying (Figure 10b). The interior of the substrate had been abraded and cleaned to promote its bonding with the plaster, but a sufficiently strong bond was not achieved to prevent severe warping and distortion on plasma spraying. A variation of this approach which included a copper water line imbedded in the plaster was also tried at the same time, with identical unsatisfactory results.

The third design, depicted in Figure 10c, employed a solid-block substrate. Because 1-in.-thick stock of Hastelloy X and Type 347 stainless steel substrate material was not readily available, these materials were used only as the top halves of blocks, while the bottom halves were machined from mild steel. The two halves were fastened together with screws entering from the bottom to obtain a specimen substrate of the required dimensions. Two 28-gage Chromel and Alumel wires inserted through two stepped holes having a final diameter 0.013 in. were welded in place at the outer surface of the substrate (the surface to be coated) to form a three-leg Chromel-substrate-Alumel thermocouple at the substrate-coating interface. Each thermocouple junction

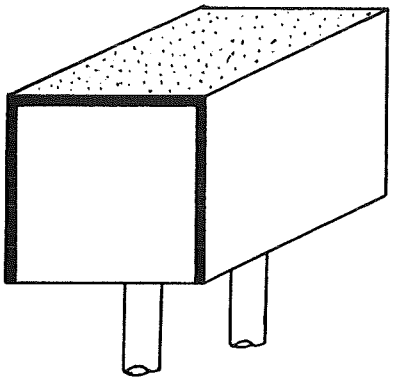

a. Water-Cooled Copper Spraying Form with 0.010-in.-Thick Substrate

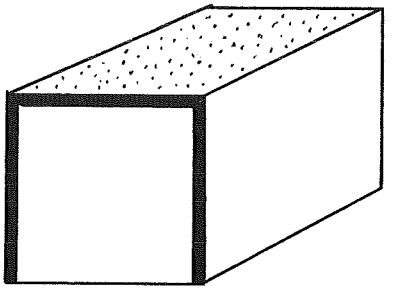

b. Ceramic Block Spraying and Testing Form with 0.010-in.-Thick Substrate

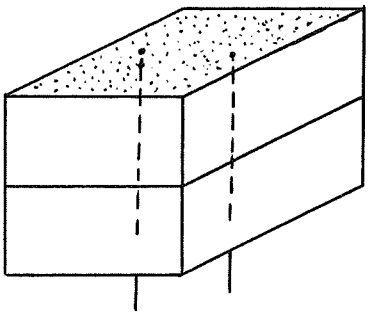

c. Two-Piece Solid Block with Chromel-Substrate-Alumel Junction Thermocouple (Junction at Substrate-Coating Interface)

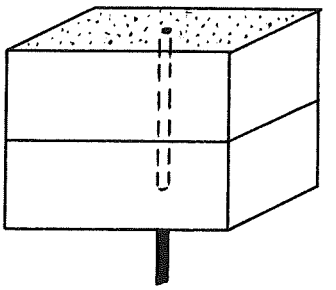

d. Two-Piece Solid Block with 0.020-in.-Diameter Sheathed Chromel-Alumel Grounded Junction Thermocouple (Junction at Substrate-Coating Interface)

FIGURE 10. EVOLUTION OF SPECIMENS FOR SHORT-TERM, UNCOOLED ROCKET FIRINGS

(Rocket exhaust parallel to short side of specimen)

was located 1/4 in. from the center and 5/8 in. from either end of the surface to be coated so that the thermocouple would monitor the average temperature of the central 1/2 in. of the specimen along the axis of the rocket exhaust. After attachment of thermocouple wires, the surface to be coated was hand polished on emery cloth to remove excess weld metal, roughened by vapor blasting at 50 psig, and ultrasonically cleaned in trichlorethylene and absolute alcohol. Several attempts were made to effectively insulate the thermocouple wires from the walls of the holes through which they passed, but the results were uncertain. Plastic insulation and organic and refractory cement slurries were used in these attempts.

Several serious deficiencies in this specimen design soon became apparent. Chief among them were:

(1) The actual size of the thermocouple junctions could not be determined, with the result that the depth below the substrate surface of the initial wire-substrate contact point could not be established. The exact location at which temperature was monitored was therefore unknown.

(2) The adequacy of thermocouple-wire insulation could not be assessed. Electrical continuity checks yielded positive results even when the thermocouple was short-circulated by wire-substrate contact at points other than at the welded junction.

(3) The thin thermocouple wires and delicate welded junctions were easily broken during specimen preparation and mounting even when specimens were handled as carefully as possible.

The upper half of each substrate block was screwed to a water-cooled chill plate and coated using optimized plasma-spraying parameters. In all, four specimens of this design were successfully plasma sprayed. Two of these were subjected to rocket firings, and two were destroyed by thermocouple failure during mounting in the rocket motor. Because of the uncertainties and difficulties involved, the design was discarded at this point.

The fourth and final design for uncooled specimens, depicted in Figure 10d, was a two-piece solid block identical to that just described except for the thermocouple arrangement. In this case, a single stepped hole with a final diameter 0.003 in. in excess of the thermocouple diameter was drilled through the block so that it emerged at the center of the surface to be coated. A sheathed thermocouple was inserted in the hole and soft soldered to the back of the upper block so that its flat tip was flush with the surface to be coated. The 0.003-in.-thick Type 347 stainless steel sheath had an outside diameter of 0.020 in. and was capped by a flat end of the same material. Chromel and Alumel wires were welded to the end cap to form a grounded-junction thermocouple. With this arrangement, the depth of the thermocouple below the coating-substrate interface was the thickness of the end cap. This thickness varied from 0.003 to 0.009 in. as determined by measurements on radiographs.

Following attachment of thermocouples, specimens were roughened by vapor blasting at 50 psig and were ultrasonically cleaned in trichlorethylene and absolute ethyl alcohol. During plasma spraying, the upper half of the specimen block was screwed to a water-cooled copper chill plate specially constructed to provide support for the thermocouple and the lower half of the block. Plasma-spraying procedures and parameters used were those described earlier.

The instrumented specimen afforded an opportunity to monitor the coating-substrate interface temperature during application of a plasma-sprayed coating. The output from the thermocouple was fed to a strip-chart recorder operating at a chart speed of 6 in./min. Each traverse (one complete scan of the plasma flame over the specimen surface) was clearly apparent as a temperature spike on a typical recorder trace, such as the one shown in Figure 11 for deposition of a single coating layer. The measured interface temperature increased with each successive traverse until a maximum value was attained. In the example shown, the interface substantially attained its maximum temperature on the fifth traverse as a pseudoequilibrium was established between the heat arriving at the exposed surface from plasma spraying and the heat dissipated by the specimen block.

Figure 12 summarizes substrate surface temperatures recorded during plasma spraying of one complete coating system. It may be noted that after deposition of the first oxide-containing layer (Layer 2), maximum substrate temperatures obtained during deposition of subsequent layers either did not increase or were reduced in spite of the increasing severity of plasma spraying conditions. This situation may be explained by assuming that the additional oxide deposited increased the thermal resistance of the total coating to an extent which more than compensated for the additional heat arriving at the specimen due to increasing severity of spraying conditions. The trend just discussed was reversed only during application of the final oxide layer, which could be deposited only with very high plasma-arc powers and with a spraying distance so small that the specimen surface was immersed in the plasma flame. Even under these extreme conditions, the measured substrate surface temperature did not exceed 500 F.

The above measurements of substrate surface temperature indicated that the coating apparently provided an effective thermal barrier and that even a relatively poorly cooled substrate with a 1/2-in.-thick block between the substrate-coating interface and the chill plate was not heated to high temperatures during plasma-arc deposition of the most refractory of the candidate coating-system materials.

Preparation of Cooled Specimens for Rocket Testing

Specimen design for cooled rocket firings was essentially an adaptation of the successful water-cooled jig used for deposition of coatings on thin substrates (Figure 2). Basically, the specimen consisted of a 0.010-in.-thick Type 347 stainless steel substrate whose backside was in direct contact with a thin curtain of rapidly flowing cooling water at 60 psig. Ribs supported the thin substrate against the pressure of the coolant and also divided the water curtain into four streams which flowed parallel to the axis of the rocket exhaust from leading to trailing edge. Stagnation of coolant at any point was prevented both by the ribs and also by filling and emptying the cooling channels through narrow slots connecting the channels with reservoirs extending the length of the specimen. Essential features of the specimen design are depicted schematically in Figure 13 and as a disassembled specimen and one coated and ready for mounting in the rocket motor in Figure 14.

Block end plates and the 0.010-in.-thick Type 347 stainless steel substrate were copper brazed in a hydrogen-atmosphere furnace after cleaning all components of the assembly. In this operation it was necessary to place the exact amount of braze to make the joints but not block critical flow passages. Several specimens were brazed and examined destructively to establish the amount of braze material required. The correct amount of braze material was placed at the interior ribs by cementing short lengths of

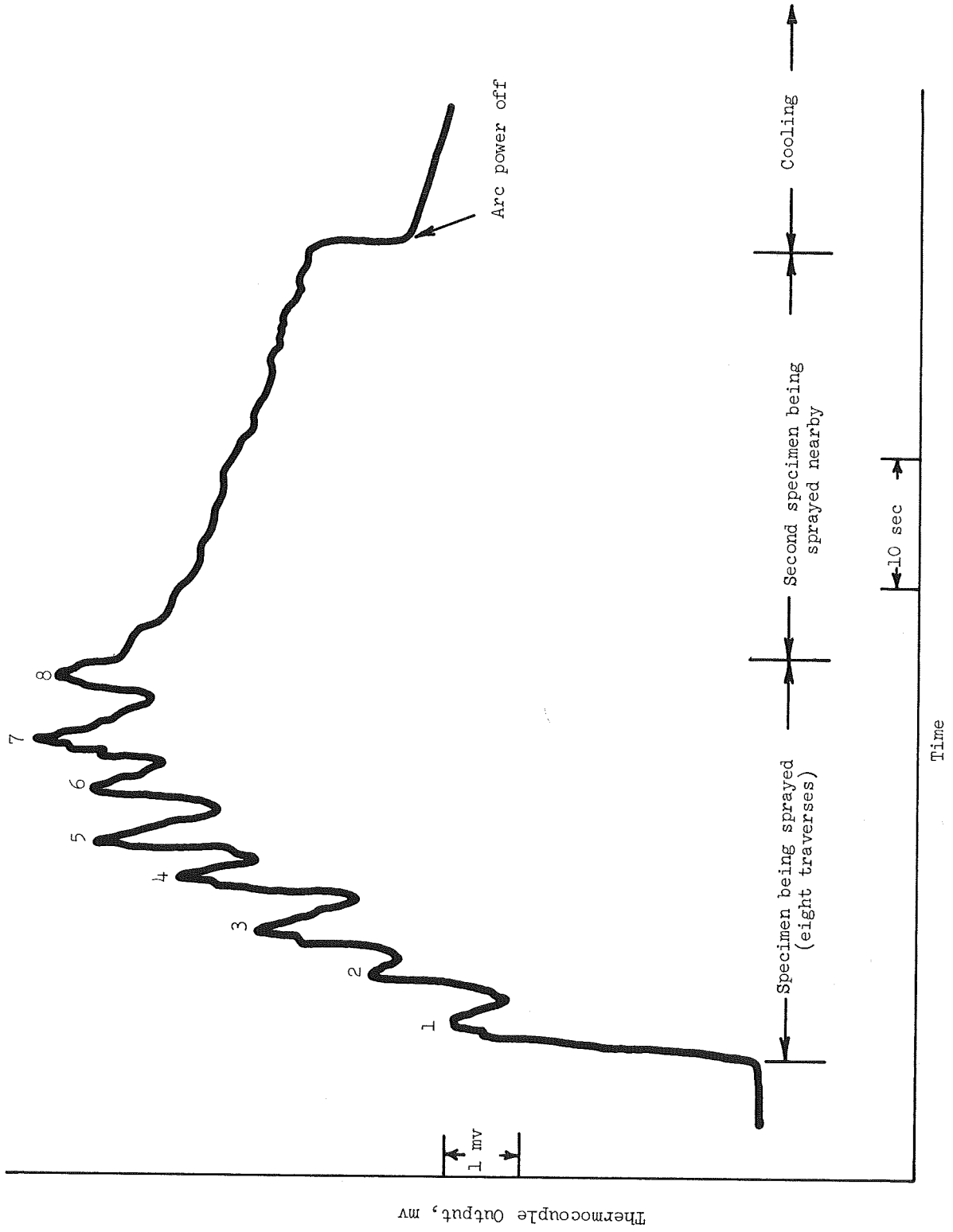

FIGURE 11. TYPICAL RECORDER TRACE OF SUBSTRATE SURFACE TEMPERATURE DURING PLASMA SPRAYING OF BLOCK 1-1, COATING SYSTEM 1

Coating System 1, Block 1-1

Plasma-Spraying Conditions					
Parameter	Layer Number				
	1	2	3	4	5
Arc Current, amp	300	400	500	600	700
Arc Gas Flow, cfm	0.92	0.65	0.65	0.65	0.65
Powder Gas Flow, cfm	0.17	0.12	0.11	0.11	0.16
Powder Feeder Setting	20	20	20	20	20
Gun-Substrate Distance, in.	4	3.5	3	1.5	1
Total Spray Time, sec	34.5	34.5	42.5	38	29.5

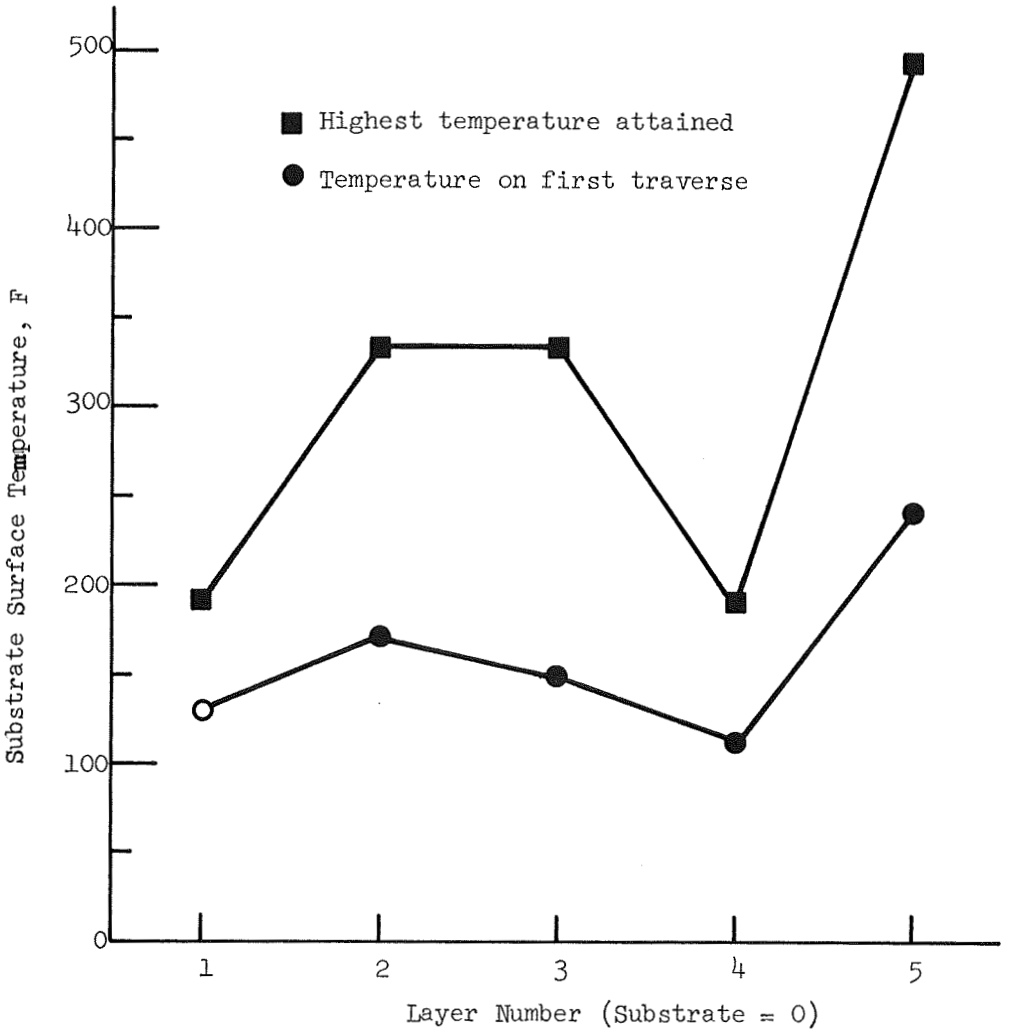

FIGURE 12. SUMMARY OF SUBSTRATE SURFACE TEMPERATURES DURING PLASMA SPRAYING OF BLOCK 1-1, COATING SYSTEM 1

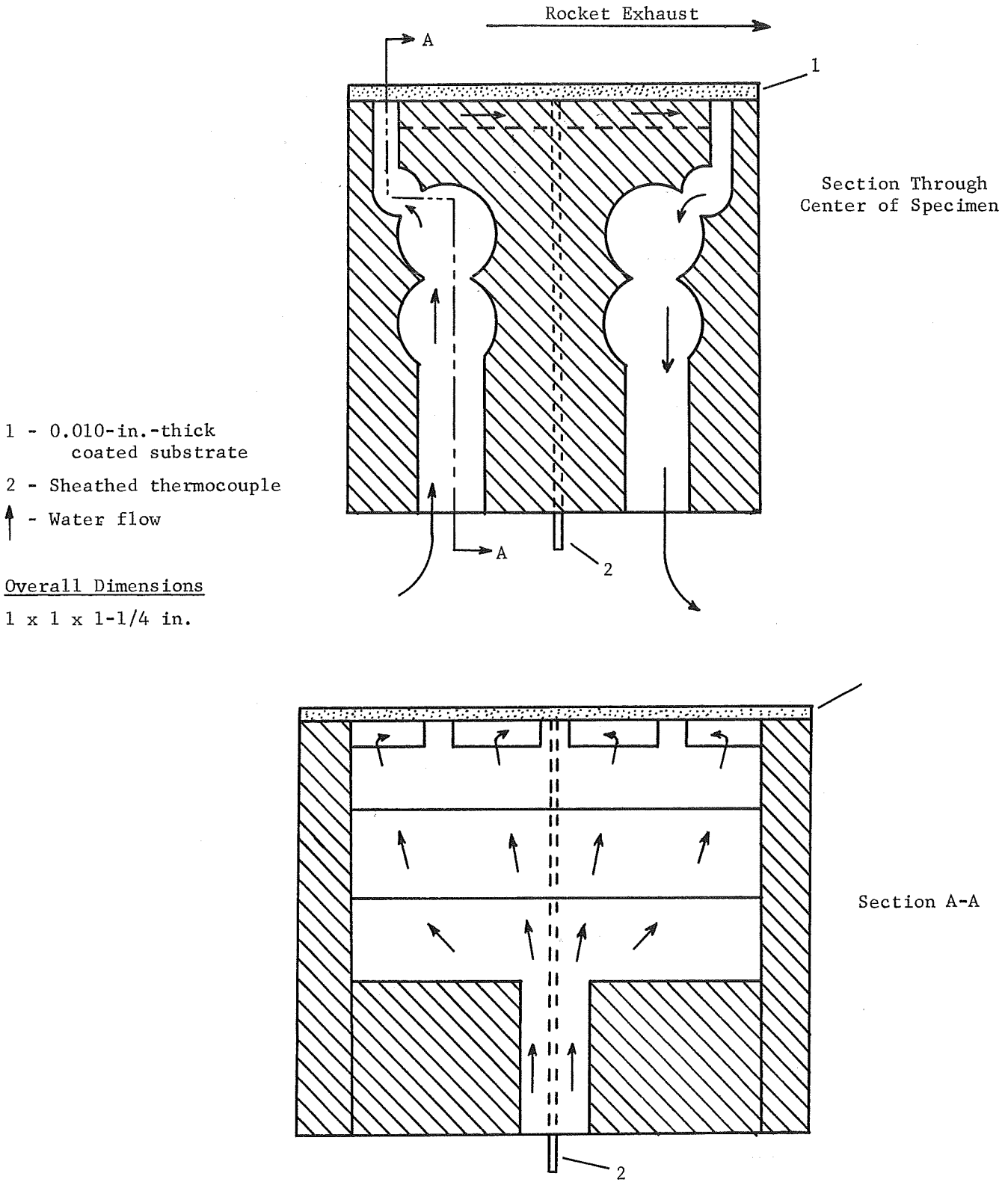

FIGURE 13. BASIC DESIGN OF COOLED SPECIMENS

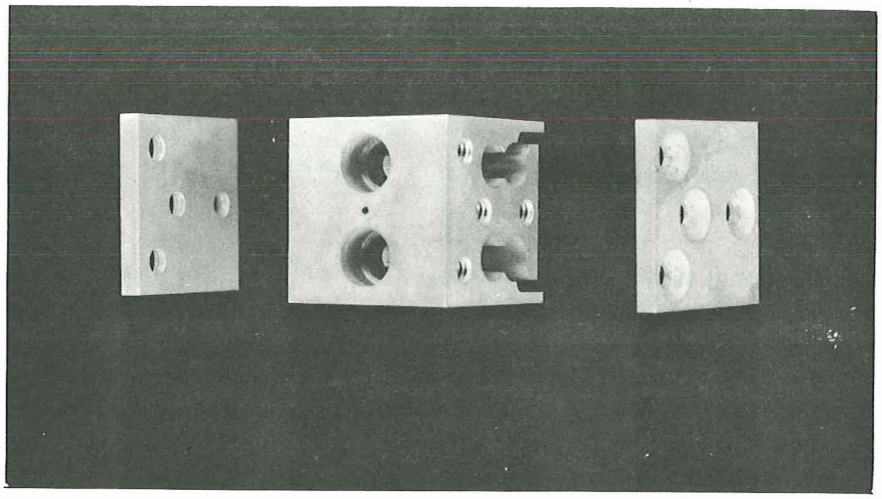

1X a. Disassembled 8D585

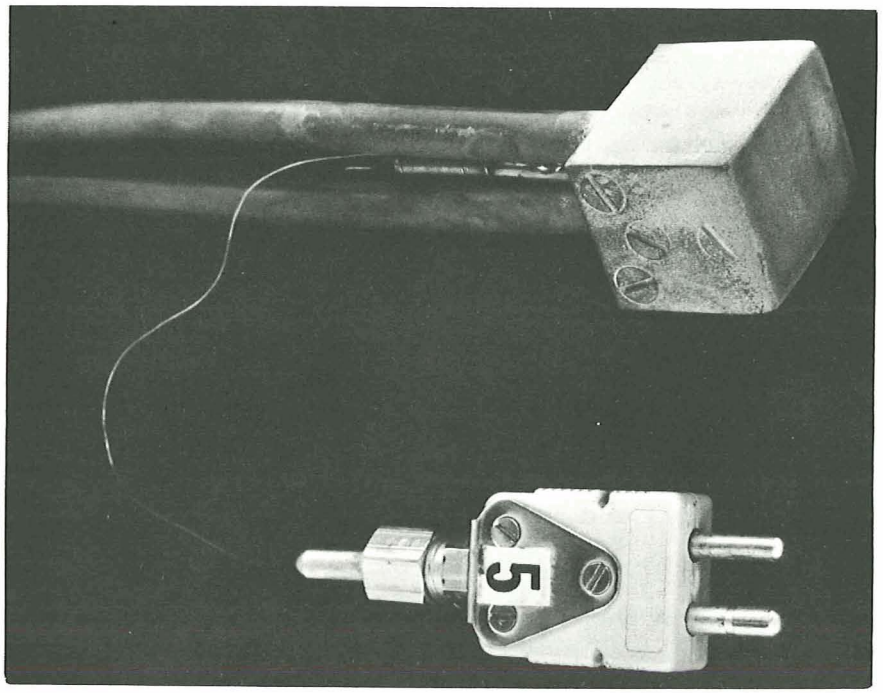

1X b. Coated and Ready for Mounting 8D586

FIGURE 14. WATER-COOLED ROCKET-TEST SPECIMEN

copper wire with a dilute solution of Duco cement in acetone, and by depositing a fillet of copper at the substrate-block junction as a slurry of copper powder, Duco cement, and acetone. The interiors of the rectangular cooling channels and of the thermocouple hole were coated with a thin layer of braze stop-off solution to prevent wetting these locations with copper. Extreme care was required in placing copper and stop-off around the thermocouple hole since a pressuretight water seal was required yet excess braze would fill the hole by capillary action thus preventing contact of the thermocouple with the backside of the substrate. Assemblies were brazed in dry hydrogen at 2150 F and allowed to cool in hydrogen in the cold zone of the furnace.

Following brazing, 5/16-in.-diameter copper water leads and a 0.040-in.-ID x approximately 2-in.-long stainless steel thermocouple guide tube were silver soldered in position on the back of the specimen block. Excess solder was ground off, and the thermocouple hole was cleared of any obstructions by reaming it along its entire length with a 0.030-in.-diameter drill bit. Excess substrate material was sheared off, and the substrate edges were ground flush with the sides of the specimen block and rounded slightly to facilitate adherence of the plasma-sprayed coating. Each specimen was pressurized with 300-psig carbon dioxide and checked for leakage by watching for bubbles when the pressurized specimen was placed in an acetone bath. Dirt, grease, and oxide obtained during the above operations were removed by vapor blasting at 50 psig and ultrasonically cleaning in trichlorethylene and ethyl alcohol. Specimens were then instrumented with 0.020-in.-diameter sheathed thermocouples of the type previously used on uncooled specimens and discussed above. Each thermocouple was spring loaded against the back of the stainless steel substrate by soft soldering one end of an extended spring to the thermocouple sheath and the other end to the thermocouple guide tube.

Coating System 4 was applied to the 0.010-in.-thick cooled substrate by plasma spraying in dry argon. Spraying parameters were essentially those given in Table 11. Specimens were plasma sprayed in batches of two and were cooled by approximately 50 F water flowing through them in a parallel-flow arrangement at a line pressure of approximately 60 psig. Because the oxide layers previously deposited on some uncooled specimens were found to be excessively thin, coating layer thicknesses were measured with particular care. The total thickness of the uncoated specimen was measured at four selected points both before and after placement in the atmosphere chamber. All in-chamber micrometer measurements were made at the same points when the cooling water was not flowing. Repeated measurements at the same point agreed to within less than 0.0005 in., the practical limit of accuracy for in-chamber measurements. After deposition and in-chamber measurement of all coating layers, specimens were removed from the atmosphere chamber and remeasured; both sets of measurements were in good agreement.

During plasma spraying the temperature at the backside of the substrate of some specimens was monitored by feeding the output of the spring-loaded thermocouple into a strip-chart recorder. In order to check thermocouple response, the first 20 sec of spraying of the first specimen was done without cooling water flowing. Maximum temperatures attained during each of the four uncooled traverses of the plasma torch were 115, 140, 170, and 185 F, in that order. The rest of the first coating layer was deposited with water flowing through the specimen, and a maximum temperature of 75 F was recorded for the cooled specimen. The highest temperature attained during application of the entire coating system was 135 F which was measured during application of the BeO fourth layer. The 135 F maximum occurred on the sixteenth of forty-eight traverses of the plasma torch, and progressively lower temperatures were attained as

the oxide thickness increased on successive traverses. Similar results were obtained during application of coatings to several other specimens.

ROCKET TESTING

Testing Facilities and Test Procedures

Rocket firings were conducted with a small-scale oxygen/hydrogen rocket motor permanently mounted in a protective bunker at the West Jefferson site of Battelle-Columbus. The motor, shown in Figure 15, consists of a combustion chamber and a removable retaining ring containing the nozzle assembly. The chamber section is constructed of copper cooled by water flowing through internal channels; separate water lines provide cooling to all or part of the nozzle assembly. The motor was operated with gaseous O_2/H_2 fuel ratios near maximum specific impulse (I_{sp}). Heat-transer rates up to 35 Btu/(in.^{2})(sec) (equivalent cold-wall value) may be obtained at the flat face of a slit nozzle during operation at a chamber pressure of 455 psia. An electronic timing mechanism permits rocket firing durations reproducible to 0.01 sec. Rocket firings conducted in this program were exhausted into a large, low-pressure stainless steel scrubber tank to prevent contamination of the atmosphere by toxic and/or radioactive materials contained in coating particles eroded from specimens. Smears taken in the area after specimen firings indicated no uncontained contamination from thoria or beryllia.

For the rocket firings of this program, a slit nozzle configuration was used. A 0.10 by 1-in. nozzle slit was formed by the coated surface of the test specimen, the exposed surface of a water-cooled copper calorimeter, and two 0.10-in.-thick copper spacer/alignment bars placed between the specimen and calorimeter. Nominal overall dimensions of both the specimen and calorimeter were 1 by 1 by 1-1/4 in. After the four-piece nozzle assembly was securely clamped together and aligned, it was mounted in a brass retaining ring with cast plaster of Paris. The retaining ring was bolted in place on the combustion chamber to form the complete rocket motor.

A quartz window in the copper calorimeter permitted a recording radiation pyrometer to be sighted on the surface of the specimen coating at the center of the area exposed to the rocket exhaust. Differential thermocouples were used to monitor the temperature rise of cooling water flowing through the calorimeter and, where applicable, through the coated specimen. A thermocouple imbedded in the specimen detected the temperature attained at or near the coating-substrate interface. Combustion-chamber pressure was monitored by a pressure transducer. Specimen surface temperature, coating-substrate interface temperature, chamber pressure, and cooling-water temperature rise were monitored throughout each firing by a high-speed, rapid-response multichannel strip-chart recorder equipped with light-activated chart paper and a timing index. Each component of the monitoring system was calibrated against standard emf sources immediately prior to each rocket firing. Pressures and flow rates of propellant gases and of cooling water were also calibrated prior to each firing.

Test plans called for initial tests to be conducted on four coating systems selected under Task I. Initial tests would be conducted on uncooled specimens for short durations. Longer duration erosion tests on cooled configurations would then determine the most

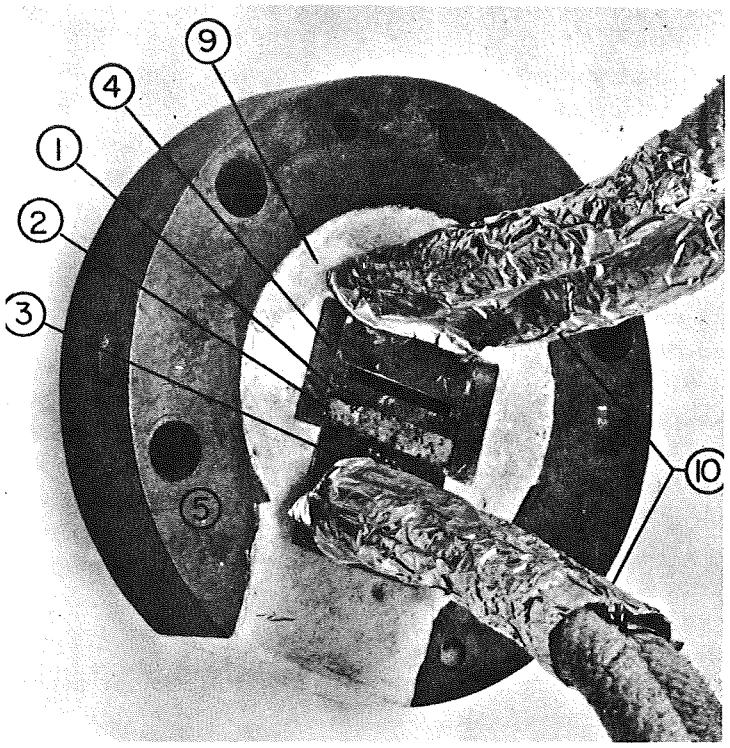

Photograph

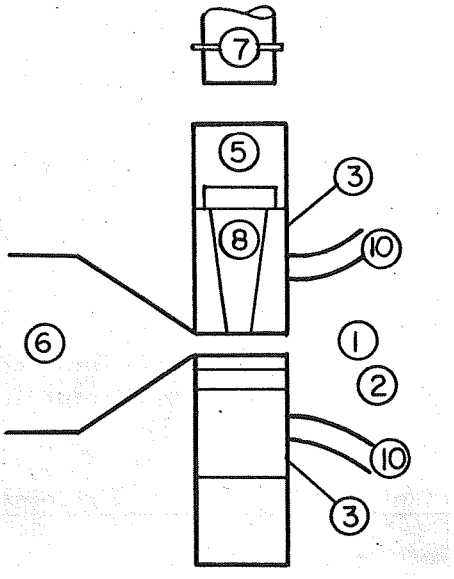

Sectional Schematic

① Test specimen
② Insulation backup
③ Water-cooled calorimeter
④ Spacer blocks
⑤ Mounting ring
⑥ Combustion chamber
⑦ Optical pyrometer
⑧ Quartz window
⑨ Refractory ceramic potting material
⑩ Cooling water lines

FIGURE 15. HIGH-HEAT-FLUX MATERIALS - EVALUATION APPARATUS

promising coating system. Three repeated starts on the same specimen would determine the final candidate coating system's ability to survive cyclic exposure. Following firings of 10, 30, and 60 sec in duration with water as the coolant, the final qualification multichannel test-specimen configuration would be evaluated in two 10-sec tests with a liquid-hydrogen coolant.

In all of these tests, the multilayer coating interface with the substrate was not to exceed 1600 F. The imposed heat flux was to be equivalent to a cold-wall flux of 30 to 35 Btu/(in.^{2})(sec). Oxygen-to-hydrogen ratio was to be kept near maximum I_{sp}. A thermocouple imbedded in the substrate of each specimen would provide backface temperature data. Surface temperature of the specimen was to be measured during test exposure.

Establishment of Test Parameters

In evaluating the four systems developed in Task I, motor operation is already specified by the required cold wall heat-flux level of 30 to 35 Btu/(in.^{2}sec) which in turn requires a steady-state chamber pressure of 415 and 455 psi, respectively. Thus, in order not to exceed a backface temperature of 1600 F on the uncooled specimens, it is necessary to limit the test exposure to a short interval.

A thermal analysis was performed to determine test-specimen response in the rocket exhaust and thus establish the test-exposure duration. This analysis was based on Coating System 1 on a Hastelloy X block. The TWODHT computer program, which was used in the Task I analyses, was used. The problem considered was the rocket-motor test-slit nozzle rather than a circular cross-section nozzle.

Heat transfer into the specimen was shown by a two-dimensional analysis to be satisfactorily represented by a one-dimensional analysis. The computer input conditions used were those associated with the rocket motor producing a cold-wall heat flux of approximately 35 Btu/(in.^{2}sec). These conditions are a chamber pressure of 455 psi and a fuel mixture of 5:1. The remaining gas input parameters were obtained from NASA SP-3011, "Thermodynamic and Transport Properties for the Hydrogen-Oxygen System". The rocket-motor input parameters were checked by using a separate steady-state heat-transfer program utilizing the Bartz equation. The Bartz relationship is also used in TWODHT to determine the convective heating rates and the resulting heat-transfer coefficient was multiplied by 0.7 as agreed upon at the beginning of this contract. (Calorimeter tests later confirmed this.)

The computer-model input was a pressure ramp from ambient to 455 psi in 0.3 sec and then constant, which corresponds to the actual rocket-motor behavior when choking before the test specimens. All other parameters, such as temperatures, were step conditions.

In the computation, 59 nodes were used. One node was used for each of the five coating layers. Thus, the first node was 0.003 in. thick for the thoria, the second, third, fourth, and fifth nodes were each 0.002 in. thick, corresponding to the thoria-10 v/o niobium, 50 v/o thoria/niobium-50 v/o Hastelloy C, 20 v/o thoria/niobium-80 v/o Hastelloy C, and for the Hastelloy C coating layers. The next four nodes were 0.0025 in. thick and were used for Hastelloy X. The next 12 nodes were 0.0025 in. thick, the next 24 nodes were 0.005 in. thick, the next 4 nodes were 0.010 in. thick, and the last 10 nodes were 0.080 in. thick, and were all used for Hastelloy X. Several

different node-thickness combinations were tried before the above combination was shown to make the calculation results insensitive to node thickness.

Figure 16 shows the temperature profile for the first 0.171 in. for several instants of time for Coating System 1 on the 1-in. Hastelloy block. The latest time shown, 0.252 sec, corresponds to when the Hastelloy C-Hastelloy X bond interface is approximately 2060 R (1600 F), and is the test time limit for this configuration. The data are cross-plotted in Figure 17 where the temperatures of three different locations are shown versus time. The locations plotted are the surface, T_s, the Hastelloy C-Hastelloy X bond interface, T_I, and at a depth of 10 mils in the thick Hastelloy X block. This figure shows the predicted interface temperature rise to the selected limiting value of 2060 R. This exposure time was used to start testing the uncooled specimens. The time was to be varied as necessary to achieve an interface temperature of 2060 R.

A similar analysis was conducted for Coating System 1 on an uncooled 10-mil substrate. Approximately 0.2 sec was required to reach a backface maximum temperature of 1600 F for this configuration. The coating on the 1-in. substrate thus gives a longer time and also reaches a higher surface temperature.

After determining the test exposure time for uncooled specimens, preliminary firings were made to check out the rocket facility because the facility had been moved to a new location just prior to starting tests on this program. The rocket motor was fired several times at pressures of 200 psi and 345 psi with water-cooled copper calorimeters of the same size in place of specimens. Lower pressure conditions were used because of the limited cooling of the then available calorimeters. These firings provided a satisfactory check of the chamber pressure-heat flux relationship. A check of the actual motor startup transient showed that the chamber pressure rose to 70 percent of final steady state pressure in 0.3 sec and the remaining 30 percent was achieved in the next second. These conditions differed from those used in the computer analysis because choking was at the calorimeter exit (selected mode of operation for the evaluation tests) rather than at the calorimeter entrance. Under these startup conditions, the pressure at the initially selected test duration time of 0.26 sec will be approximately 300 psi. No additional computer analyses were made for these starting conditions because initial uncooled specimen tests produced the limiting back wall temperatures and produced partial coating surface failures.

Six additional firings were made to determine the actual firing time relative to the preselected time set on the electronic-timer firing mechanism. Firing durations of 0.22, 0.24, and 0.26 sec were investigated. In all cases, the precision and reproducibility of rocket motor running times were satisfactory in relation to the accuracy of time measurements possible with the galvanometer-type high-speed recorder used to monitor testing parameters and specimen temperatures.

Rocket Firings With Uncooled Specimens

Figure 18 compares the measured values of chamber pressure and output of the substrate-coating interface thermocouple for all short-term rocket firing tests on uncooled, solid-block specimens. Selected pressure-temperature-time data are given in Table 20, and temperature data derived from the Figure 18 curves are presented as a function of time in Figure 19. The posttest condition of each specimen tested and the

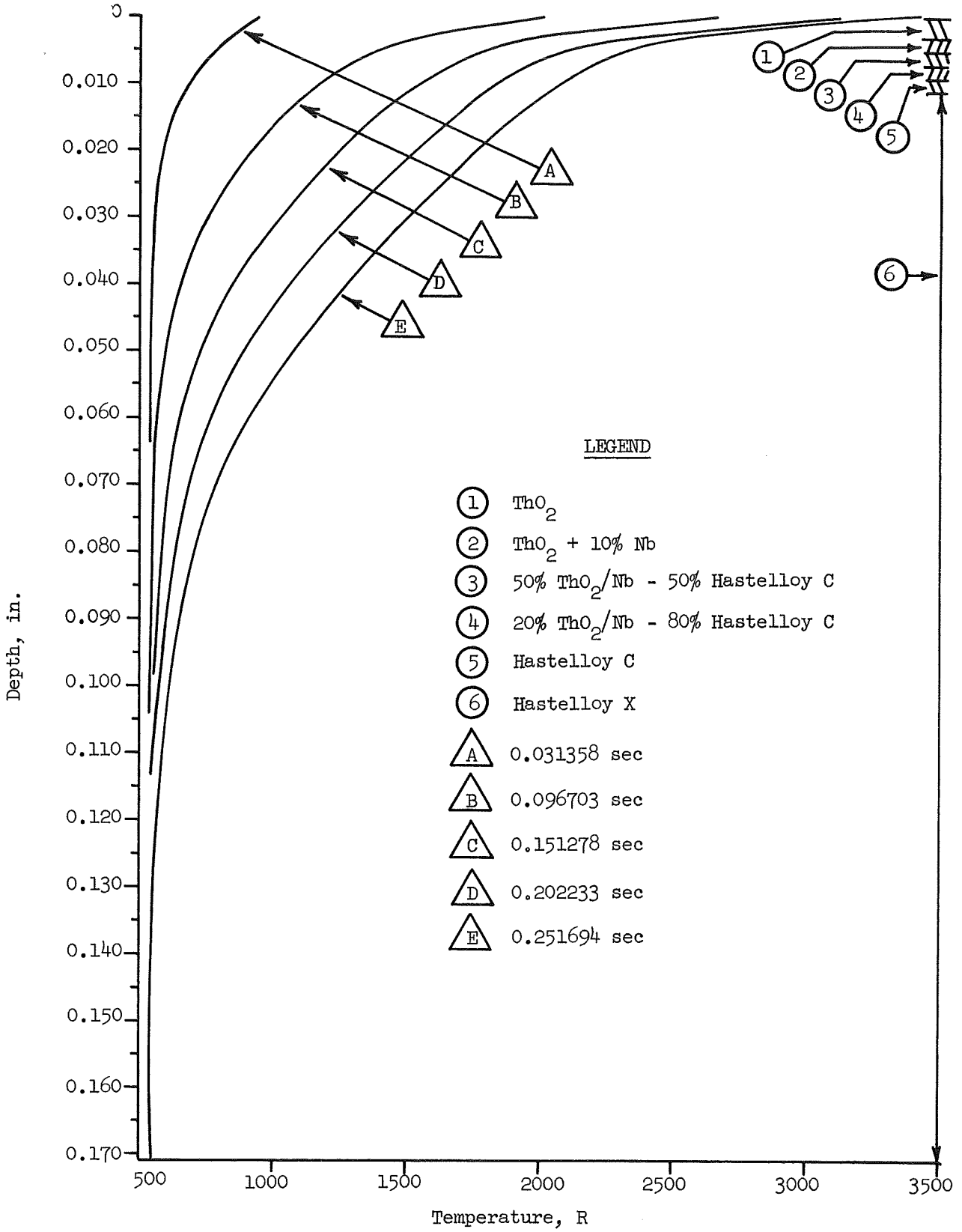

FIGURE 16. TEMPERATURE VERSUS DEPTH DURING ROCKET TESTING OF COATING SYSTEM 1, BASED ON THERMAL ANALYSIS

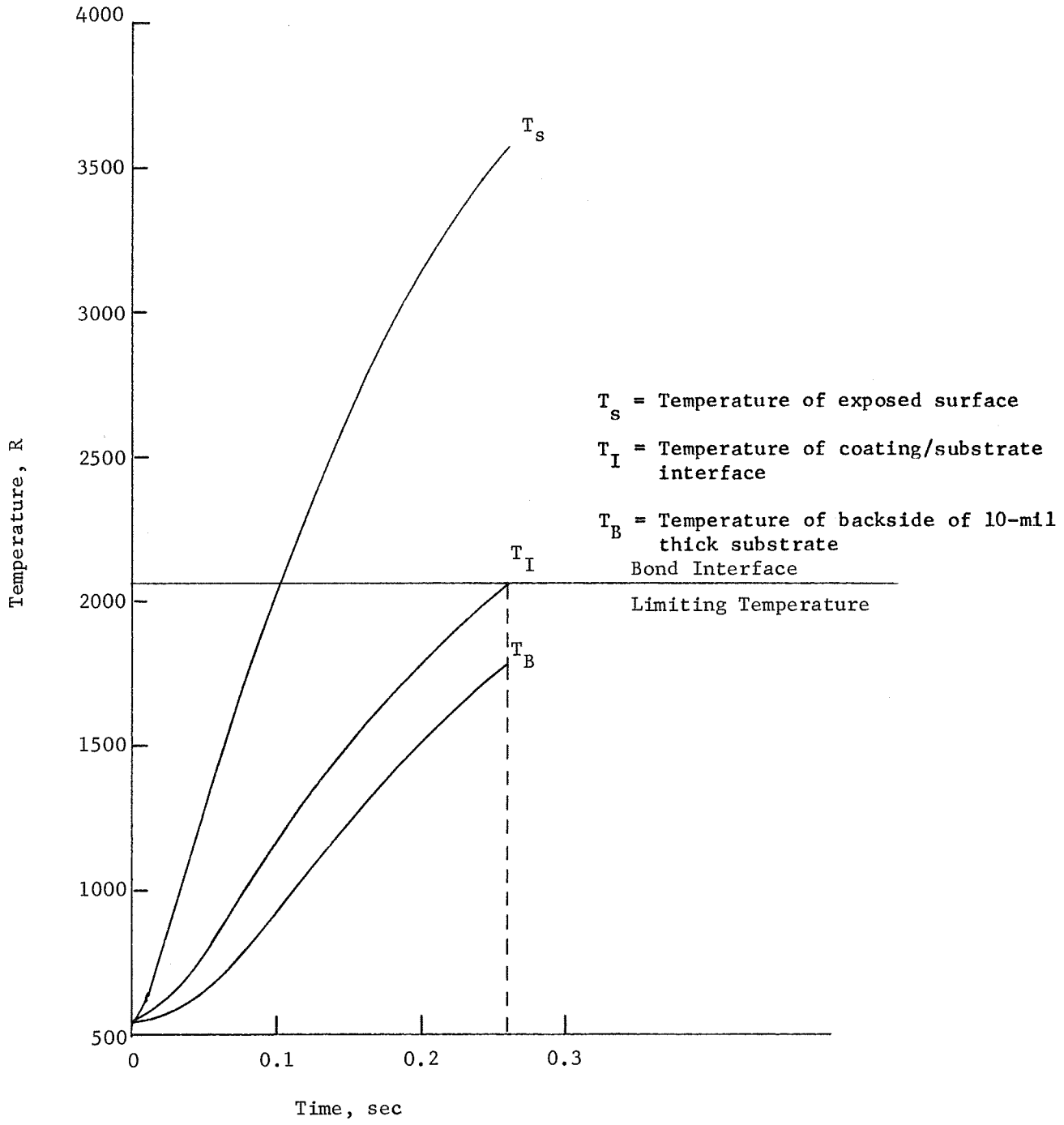

FIGURE 17. TEMPERATURE VERSUS TIME DURING ROCKET TESTING OF COATING SYSTEMS, BASED ON THERMAL ANALYSIS

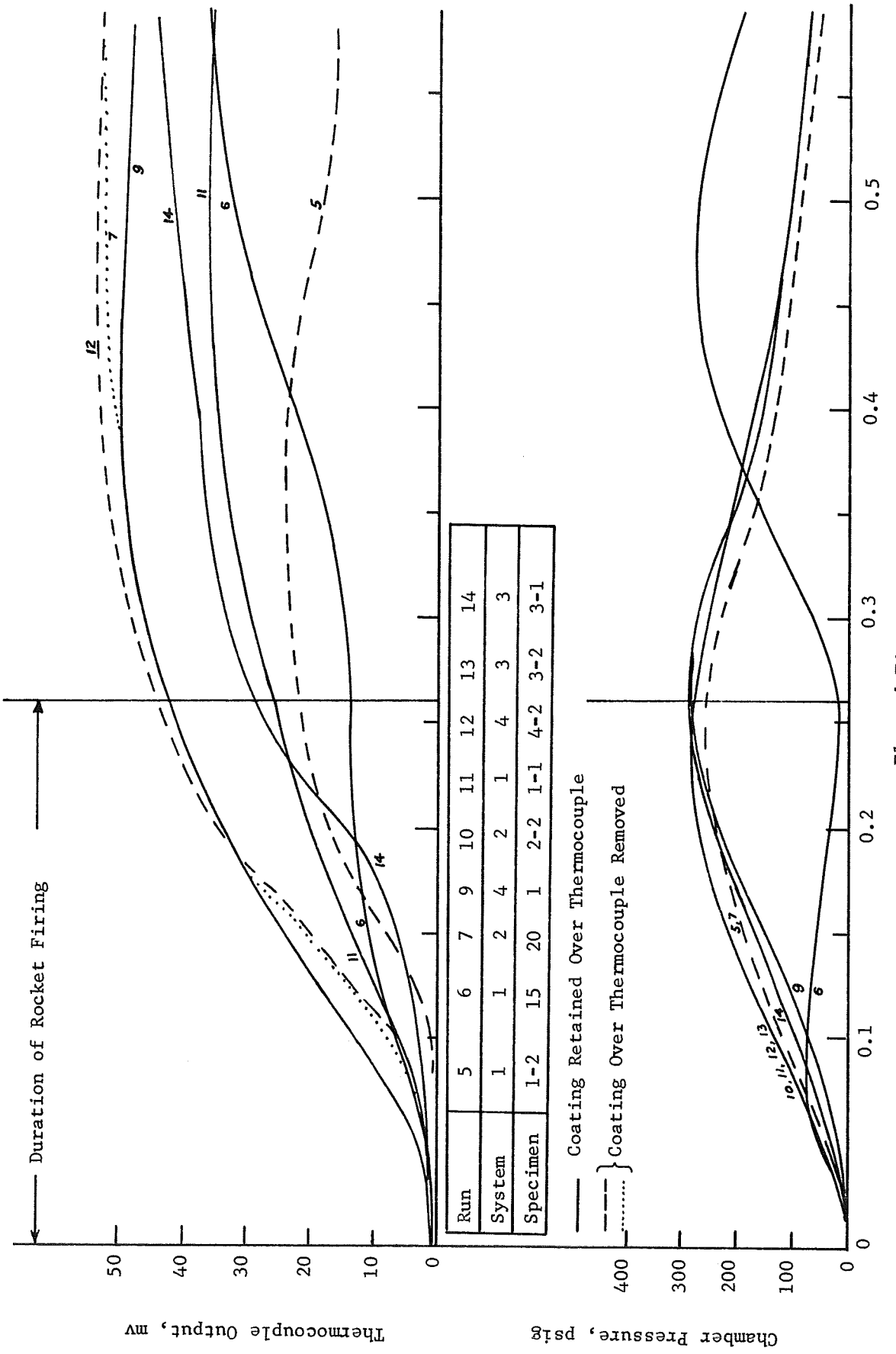

FIGURE 18. CHAMBER PRESSURES AND SUBSTRATE SURFACE TEMPERATURES ENCOUNTERED IN SHORT-TERM ROCKET TESTS

TABLE 20. SUMMARY OF 0.26-SEC ROCKET FIRINGS ON UNCOOLED SOLID-BLOCK COATED SPECIMENS

	Run 11	Run 6(a)	Run 5	Run 10	Run 7(b)	Run 14	Run 13	Run 9	Run 12
Coating System No.	1	1	1	2	2	3	3	4	4
Specimen No.	1-1	15	1-2	2-2	20	3-1	3-2	1	4-2
Thermocouple No.	4	(c)	7	10	(c)	2	5	7	8
Maximum Pressure, psia	307	313	290	288	290	310	300	310	297
Time of Maximum Pressure, sec	0.249	0.272	0.253	0.245	0.246	0.249	0.256	0.249	0.252
Time Temperature Rise Begins, sec	0.03	0	0.10	(d)	0.03	0.05	(d)	0.03	0.03
Time of Maximum Temperature, sec	0.625	0.619	0.332	--	0.461	0.667	--	0.400	0.441
Temperature at 0.10 Sec, F	307	850	42	--	375	193	--	628	297
Temperature at 0.20 Sec, F	878	1214	833	--	1596	878	--	1578	1578
Temperature at 0.30 Sec, F	1260	1433	1032	--	2120	1520	--	2095	2233
Temperature at Maximum, F	1591	1887	1048	--	2303	1925	--	2233	2400
Temperature at Time of Maximum Pressure, F	1078	1446	960	--	1887	1308	--	1864	1980
Coating Over Thermocouple	On	On	Off	On	Off	On	Off	On	Off

(a) Misfire. Zero time is 0.271 sec actual time from start of first firing attempt. Pressure at 0.271 sec = 41 psia. Temperature at 0.271 sec = 740 F (16.1 mv).
(b) Third firing. No data were obtained on the first two firings.
(c) Two-wire exposed thermocouple.
(d) Thermocouple failure.

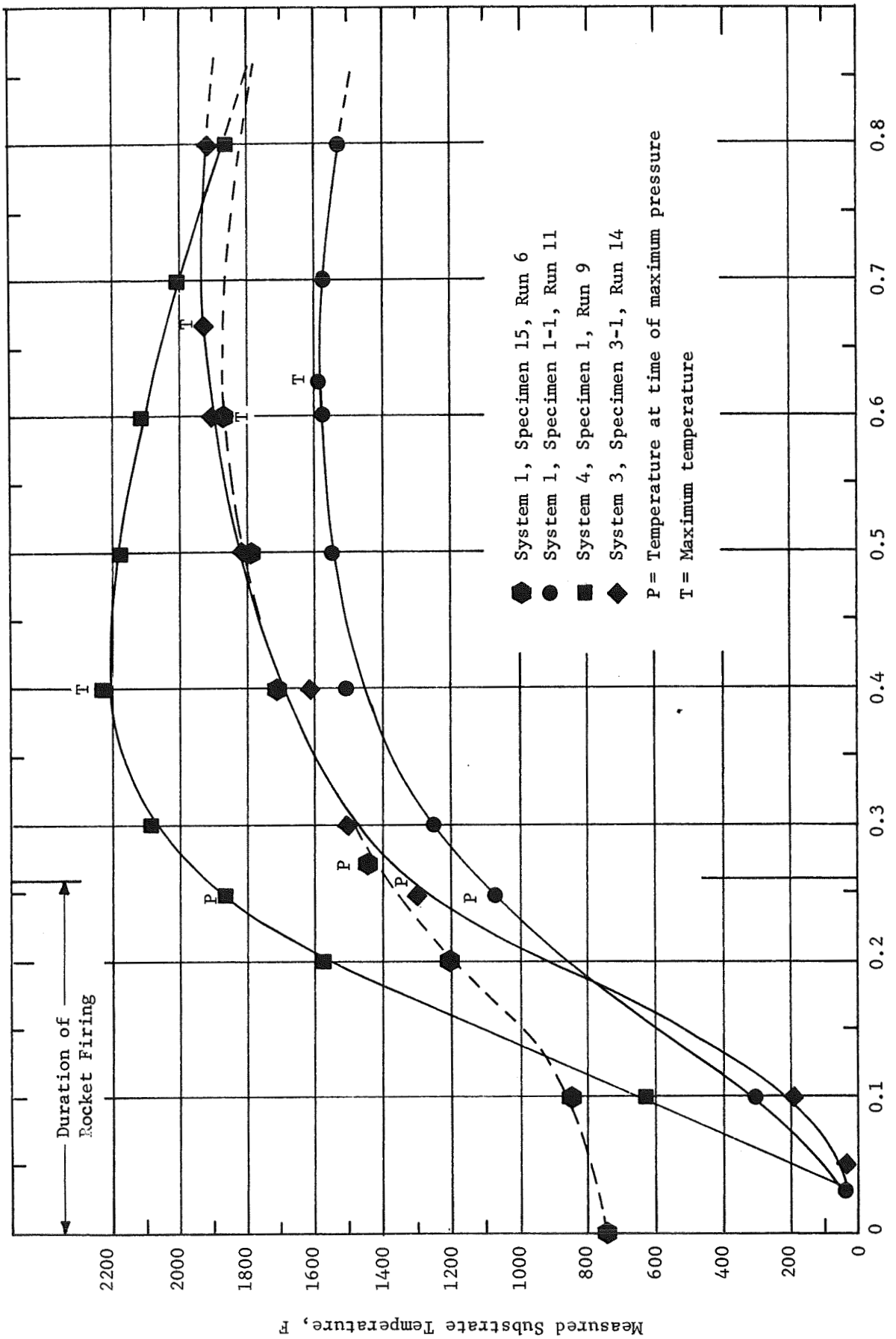

FIGURE 19. TEMPERATURE OF COATING-SUBSTRATE INTERFACE DURING ROCKET FIRING TESTS ON UNCOOLED SOLID-BLOCK COATED SPECIMENS

microstructure of exposed and unexposed areas of selected specimens are shown in Figures 20 through 27. Unexposed areas shown are typical areas in the 1/8 by 1-in. strips of coating at the specimen edges; these areas were under spacer bars during rocket firings. All rocket firings were conducted under conditions which would produce a steady-state chamber pressure of 455 psi, an approximate gas temperature of 5300 F, and a nominal cold-wall equivalent heat flux of 35 Btu/(sec)(in.^{2}). A propellent weight ratio of O_2:H_2 = 5:1 was used in all cases. Chamber pressure was highly reproducible, attaining a maximum value of 300 ± 13 psia at a time of 0.250 ± 0.003 sec.* Maximum indicated temperatures at coating-substrate interfaces ranged from 1048 to 2400 F, with the highest temperatures recorded by thermocouples exposed by loss of coating. Although the entire coating was removed from Specimen 1-2, a very low interface temperature was indicated because the epoxy used to mount the thermocouple had charred, allowing the thermocouple junction to slip into the interior of the specimen block. All other thermocouples were soldered in place to prevent recurrence of this difficulty. Maximum interface temperatures indicated by the four thermocouples which functioned and remained coated ranged from 1591 to 2223 F. Persistent difficulties with the radiation pyrometer focused on the coating prevented meaningful measurements of specimen surface temperature.

Although rocket firing conditions were highly reproducible, the coating systems behaved inconsistently. For every coating system, one specimen suffered appreciable or total loss of coating while a second specimen survived an identical rocket firing with little or no damage. All specimens of each coating system were nominally identical; in most cases the two specimens tested were plasma sprayed simultaneously. The conflicting results seemed to be due to subtle and undetected differences in either the coating operation and/or in the rocket firings.

One specimen-to-specimen difference likely to occur during coating application is a variation of layer and total coating thicknesses, which may result in appreciable differences in temperature and heat-flux profiles through the coating during rocket firings. Coating thicknesses were determined from the change in total specimen thickness as indicated by a series of micrometer measurements taken inside the spray chamber. Because the 0.002 to 0.0035-in. thickness of individual coating layers constituted only about 0.4 to 0.7 percent of the total measured thickness of approximately 0.5 in., improper coating thicknesses could result from very slight errors in micrometer measurements; the measurement difficulty is illustrated by Specimen 1, whose actual total coating thickness was found to be roughly one-third the value measured by micrometer. Uncertainties in coating thickness are unavoidable with the micrometer measurement technique, but the magnitude of the error in this instance was unusually excessive. It was recognized that development of techniques for making precise nondestructive thickness measurements on the thin complex coatings involved would require research and experimentation beyond the scope of this program.

Coating edge effects may also be introduced during plasma spraying due to stresses at specimen edges. The relatively sharp corners required to provide a tight seal between the specimen and the rocket motor also contribute to stresses in the coating near specimen edges. In efforts to reduce these effects, specimens were "oversprayed" to prevent increased coating thickness at the edges and the coating was extended part way down the sides of the specimen blocks.

*Run 6 was not included in the time average. This run misfired, resulting in a low-pressure (approximately 40 psia) plateau in the pressure curve (cf., Figure 18).

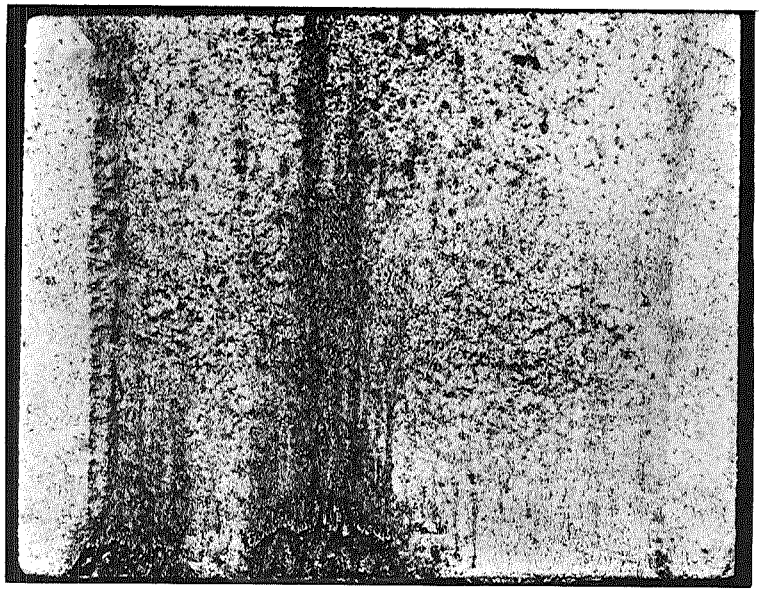

3X 5D093

a. Specimen 15

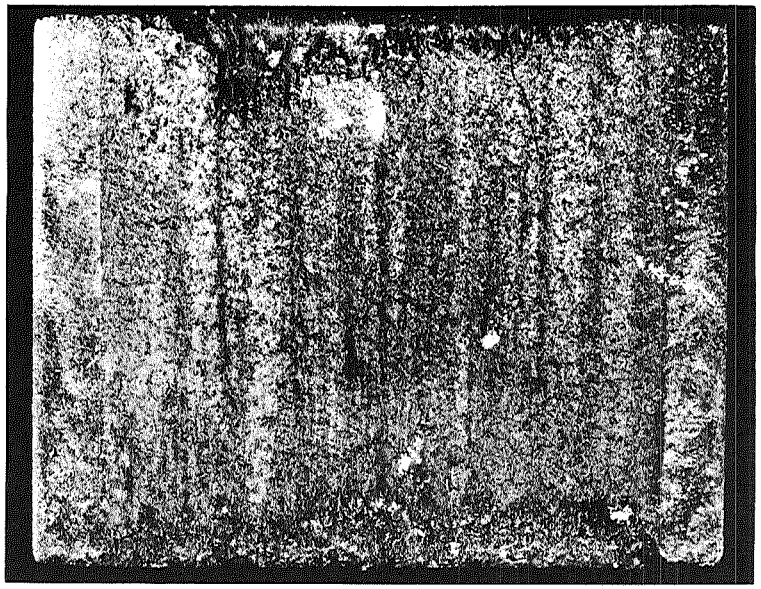

3X 5D509

b. Specimen 1-1

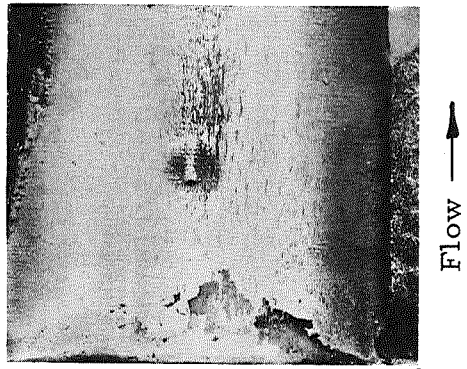

2X 5D089

c. Specimen 1-2

FIGURE 20. UNCOOLED, SOLID-BLOCK SPECIMENS (COATING SYSTEM 1) AFTER SHORT-TERM ROCKET-FIRING TEST

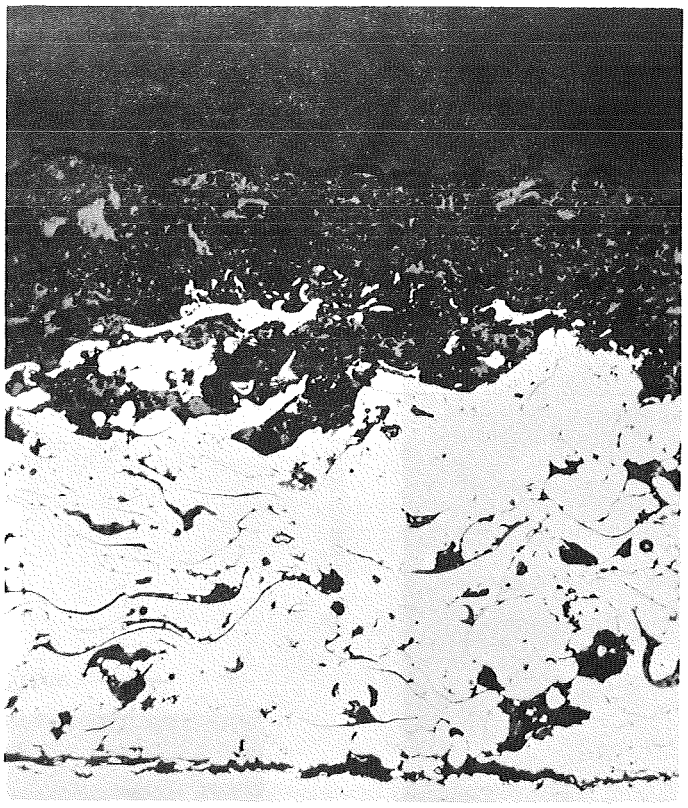

250X 5D328

a. Area Not Exposed to Rocket Exhaust

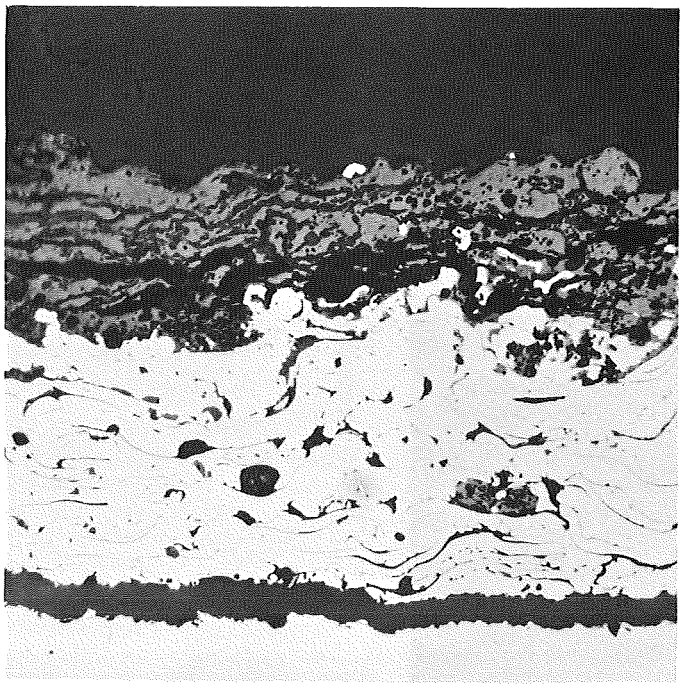

250X 5D329

b. Area Exposed to Rocket Exhaust

FIGURE 21. MICROSTRUCTURE OF SPECIMEN 15 (COATING SYSTEM 1) AFTER SHORT-TERM ROCKET-FIRING TEST

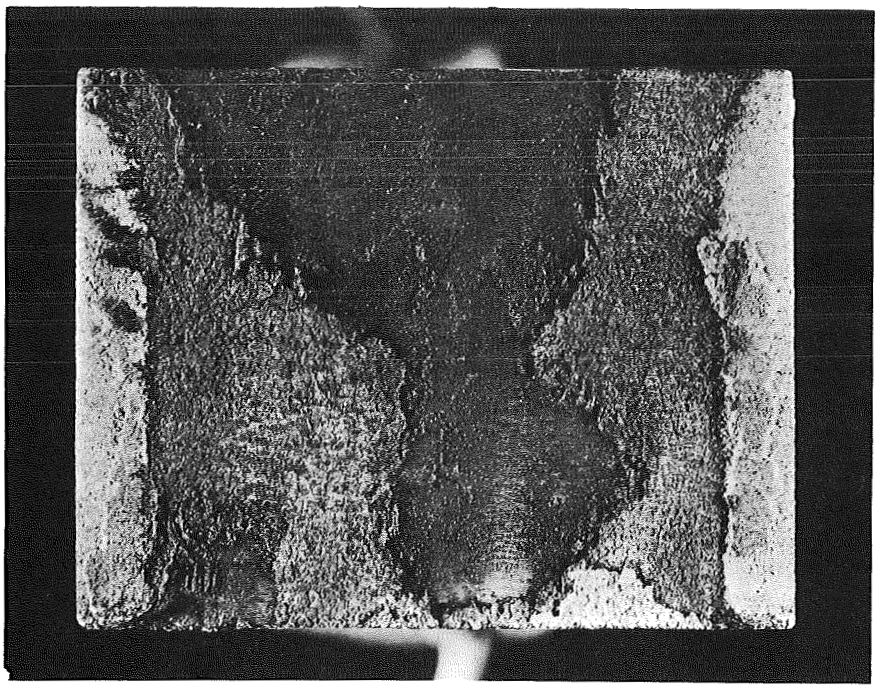

3X 5D091

a. Specimen 20 After Three Rocket Firings

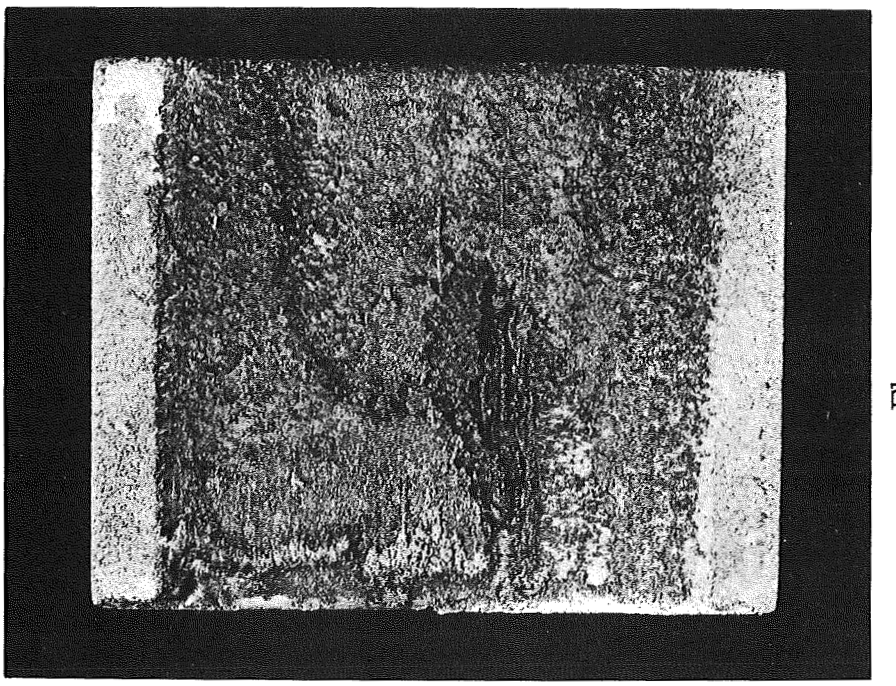

3X 5D510

b. Specimen 2-2

FIGURE 22. COATING SYSTEM 2 UNCOOLED SOLID-BLOCK SPECIMENS AFTER SHORT-TERM ROCKET FIRINGS

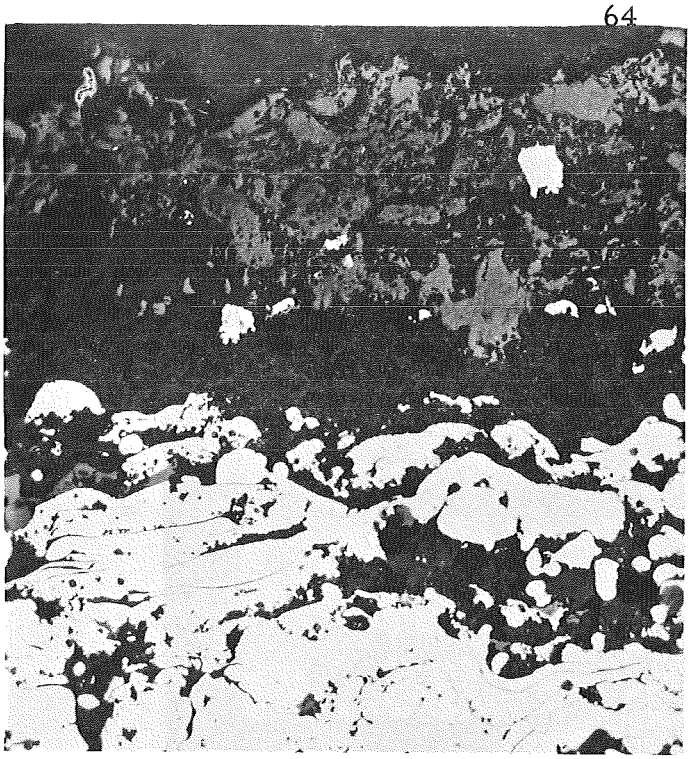

250X 5D330

a. Area Not Exposed to Rocket Exhaust

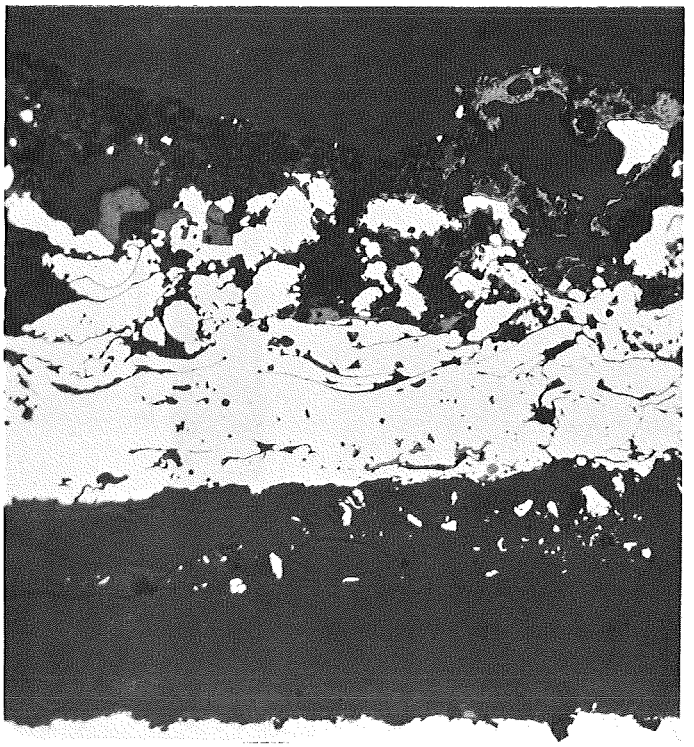

250X 5D331

b. Area Exposed to Rocket Exhaust

FIGURE 23. MICROSTRUCTURE OF SPECIMEN 20 (COATING SYSTEM 2) AFTER THREE ROCKET-FIRING TESTS

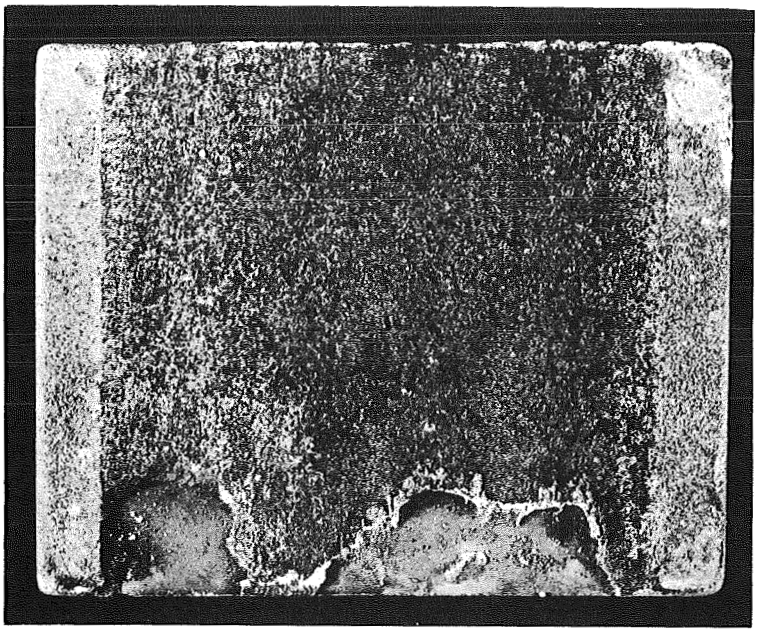

3X 5D511

a. Specimen 3-1

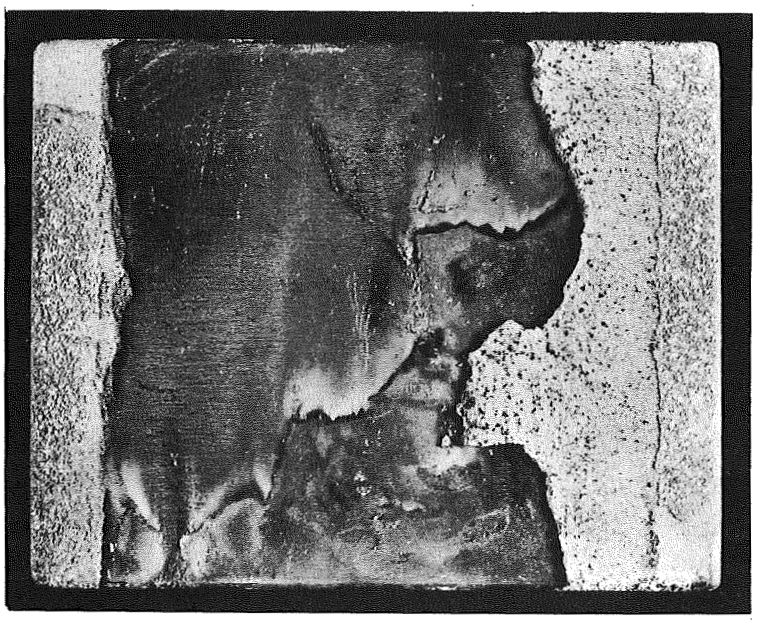

3X 5D512

b. Specimen 3-2

FIGURE 24. UNCOOLED, SOLID-BLOCK SPECIMENS (COATING SYSTEM 3) AFTER SHORT-TERM ROCKET-FIRING TEST

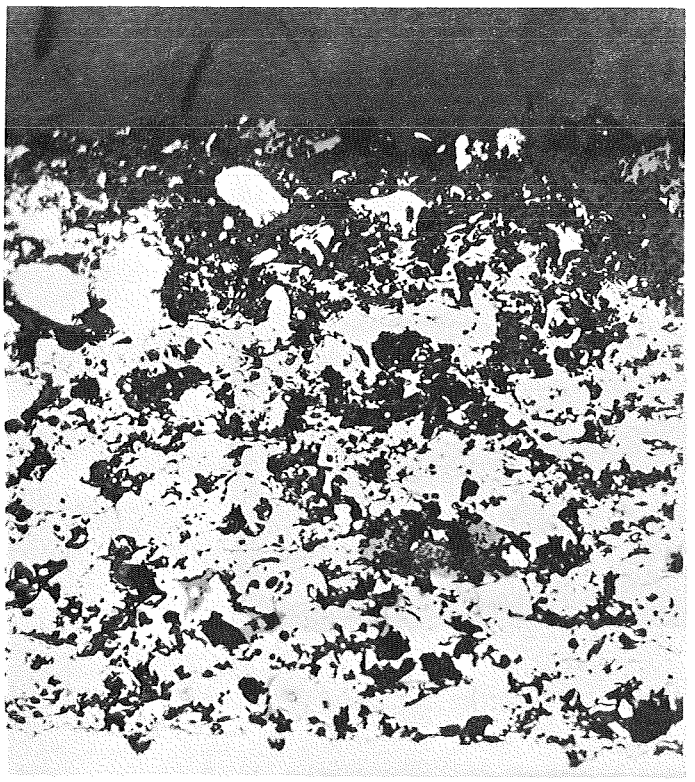

250X 5D843

a. Area Not Exposed to Rocket Exhaust

250X 5D842

b. Area Exposed to Rocket Exhaust

FIGURE 25. MICROSTRUCTURE OF SPECIMEN 3-1 (COATING SYSTEM 3) AFTER ROCKET-FIRING TEST

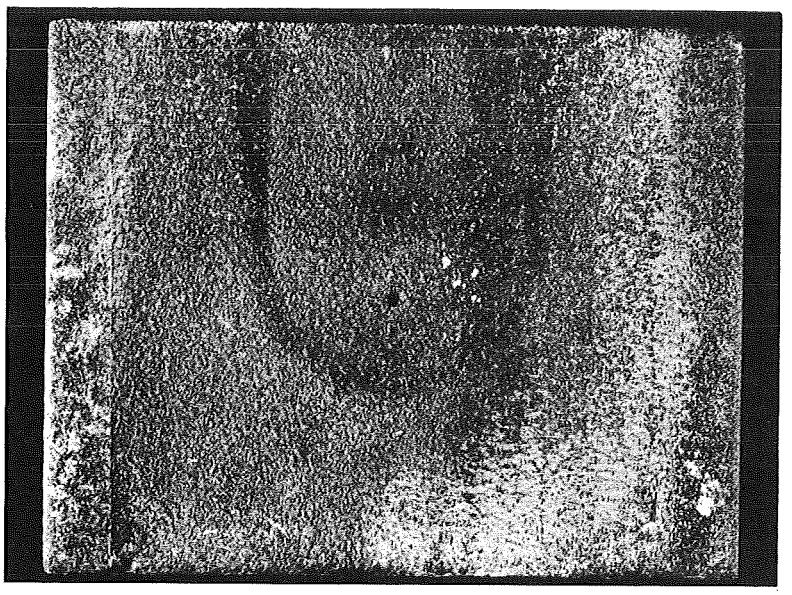

3X 5D508

a. Specimen 1

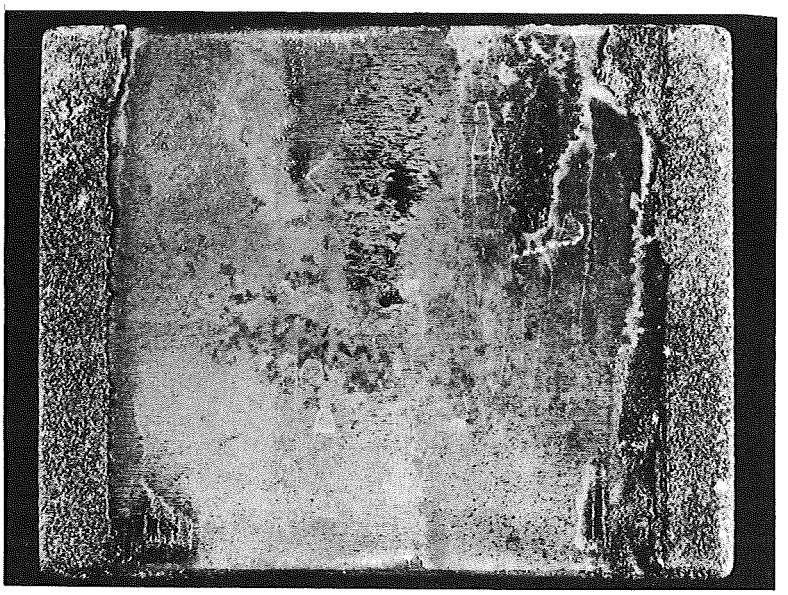

3X 5D513

b. Specimen 4-2

FIGURE 26. UNCOOLED, SOLID-BLOCK SPECIMENS (COATING SYSTEM 4) AFTER SHORT-TERM ROCKET-FIRING TEST

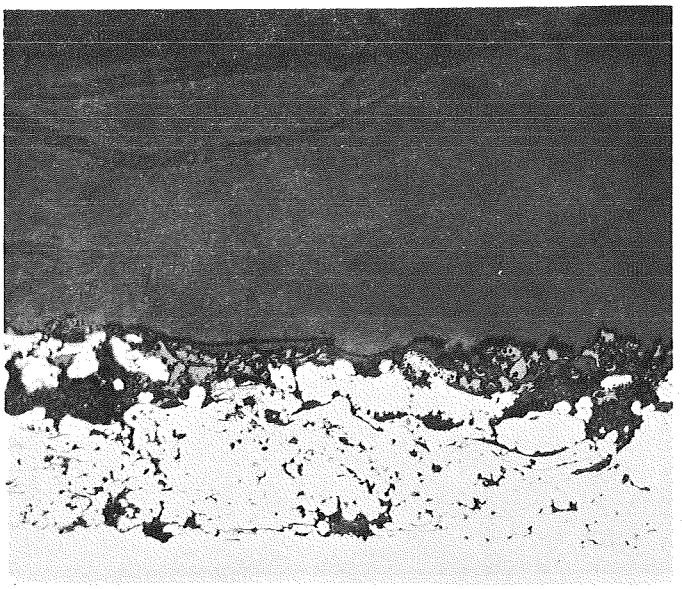

250X 5D844

a. Area Not Exposed to Rocket Exhaust

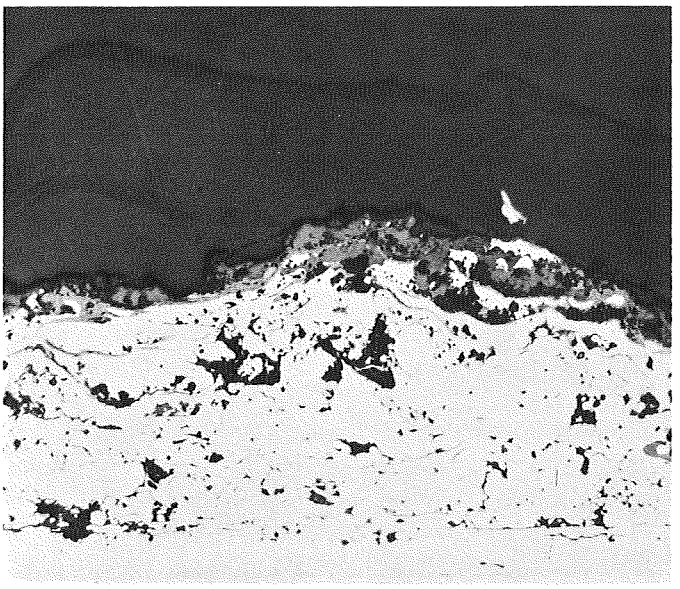

250X 5D845

b. Area Exposed to Rocket Exhaust

FIGURE 27. MICROSTRUCTURE OF SPECIMEN 1 (COATING SYSTEM 4) AFTER ROCKET-FIRING TEST

The primary difference among specimens during testing was thought to be the location of the specimen surface relative to the rocket-motor slit. Every effort was made to align specimens so that the coating surface was a few mils below the lower edge of the motor slit, but precise alignment was made difficult by the deep and narrow (1 by 1 by 1/8 in.) slit formed by the specimen, calorimeter, and spacer bars. If any portion of the coated specimen projected into the motor slit, the edge of the coating would be directly exposed to the high-velocity exhaust gases during a rocket firing. The coating could be easily spalled or entirely removed under such conditions, particularly if residual stresses were present at the coating edge as discussed above. Such direct exposure of the coating edge would not be encountered in actual service of the coating in a rocket nozzle of circular cross section.

Interpretation of Test Results on Uncooled Specimens and Selection of Final Coating System

Coating System 1 was most effective in maintaining a low substrate surface temperature in two tests, and suffered only minor loss of coating. In tests on Spec. 1-2, however, the coating was completely lost. In this case, the coating apparently spalled off after run completion since no rapid rise in temperature occurred during the run to indicate loss of coating. The results of the single-fire, short-term tests raised serious doubts of the ability of this system to withstand subsequent rocket startups. One cause for concern was the marked dark-colored striations on the surface on both Coating System 1 specimens. Because these striations did not appear on specimens of any other system, it was thought that they could be the result of oxidation of the niobium reinforcement present in the three intermediate coating layers. Such oxidation would result in a low-melting eutectic oxide which would continuously degrade the coating. Even if this problem were to be overcome by elimination of the niobium component, a serious difficulty would still remain. As discussed earlier, measurements indicated a very low coating bond strength for Coating System 1. A postulated explanation of the lack of bond strength is that the coating system contained no material which forms an effective barrier to oxygen diffusion to the substrate surface. Any oxygen or moisture impurity present during plasma spraying could diffuse through the coating and form an oxide on the heated, easily oxidizable Hastelloy substrate, thereby contributing to an expansion mismatch and weakening the bond. Areas of oxide (dark phase) at the coating-substrate interface may be seen in Figure 21a. Oxidation and resultant coating separation is even more apparent in the portion of the specimen exposed to the rocket exhaust (Figure 21b). Thus, Coating System 1 was rejected on the basis of loss of coating constituents and marginal bond strength; it was thought that both factors would lead to serious problems during long-term runs or subsequent rocket restarts.

Coating System 2 was rejected for further study on the basis of the excessive erosion and coating loss apparent in Figure 22 and oxidation and coating separation, as shown in Figure 23b.

In tests on Coating System 3, the entire coating was lost on the first test and partial adhesion was maintained in the second test. Of greater consequence, oxidation and separation were noted at the coating-substrate interface in the fired area; the interface is not shown in Figure 25b, however. Although oxidation and separation were not as severe as that for Coating System 2, it was thought that subsequent restarts and/or longer term firings would probably further oxidize the substrate and lead to inadequate

bond strength. Previous measurements had indicated a moderate bond strength before testing. Coating System 3, therefore, was considered to be marginally satisfactory.

The coating of one of the Coating System 4 specimens (Specimen 1) was essentially unaffected by the rocket firing. No spalling or erosion occurred (Figure 26a), and almost no oxidation or separation was detected at the substrate-coating interface (Figure 27). Specimen 4-2, however, showed complete loss of coating as shown in Figure 26b. This was attributed to a poor interface bond during specimen preparation. The successful behavior of Specimen 1 was attributed to the use of Type 304 stainless steel as the substrate, giving initial layers which were less susceptible to oxidation than the Hastelloys used in the other three systems. Also, pretest measurements indicated a Coating System 4 bond strength which was three to five times greater than that of any other coating system as noted earlier. It is apparent, however, that additional work is required to achieve specimen uniformity. Figure 27 shows that a good bond was present on Specimen 1 before testing and was not degraded during the rocket firing. The only negative aspect of Coating System 4 was the excessively high substrate surface temperature attained during the rocket firing. However, Figure 27 shows that the thickness of the total coating system was thinner than that desired and that the two outermost oxide layers were extremely thin (<1 mil rather than the desired 5.5 mils). In a coating of the proper thickness, roughly three-quarters of the thermal gradient occurs across the outermost oxide layers. Thus, the extreme thinness of these layers on the tested specimen account for the high temperatures attained. The effectiveness of an outermost layer of ThO_2 to withstand a large thermal gradient and thermal stress without spalling was demonstrated by the lack of ThO_2 spalling in the case of the Coating System 1 specimens even after apparent loss of the niobium reinforcement. Therefore, it may be expected that the required thermal gradient would be generated and accommodated without spalling on a System 4 coating of the proper thickness. Thermal diffusivity data presented earlier indicated that a System 4 coating of the proper thickness should constitute an even more effective barrier than expected from initial calculations. The thinness of the specimen coating can only be accounted for by errors in measurement caused in part by the difficulty of making in-chamber measurements during coating application. Therefore, on the basis of the expectation of an acceptable temperature gradient with a coating of the proper thickness, the very high measured values of coating bond strength, and the lack of oxidation and separation at the coating-substrate interface, Coating System 4 was selected for further study.

Rocket Firings With Water-Cooled Specimens

A total of six water-cooled specimens were tested with Coating System 4. All specimens were fabricated as outlined in the section on preparation of specimens. Test plans required that one specimen was to be exposed to the rocket conditions at an equivalent cold-wall heat flux of 30 Btu/(in.^{2})(sec) for three repeated starts and three specimens were to be subjected to continuous exposure at the same heat flux at increasing times of 10, 30, and 60 sec. Of the remaining two specimens, one was to be fired 4 sec under oxidizing conditions while the other was to be fired 4 sec under reducing conditions.

The first water-cooled specimen of Coating System 4 was exposed to a 4-sec rocket firing using an oxidizing fuel mixture. Failure of the rocket-motor nozzle and the specimen occurred during the run, and the specimen was totally destroyed. Abrupt,

erratic changes in all parameters monitored on the strip chart indicated that failure began at approximately 2.5 sec. The failed nozzle and specimen are shown in Figures 28 and 29, respectively.

Sufficient evidence was not available to positively determine the cause of failure; however, several possible modes were considered. Metallographic examination of the motor nozzle indicated a weld repair which had been made prior to the start of the present program. Continuous firing over the repair may have caused oxidation of the copper and failure at the nozzle slit due to loss of heat transfer. Alignment of the specimen with the motor-nozzle slit is critical and a slight mismatch could have blown off the coating and caused melt-down of the nozzle following failure of the test specimen. Alternatively, the coating could have been deficient or cooling channels could have been blocked; however, the condition of the specimen precluded determining these possible defects. Since cooling flow was satisfactory prior to testing, however, and had been checked during plasma spraying and after installation in the rocket engine, the latter was considered unlikely.

A new nozzle was installed in the rocket motor and successfully tested in several preliminary firings. Because of the previous failure it was decided to proof test each subsequent specimen by firing for 1 sec at maximum I_{sp} prior to further testing.

Specimen TC-8 was fired under the conditions listed in Table 21 three consecutive times at 1 sec. Visual examination of the specimen after each cycle indicated no severe degradation of coating, and the specimen was removed after the third firing.

Specimen TC-4 was installed and run for 1 sec as a proof test. At the end of the firing a water leak was noted and visual examination indicated spalling of the coating. Accordingly, the specimen was removed.

Specimen TC-7 was installed and proof tested for 1 sec. On visual examination it was noted that spalling had occurred in several areas in a manner similar to that observed in Specimen TC-4. Spalling of two consecutive specimens at 1 sec indicated severe coating-adhesion difficulties; however, on the basis of three successful restarts of 1 sec on Specimen TC-8 another proof test was scheduled.

Specimen TC-2 was fired for 1 sec using conditions identical to the previous three specimens. On visual examination no degradation of the coating was noted. No recording of backface temperature was obtained, however, because of thermocouple failure. In order to obtain additional data without total specimen destruction and on the basis of the successful restart behavior of Specimen TC-8 it was decided to limit subsequent firings to 4-sec intervals. A new thermocouple was also installed and checked in order to obtain a backface temperature for the next firing. Specimen TC-2 was then fired for 4.23 sec and examined visually. At this point, it was noted that spalling of the specimen coating had occurred in localized areas, but the absence of fluctuations in monitored parameters prevented estimation of when spalling occurred.

At this point it was decided to proof test the remaining sample, Specimen TC-6A, for 1 sec and schedule short-duration tests of intervals of 2 sec to determine the point of coating failure. The specimen, however, failed by a severe water leak during the 1-sec proof test. During this test, the coolant flow rate was considerably less than that measured previously (0.66 and 0.83 lb/sec, respectively), indicating that cooling channels in the specimen may have been blocked by excess braze material.

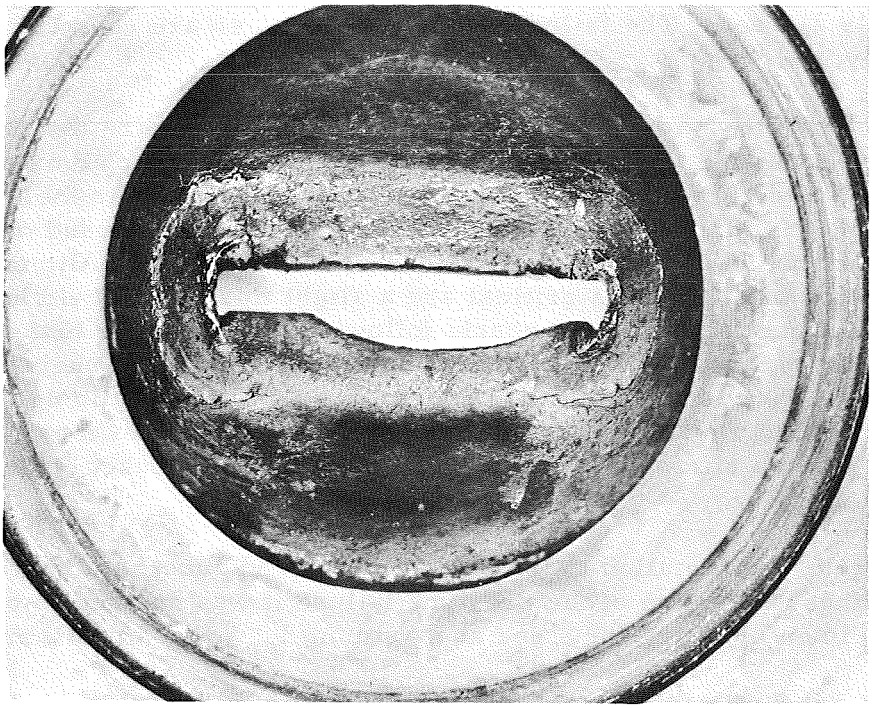

2X 8D730

a. Chamber Side, Showing Repaired Area

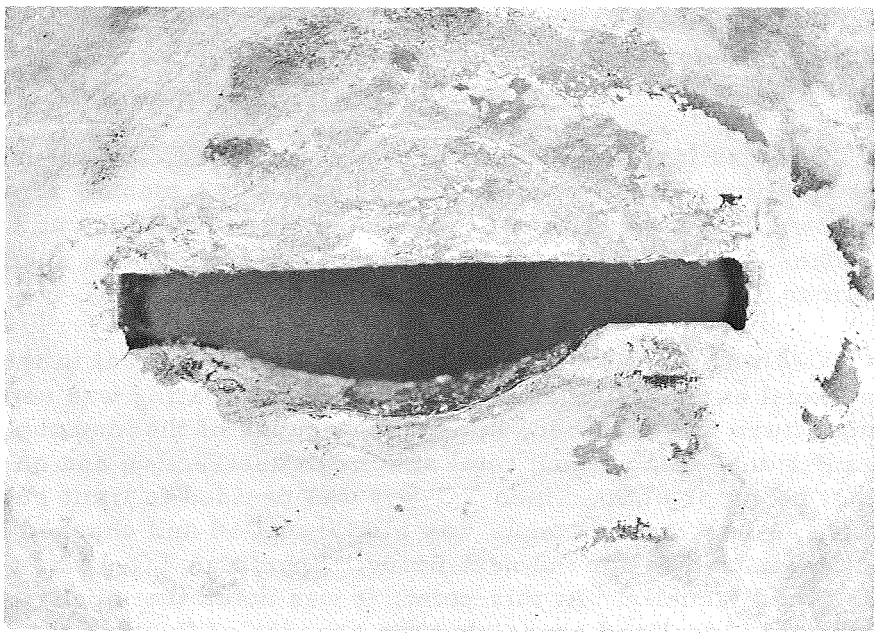

3X 8D731

b. Exit Side, Showing Fracture Cracks

FIGURE 28. FAILED ROCKET-MOTOR NOZZLE USED IN FIRST TEST ON A WATER-COOLED SPECIMEN OF COATING SYSTEM 4

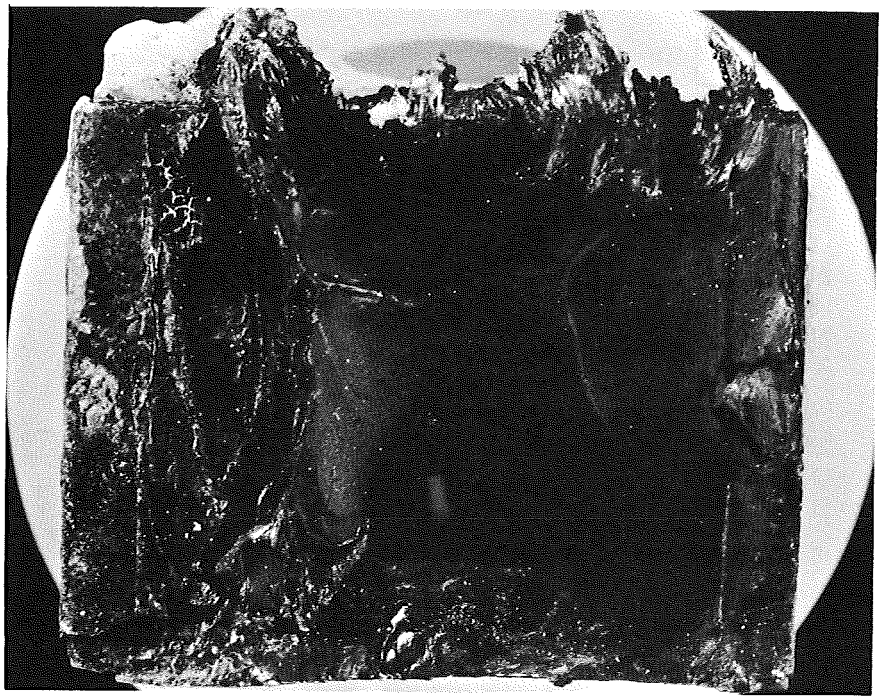

FIGURE 29. WATER-COOLED SPECIMEN DESTROYED BY ROCKET-MOTOR FAILURE

TABLE 21. FIRING CONDITIONS FOR COATING SYSTEM 4 WATER-COOLED SPECIMENS

	Run 15	Run 17A, B, C	Run 18	Run 19	Run 20	Run 21
Specimen Thermocouple No.	TC-12	TC-8	TC-4	TC-7	TC-2	TC-6A
Maximum Chamber Pressure, psia	--	385	383	385	440	398
Test Duration, sec	4.0(a)	~1/~1/~1	1.02(b)	0.98	0.99/4.23	1.0(b)
Maximum Temperature Indicated by Specimen Thermocouple, F	--	165/165/165	359	121	--	296
Maximum Surface Temperature, F	--	2525/2450/2500	3020	2875	2765/2600	2075
Specimen Coolant-Flow Rate, lb/sec	--	0.90	0.83	0.83	0.83	0.66
Condition of Coating After Test	(a)	Did not spall	Spalled	Spalled	Spalled (2)	--

(a) Catastrophic failure of motor/specimen. Data invalid.
(b) Specimen leakage through substrate.

Table 21 summarizes the pressure-temperature coolant rate-time relationships for the tests. Because of the relatively short time intervals of the firings, steady-state conditions were not achieved and heat flux would not have reached maximum values.

Thermocouple output was low, which may have been caused by poor thermal contact with the spring-loaded system utilized for the 0.010-in.-diameter sheathed couples. In addition, the surface temperature data, while consistent, must be considered on the basis of the uncertainty in emissivity data and the transparency error which would be encountered with the coatings at high temperature.

The combination of uncertainty in temperature data on both sides of the coating coupled with the lack of steady-state data precludes the calculation of meaningful heat-transfer data for the coatings.

Interpretation of Test Results on Cooled Specimens

All specimens fired in the tests in which water cooling was employed were examined metallographically to determine the mode of failure. Spalling of the coating was noted in some degree in all specimens; however, the depth and degree of spalling varied widely. Figure 30 illustrates the surface of Specimen TC-8 after three consecutive restarts. Visual examination by low-power microscope indicated that only a portion of the outermost layer of thoria had been removed, with no coating cracking. This was confirmed in examination of the metallographic sections shown in Figure 31. Comparison of the unexposed coating under the hold-down fixture with an area in the center of the test specimen indicated only the erosion of thoria. It should be also noted that the thoria on all coatings was dark in the plasma-sprayed condition, indicating substoichiometric composition in respect to oxygen. After the firings, the thoria assumed normal coloration, indicating oxidizing conditions. The photomicrographs in Figure 31 indicate good bonding between the first plasma-sprayed layer of stainless steel and the stainless substrate but show that the total coating was only about one-half the intended thickness.

Examination of Specimen TC-7 (Figure 32) indicated spalling both to the intermediate layers and to the substrate after the 1-sec firing. Photomicrographs showing the intermediate-layer spalling as well as the structure existing in the original coating are presented in Figure 33.

A similar failure occurred in Specimen TC-4 after a 1-sec run; however, a water leak through the substrate was also found. Figure 34 shows a larger degree of spalling to the substrate as compared to that which occurred in Specimen TC-7 (Figure 32); however, the water quench from leakage on rocket-motor shutdown would contribute to shock and spalling of the coating. The failed area of Specimen TC-4 (Figure 35) shows blocking of approximately one-third of the water channel, which would reduce cooling; however, the total water flow for the specimen was comparable to others which did not fail, and spalling occurred in a uniform manner over the surface of the specimen. The photomicrographs which enable comparison of the area exhibiting interlayer spalling with the unexposed area under the hold-down fixture are shown in Figure 36. Again, substrate bonding appears satisfactory; however, failure occurred in the coating layers.

Specimen TC-2, which was exposed to a 1-sec firing followed by a 4-sec firing, lost the coating in selected areas by interlayer failure, as shown in Figure 37. Photomicrographs in Figure 38, showing the unfailed fired area and the unexposed area,

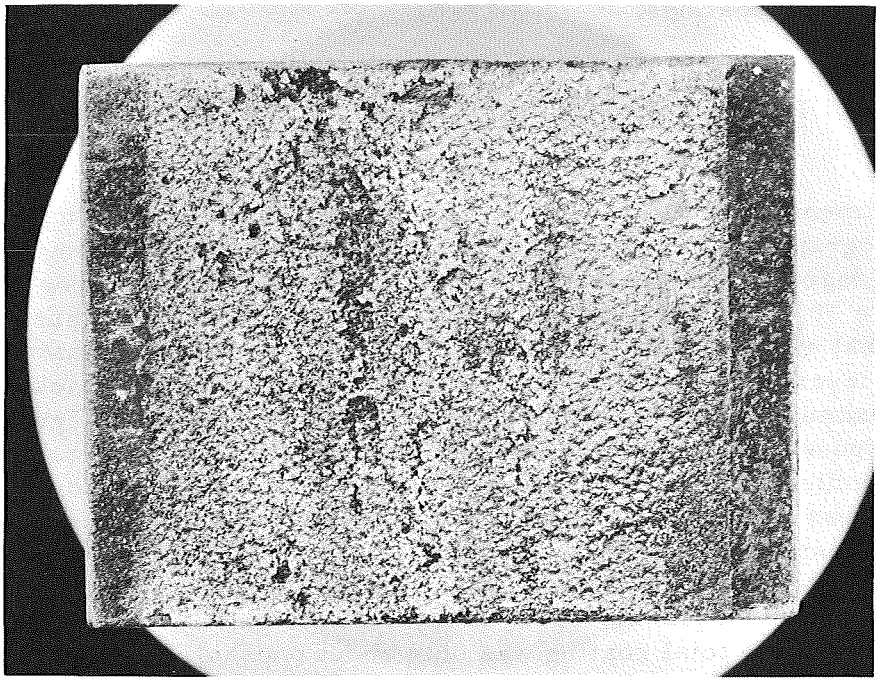

FIGURE 30. SURFACE OF SPECIMEN TC=8 AFTER THREE CONSECUTIVE 1-SECOND ROCKET FIRINGS

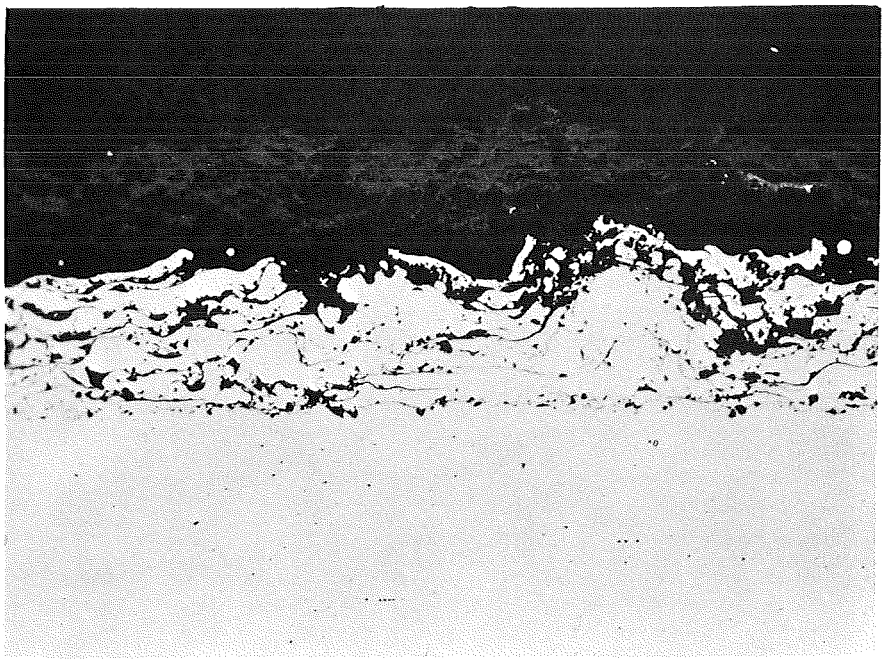

250X 9D485

a. Unexposed Under Hold-Down Fixture

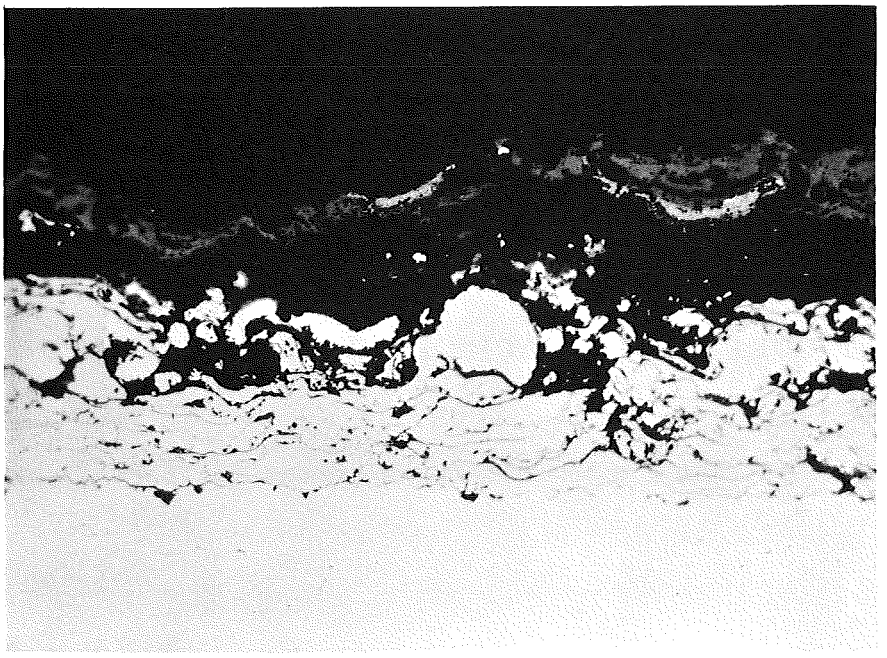

250X 9D486

b. Exposed to Rocket Environment

FIGURE 31. STRUCTURE OF COATING SYSTEM 4 ON SPECIMEN TC=8

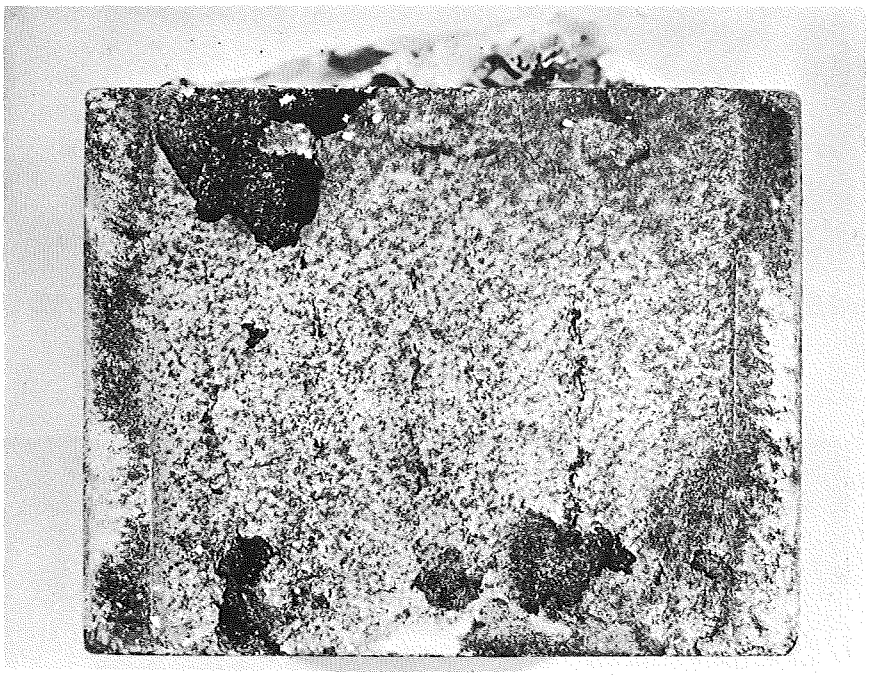

4X 9D269

FIGURE 32. SURFACE OF SPECIMEN TC=7 AFTER 1-SECOND ROCKET FIRING

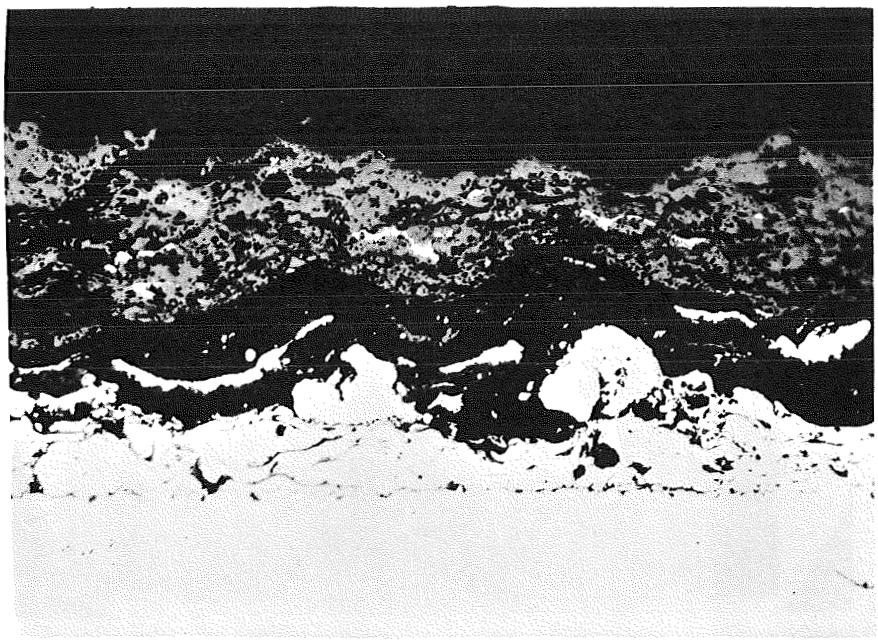

250X 9D493

a. Unexposed Under Hold-Down Fixture

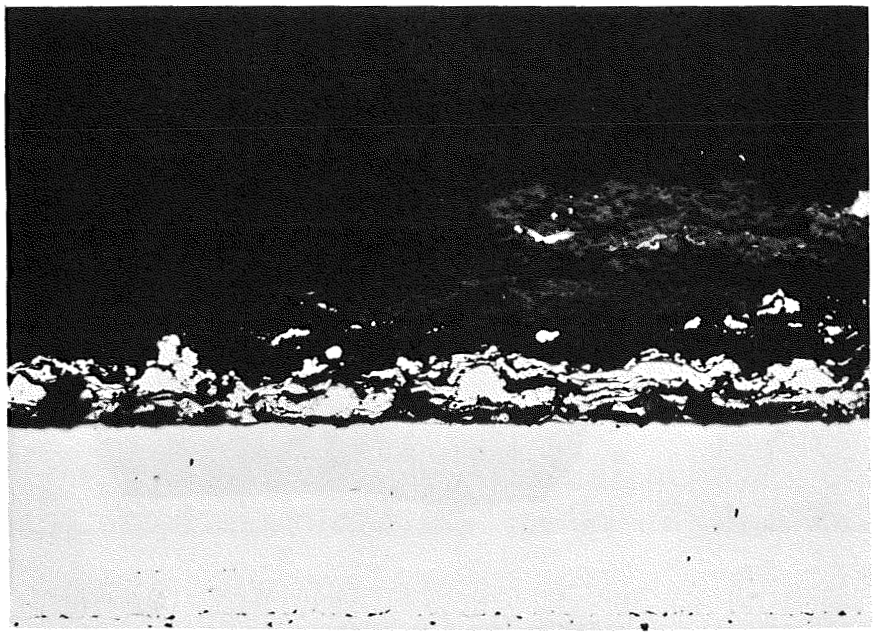

250X 1E574

b. Exposed to Rocket Environment

FIGURE 33. STRUCTURE OF COATING SYSTEM 4 ON SPECIMEN TC=7

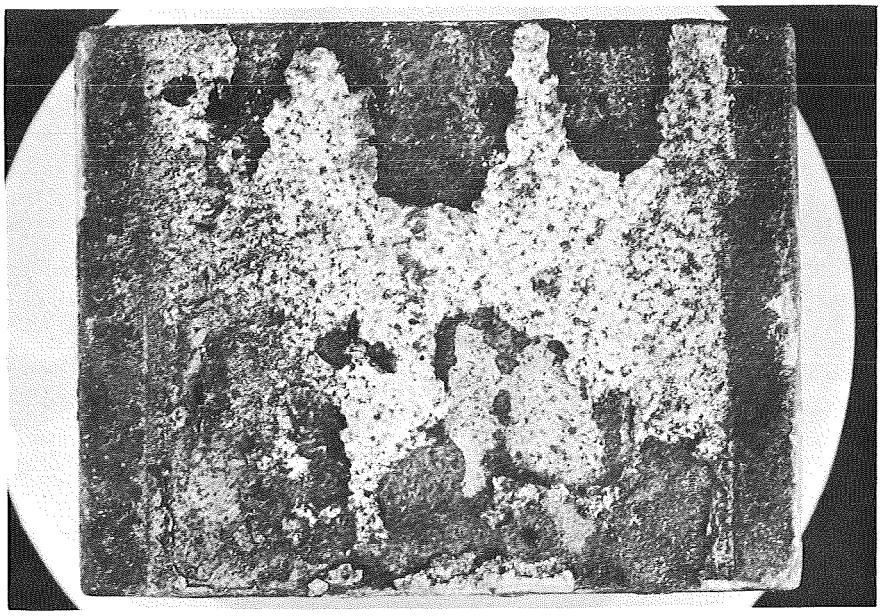

4X 9D272

FIGURE 34. SURFACE OF SPECIMEN TC=4 AFTER 1-SECOND FIRING

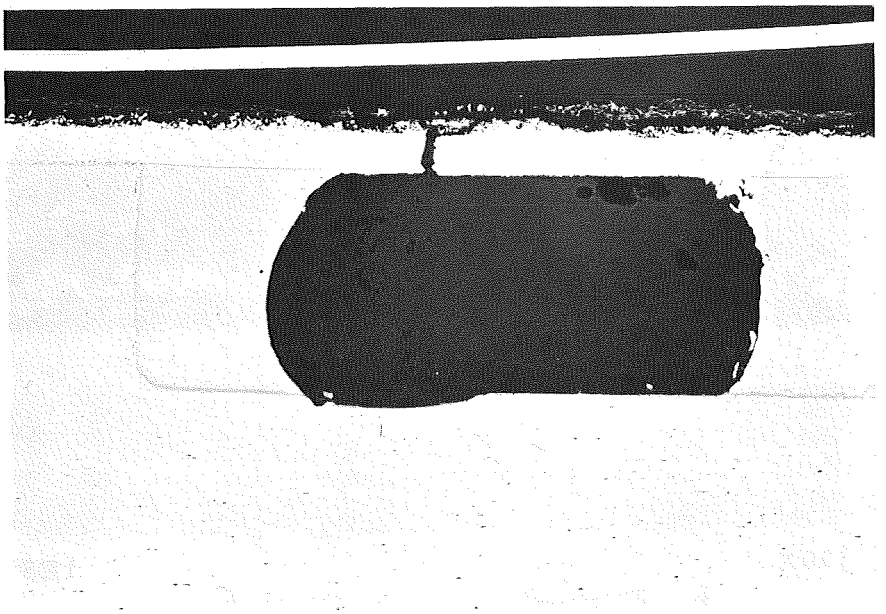

20X 9D496

FIGURE 35. LEAK IN CHANNEL PARTIALLY BLOCKED BY COPPER BRAZE IN SPECIMEN TC=4

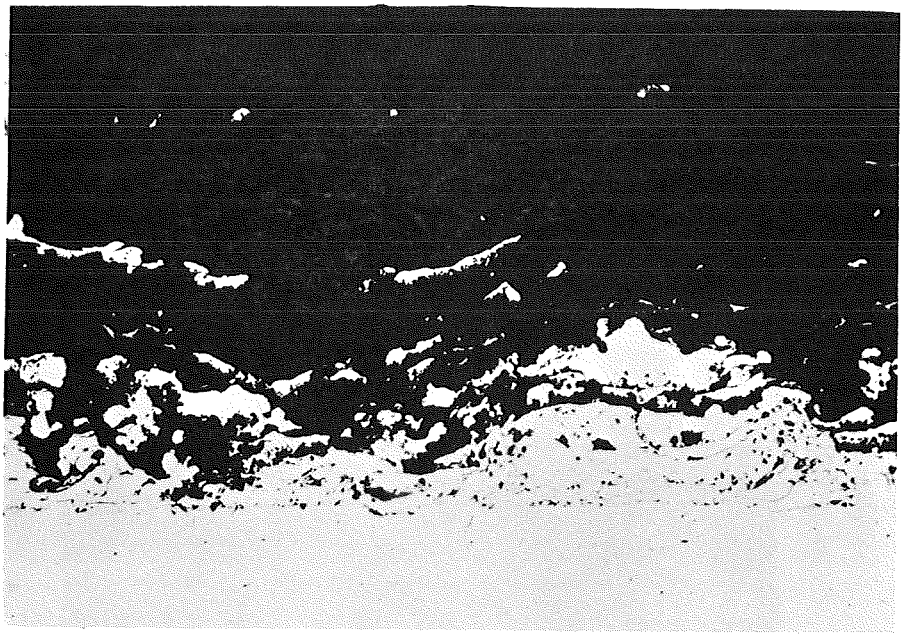

250X 1E570

a. Unexposed Area Under Hold-Down Fixture

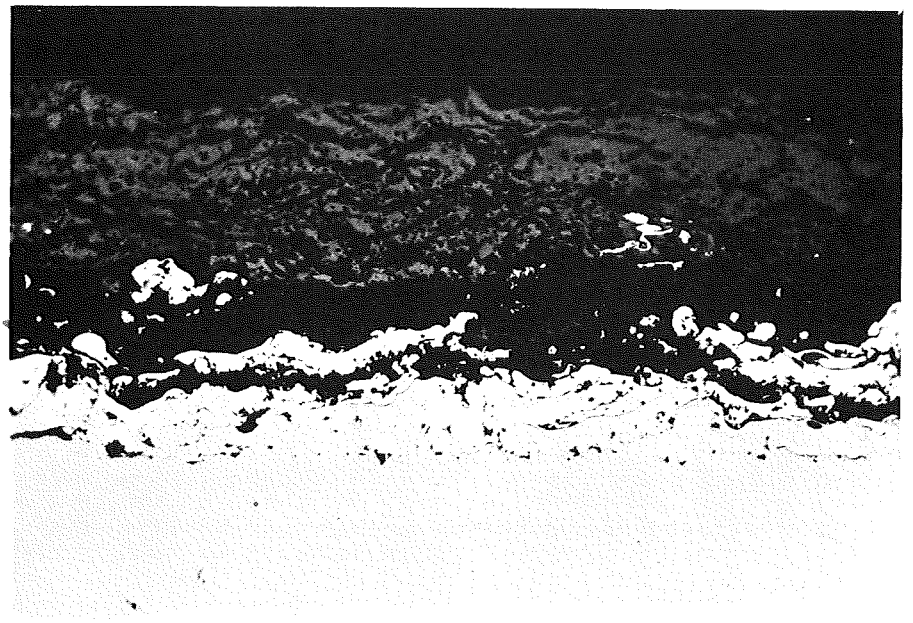

250X 1E571

b. Exposed to Rocket Environment

FIGURE 36. STRUCTURE OF COATING SYSTEM 4 ON SPECIMEN TC=4

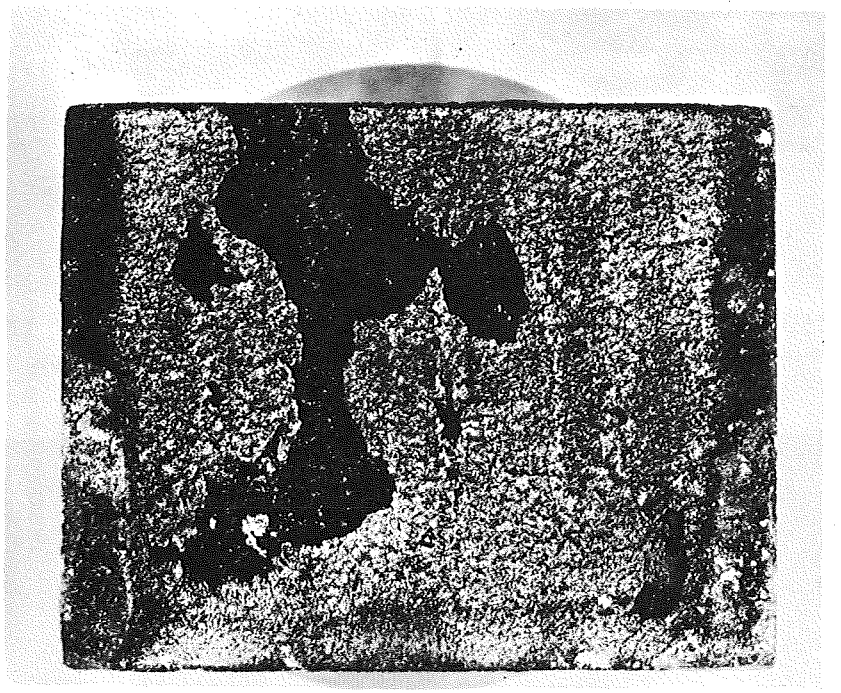

FIGURE 37. SURFACE OF SPECIMEN TC=2 AFTER 1-SECOND AND 4-SECOND ROCKET FIRINGS

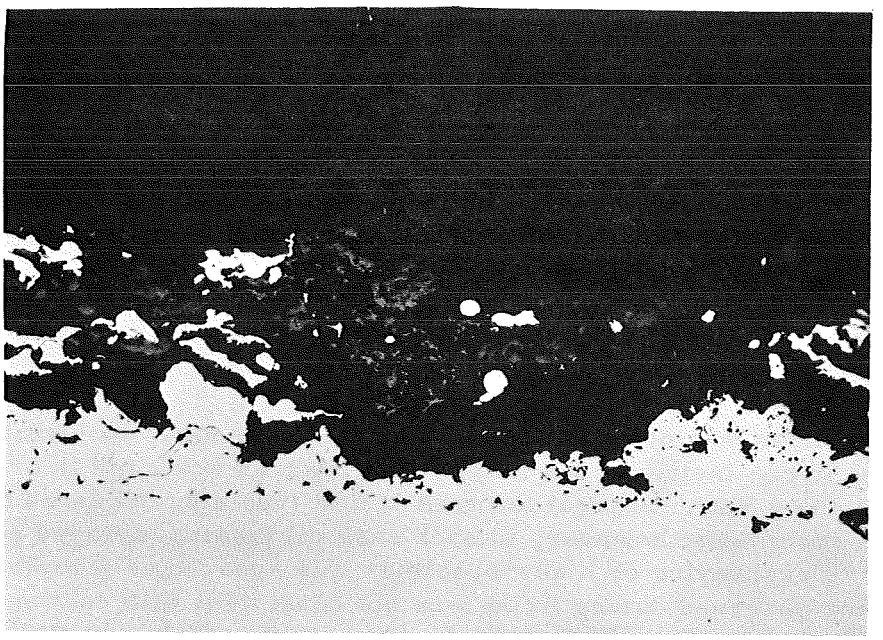

250X 1E575

a. Unexposed Area Under Hold-Down Fixture

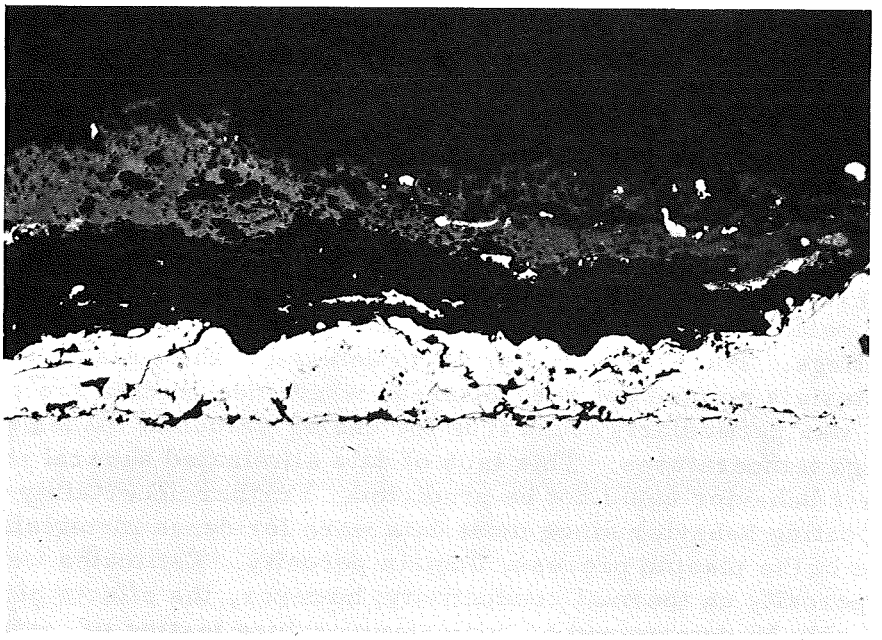

250X 9D492

b. Exposed to Rocket Environment

FIGURE 38. STRUCTURE OF COATING SYSTEM 4 ON SPECIMEN TC=2

reveal very little loss of thoria and no interlayer failure, indicating the possibility of producing coatings which can successfully withstand the environment.

An attempt to repeat the experiment on Specimen TC-6A again gave failure in the coating, as shown in Figure 39, accompanied by water leakage. Sectioning of the water-channel area again showed blockage by braze metal, as exhibited in Figure 40. In Figure 40 it can also be noted that removal of the coating was complete over a wide area and blockage by the braze alloy also occurred in the adjoining channel.

Photomicrographs of the unfailed exposed coating area and the unexposed coating in Figure 41 show that the thoria layer was not sprayed to the required thickness and that separation of the coating at the substrate had occurred.

Although failure was noted in the sprayed stainless steel-to-stainless steel substrate interface in one instance, the majority of failures occurred in or adjacent to the layers containing BeO. Several failures of this type also occurred during plasma spraying of the specimens; however, in each case all plasma-sprayed coatings were removed prior to respraying or a new specimen was sprayed as a replacement. The spalling behavior observed during firing was not consistent with coating bond strengths in excess of 3900 psi for Coating System 4 as reported in Table 19 and should not occur, according to calculations of (Z) stress reported in Table 10, which show compressive stresses in coating and substrate in the region of interface. However, the calculated tensile stress in the BeO layer and observed behavior are in agreement. Close examination of specimen areas which did not fail when exposed to cyclic operation or times up to 5 sec did not reveal potential failure areas. On this basis it is apparent that additional studies of coating variables and strength behavior under simulated test conditions are required.

DISCUSSION OF RESULTS

Although the program was separated into two primary tasks, several distinct subtasks were performed which contribute to the technology of the development of protective coatings. The literature survey to determine the suitability of existing refractory materials pointed out several areas where design data are conflicting or lacking. This was particularly found true for use of elemental oxides and mixtures of oxides at high temperatures. This lack of data eliminated several potential materials since their behavior could not be predicted. Further uncertainty was introduced in predicting coating behavior since most data were for dense materials and the coatings, by virtue of the plasma process, contain porosity. Estimates were made as to the effects of porosity on thermal conductivity; however, the effects of porosity on strength could only be determined by room-temperature testing of coated specimens. Additional work in determining the high-temperature properties of plasma-sprayed coatings would give a higher confidence level to the selection of materials and the design of coating systems.

Motor tests of coatings formulated on basis of predicted conductivities and firing tests indicate validity of the predictions. Diffusivity measurement indicates a large difference: thus, the need for rationale of difference in test results.

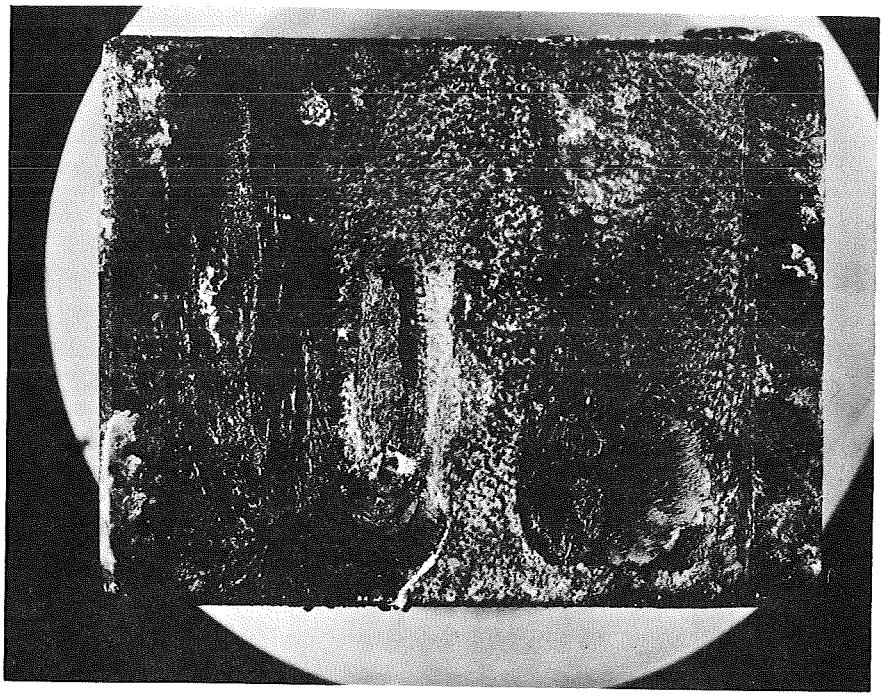

4X 9D268

FIGURE 39. SURFACE OF SPECIMEN TC=6A AFTER 1-SECOND ROCKET FIRING

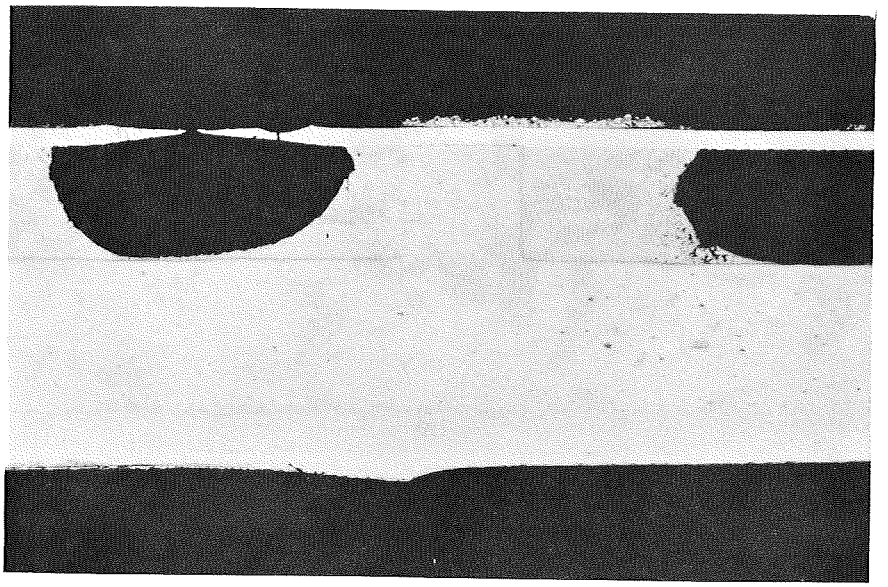

10X 9D495

FIGURE 40. LEAK IN CHANNEL PARTIALLY BLOCKED BY BRAZE IN SPECIMEN TC=6A

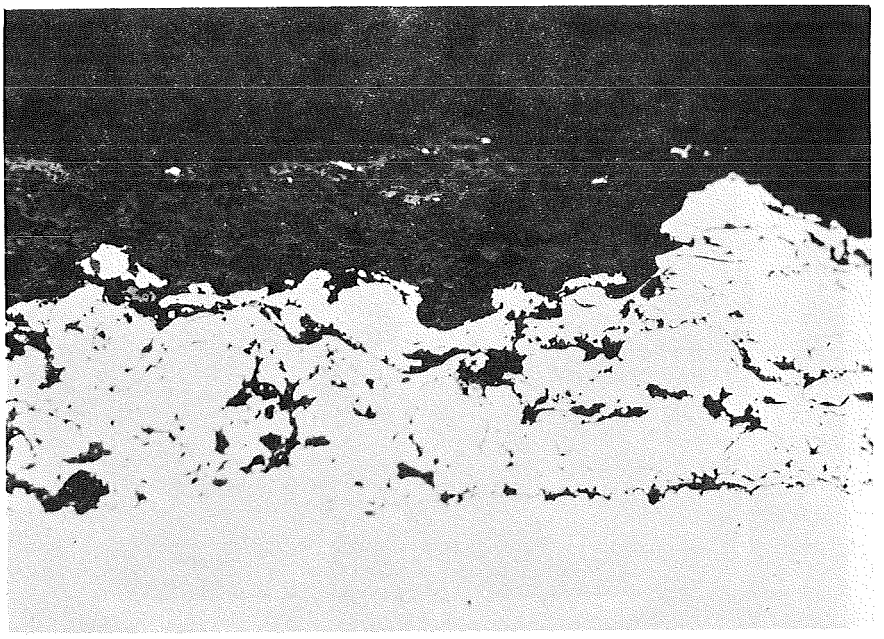

250X 9D489

a. Unexposed Area Under Hold-Down Fixture

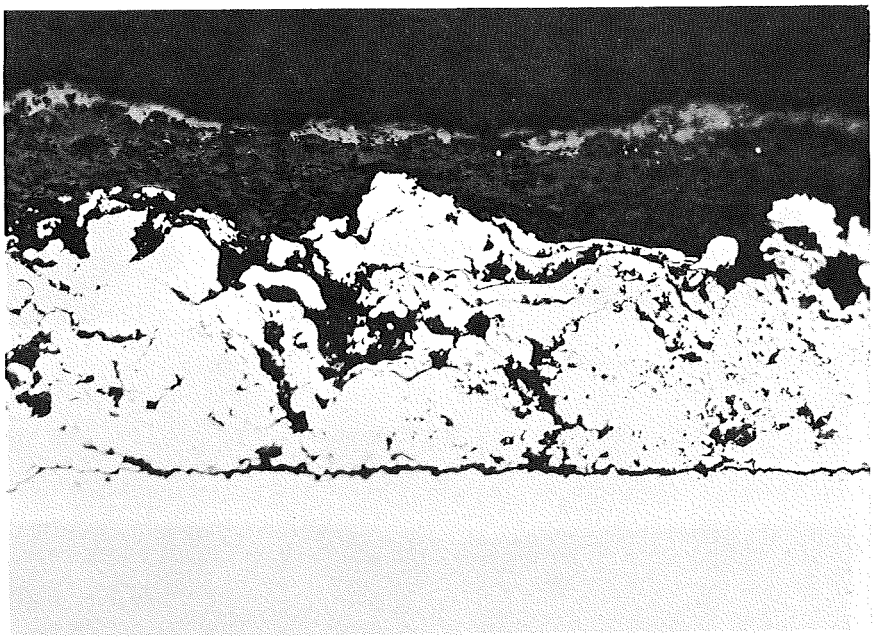

250X 9D490

b. Exposed to Rocket Environment

FIGURE 41. STRUCTURE OF COATING SYSTEM 4 ON SPECIMEN TC=6A

The selection of four coating systems for rocket testing was based primarily on stress due to thermal gradients in the coating layers. Also, an attempt was made where systems had similar stress behavior to select systems which represented "families" of materials. Both adherence and rocket testing, however, indicated that substrate adhesion was poor in the three systems on Hastelloy X, thus preventing conclusions relative to the differences between these systems. It should be pointed out that, with the number of materials selected for the outer coatings and the intermediate layers, more systems were available initially than could be evaluated within the scope of the program. At this point, however, based on the demonstrated need for better substrate adhesion, additional combinations of materials should be evaluated, although the calculated stresses may be somewhat higher.

Since coatings were ultimately to be applied to thin substrates, considerable development was done on substrate preparation and the application of coatings to achieve high bond strength without degradation of the substrate. Values approaching 4000 psi were attained which are in excess of strengths usually obtained by plasma spraying without excessive surface roughening, which in this case would degrade the substrate strength, or without subsequent heat treatment. Further increases in the adherence may be obtained by development; however, added roughening at some degradation of the substrate should be considered.

Conventional plasma spray techniques were modified to obtain thin layers of materials using codeposition. Optimization of this technique for all combinations of materials used was not within the scope of this program; however, a high degree of control was attained in many of the systems. Considerable attention was given to development of parameters for plasma spraying BeO. Although the proposed coatings could be attained, the test results indicated that further development of plasma-spray parameters is required to produce uniform coating properties or that other oxides should be selected. In addition, means should be developed to insure better control of coating thicknesses where extremes of thermal gradient occur.

A small, water-cooled test specimen was developed which is representative of substrate conditions on a regeneratively cooled nozzle. Some change or refinement of this specimen is required to eliminate problems of edge effects, fabrication, and instrumentation. Criticality of installation in the nozzle should be reduced and fabrication details need improvement to eliminate coolant-passage blockage. Temperatures at the coating-substrate interface obtained with uncooled specimens were highly reproducible, leading to the conclusion that future tests involving cooled specimens should incorporate the thermocouple in the substrate. This can be accomplished by brazing the thermocouple into a hole which penetrates the substrate to the coating interface.

Because of uncertainties in gas flow in the throat of the combustor used (due to large surface roughness relative to the throat dimensions), it is highly desirable to make further attempts to measure the gas side temperature of the coating. In this program we were unsuccessful in determining the surface temperature of the thoria, apparently due to the transparency of the coating. This difficulty has been encountered previously in measuring temperature on thin coatings and can only be resolved by determining the emissivity of the coating when a strong temperature gradient is present.

Several water-cooled specimens coated with the System 4 formulation were tested in the rocket motor. Spalling-type failures in or adjacent to the layers containing BeO prevailed in both 1-second or longer tests. Two specimens successfully withstood 1-second tests. One of these was than tested for 4 seconds. Spalling occurred in the

layers containing BeO. It is apparent that thermal-shock temperature gradients are encountered in approaching steady-state operation cause a severe loss of bonding or a reduction of strength. It also is apparent that additional studies of coating-process variables and strength behavior under simulated test conditions are required. Alternately, another oxide such as Al_2O_3 should be considered as a substitute for BeO. Although thermal conductivity is lower, requiring adjustments in layer thickness and content of metallic material, fabrication properties are more favorable.

The tests did indicate that thoria was potentially satisfactory for direct exposure to the rocket exhaust. It exhibited only minor erosion. Since Coating System 4 did not successfully fulfill the requirements in the water-cooled rocket tests, no test of the system was scheduled for firing with hydrogen as a coolant.

In summary, the program was necessarily broad in view of the overall requirements, with scope and time schedules which did not permit the solution of many pertinent problems. However, the information gained in the program provides an insight for the subsequent selection and evaluation of coatings for protection of regeneratively cooled nozzles.

CONCLUSIONS

It has been demonstrated that plasma spraying may be utilized as a technique for applying graded composition coatings to regeneratively cooled nozzles to provide environmental protection and to reduce the effective heat flux to the coolant. Four potential coating systems were fabricated for evaluation in the initial series of uncooled rocket tests; of these, one system was selected for further study in water-cooled rocket tests on the basis of low erosion and resistance to spalling. It is apparent, however, that instabilities exist in the system selected which result in spalling when approaching steady-state rocket firing conditions. Examination of the fired specimens indicated the spalling was caused by a loss of strength or bonding in those layers which contained BeO. It was concluded further studies are required to optimize the spraying parameters for BeO or that the alternate coating systems should be modified on the basis of the data obtained in the program. It was shown that thoria performs successfully as an outer layer to resist erosion by the rocket environment through successive restarts of the motor and for testing periods up to 5 sec. Further studies are required to perfect temperature-measurement techniques for both the substrate and the coated specimen surface.

REFERENCES

(1) Carpenter, H. W., "Heat Barrier Coatings for Rocket Engines", Summary of the Thirteenth Meeting of the Refractory Composites Working Groups, DMIC Memorandum 227 (September 1, 1967), pp. 16-17.

(2) ASM Metals Handbook, Volume 1: Properties and Selection of Metals, 8th Edition, American Society for Metals, Novelty, Ohio (1961).

(3) Lynch, J. F., et al., editors, Engineering Properties of Selected Ceramic Materials, American Ceramic Society, Columbus, Ohio (1966).

(4) Bradshaw, W. G. and Mathews, C. O., "Properties of Refractory Materials", LMSD-2466 (January 15, 1959).

(5) Campbell, I. E., Editor-in-chief, High-Temperature Technology, John Wiley and Sons, New York (1956).

(6) Shaffer, P. T. B., Handbook of High-Temperature Materials, Volume 1-Materials Index, Plenum Press, New York (1964).

(7) Touloukian, Y. S., Editor, Thermophysical Properties of High Temperature Solid Materials, MacMillan Company, New York (1967).

(8) Smithells, C. J., Metal Reference Book, 4th Edition, Plenum Press, New York (1967).

(9) Phillips, B., "Materials for Use Above 3000 F", Research/Development (May, 1967).

(10) "The Thermal Properties of Twenty-Six Solid Materials to 5000 F or Their Destruction Temperatures", Aeronautical Systems Division, Technical Documentary Report No. ASD-TDR-62-765 (January, 1963).

(11) Kaufman, L. and Clougherty, E. V., "Investigation of Boride Compounds for Very High Temperature Applications", Semiannual Report No. 2 on U. S. Air Force Contract AF-33 (657)-8635 (April, 1963).

(12) Long, L. C. and Joiner, J. R., "Refractories in a Reactive Atmosphere", Air Force Flight Dynamics Laboratory Technical Memorandum FDTR-TM-67-1 (April, 1967).

(13) Kaufman, L. and Clougherty, E. V., "Investigation of Boride Compounds for High Temperature Applications", 5th Plansee Proceedings (1964).

(14) Stonehouse, A. J., et al., "The Physical and Mechanical Properties of Beryllides", International Symposium on Compounds of Interest in Nuclear Reactor Technology, IMD Special Report No. 13, 445-455 (1964).

(15) Krochmal, J. J., "4000 F Oxidation Resistant Thermal Protection Materials", presented at Aeronautic and Space Engineering and Manufacturing Meeting in Los Angeles, California (October 3-7, 1966).

(16) Ryshkewitch, E., Oxide Ceramics-Physical Chemistry and Technology, Academic Press, New York (1960).

(17) Kubaschewski, O. and Evans, E. L. L., Metallurgical Thermochemistry, 3rd Edition, Pergamon Press, Oxford, England (1958).

(18) Schick, H. L., Thermodynamic of Certain Refractory Compounds, Academic Press, New York (1966).

(19) Elliott, J. F. and Gleiser, M., Thermochemistry for Steelmaking, Volume 1, Addison-Wesley Publishing Company, Reading, Massachusetts (1960).

(20) Mezaki, R., et al., "High-Temperature Thermodynamic Properties of Some Refractory Borides", Thermodynamics of Nuclear Materials, International Atomic Energy Agency, Vienna, pp 774-788 (1962).

(21) JANAF Thermochemical Tables, Dow Chemical Company, Air Force Contract AF-04 (611)-7554.

(22) Brett, J., et al., "Experimental Study of Factors Controlling the Effectiveness of High-Temperature Protective Coatings for Tungsten", Air Force Materials Laboratory Technical Report No. AFML-TR-392, prepared under Air Force Contract No. AF-33 (657)-8787 (August, 1965).

(23) Levin, E. M., et al., Phase Diagrams for Ceramists, American Ceramic Society, Columbus, Ohio (1964).

(24) Hansen, M. and Anderko, K., Constitution of Binary Alloys, 2nd Edition, McGraw-Hill Book Company, New York (1958).

(25) Elliott, R. P., Constitution of Binary Alloys-First Supplement, McGraw-Hill Book Company, New York (1965).

(26) Nuss, J. W., "Chemical Reactions of Refractory Oxides with Refractory Carbides", Summary of the Eleventh Refractory Composites Working Group Meeting, AFML-TR-66-179, pp 507-ff (July, 1966).

(27) Wilson, E. L. and Jones, R. M., "Finite Element Stress Analysis of Axisymmetric Solids with Orthotropic, Temperature-Dependent Material Properties", Air Force Report No. BS-TR-67-228, Aerospace Report No. TR-0158 (S3816-22)-1.

(28) Boganov, A. G., Pirogov, Yu A., and Makatov, L. P., "Investigation of the Effective Thermal Conductivity and Total Emissivity of Heat-Resistant Ceramic Coatings of Refractory Oxides Produced by Gas-Flame Spraying", Teplofizik Vysokikh Temperatur (Thermophysics of High Temperatures), 3 (1), 64-69 (1965).

CGB:RLH:DEK/js